THE ASYMPTOTIC ANALYSIS OF SOME PDE AND STEKLOV EIGENVALUE PROBLEMS WITH PARTIALLY REACTIVE PATCHES IN 3-D

DENIS S. GREBENKOV * AND MICHAEL J. WARD †

Abstract. We consider steady-state diffusion in a three-dimensional bounded domain with a smooth reflecting boundary that is partially covered by small partially reactive patches. By using the method of matched asymptotic expansions, we investigate the competition of these patches for a diffusing particle and the crucial role of surface reactions on these targets. After a brief overview of former contributions to this field, we first illustrate our approach by considering the classical problems of the mean first-reaction time (MFRT) and the splitting probability for partially reactive patches characterized by a Robin boundary condition. For a spherical domain, we derive a three-term asymptotic expansion for the MFRT and splitting probabilities in the small-patch limit. This expansion is valid for arbitrary reactivities, and also accounts for the effect of the spatial configuration of patches on the boundary. Secondly, we consider more intricate surface reactions modeled by mixed Steklov-Neumann or Steklov-Neumann-Dirichlet problems. We provide the first derivation of the asymptotic behavior of the eigenvalues and eigenfunctions for these spectral problems in the small-patch limit for a spherical domain. Extensions of these asymptotic results to arbitrary domains and their physical applications are discussed.

1. Introduction. Many vital processes in microbiology rely on diffusive search for small targets, such as proteins searching for their partners or specific sites on a DNA chain, ions searching for channels on the plasma membrane of the cell, viruses searching for nuclear pores, etc. [1, 81, 18, 71, 60]. In heterogeneous catalysis, reactants move toward active sites on a solid catalytic surface to be chemically transformed [73, 86, 64]. In nuclear magnetic resonance experiments, spin-bearing molecules diffuse in tissues or mineral samples and may relax their magnetization on magnetic impurities that are located on confining walls [21, 46, 77]. Various search problems on a macroscopic scale such as animal or human behavior are inspired by ecology [79, 60]. These and many other natural phenomena are often modeled by reflected Brownian motion that is confined inside a bounded domain by an impenetrable boundary. This stochastic process is stopped (or killed) under certain conditions that represent interactions of the diffusing particle with prescribed regions (called "targets") that are located either inside the domain or on its boundary. Depending on the context and application, such interactions may represent a chemical reaction, a binding, a conformational change to a different state, a relaxation of magnetization or fluorescence, an escape from the domain, etc. One of the simplest and most studied stopping condition is the first arrival onto the targets. In this scenario, the efficiency of the diffusive search is usually characterized by the distribution of the first-passage time (FPT) to single or multiple targets [102, 108, 94, 92, 37, 60].

From a mathematical viewpoint, many former works have been dedicated to the analysis of the *mean* first-passage time (MFPT) and its dependence on the shape, size, and spatial arrangement of the targets in the confining domain. If $\mathbf{X}$ denotes the starting point of reflected Brownian motion in a bounded domain $\Omega \subset \mathbb{R}^d$ with a smooth boundary $\partial\Omega$, the MFPT $T(\mathbf{X})$ to a target region $\partial\Omega_a \subset \partial\Omega$ satisfies the

*Laboratoire de Physique de la Matière Condensée, CNRS – Ecole Polytechnique, Institut Polytechnique de Paris, 91120 Palaiseau, France. Email: denis.grebenkov@polytechnique.edu (corresponding author),

†Department of Mathematics, University of British Columbia, Vancouver, B.C., Canada, V6T 1Z2. Email: ward@math.ubc.ca

Poisson equation with mixed Dirichlet-Neumann boundary condition:

$$-D\Delta T(\mathbf{X}) = 1\,, \quad \mathbf{X} \in \Omega\,, \tag{1.1a}$$

$$T(\mathbf{X}) = 0\,, \quad \mathbf{X} \in \partial\Omega_a\,, \tag{1.1b}$$

$$\partial_n T(\mathbf{X}) = 0\,, \quad \mathbf{X} \in \partial\Omega_r = \partial\Omega \backslash \partial\Omega_a\,, \tag{1.1c}$$

where $D > 0$ is a constant diffusion coefficient, Δ is the Laplace operator, and ∂_n is the outward normal derivative. The Dirichlet condition on $\partial\Omega_a$ characterizes the first-arrival stopping condition (if the particle starts from $\partial\Omega_a$, the process is immediately stopped, yielding $T = 0$), whereas the Neumann condition on $\partial\Omega_r$ ensures zero flux across the reflecting part of the boundary. The mixed boundary condition presents the major challenge in solving this boundary value problem (BVP) in general domains, in which a trivial separation of variables, such as in rectangles or concentric spheres, is not applicable. Despite the existence of advanced techniques such as dual integral or series equations [115], or the generalized method of separation of variables [62, 49], the disk with an arc-shaped target is presumably the only nontrivial example for which an exact explicit solution of (1.1) has been found [111, 107, 47, 91].

For this reason, various approximate, numerical and asymptotic techniques have been developed over the past two decades. When the target $\partial\Omega_a$ is small, determining the asymptotic behavior of the MFPT is usually referred to as *the narrow escape problem* (see an overview in [72]). The presence of a small Dirichlet patch $\partial\Omega_a$ on an otherwise reflecting boundary is a *singular* perturbation [97, 93, 119]. In fact, if $\partial\Omega_a$ was absent, the MFPT would be infinite. As a consequence, the solution of (1.1) diverges in the small-patch limit $\partial\Omega_a \to \emptyset$. The very first asymptotic result for the MFPT to a small circular patch of radius ϵ on a spherical boundary of radius R dates back to Lord Rayleigh, who found (in the context of acoustics) that, to leading-order in ϵ, $T \sim |\Omega|/(4D\epsilon)$, where $|\Omega| = 4\pi R^3/3$ is the volume of the spherical domain [3]. Even though the particle escapes through the two-dimensional boundary patch, the MFPT scales inversely with the radius of the patch ($\sim \epsilon$) and not with its area ($\sim \epsilon^2$). This is a characteristic feature of a perfectly reactive circular patch with Dirichlet condition, also known as the diffusion-limited regime in diffusion-controlled reactions [96, 121, 20, 10, 106, 64], and this behavior is typical for Dirichlet patches of arbitrary shape. However, as we will discuss below, an additional scaling regime emerges for more sophisticated reaction mechanisms. Rayleigh's leading-order result has been generalized to other domains and patch shapes, both in two and three dimensions, and the asymptotic results have been applied to many specific problems in microbiology (see [69, 114, 111, 112, 109, 70, 113] and the overviews in [71, 72]).

However, to obtain more refined asymptotic results, the method of *matched asymptotic expansions* [80], as tailored in [119] and [118] to analyze PDE problems with strong localized perturbations, has been implemented to systematically calculate higher-order asymptotic approximations of the MFPT, the splitting probability, and related first passage quantities in both two- and three-dimensional settings with either boundary patches or interior targets ([35, 30, 99, 29, 26, 31, 38, 13, 14, 74]). Some asymptotic results for related problems on unbounded domains are given in [87, 89, 83] (see also the references therein). An alternative approach to the method of matched asymptotics was described in [28]. Even though our discussion is focused on ordinary diffusion, extensions to more sophisticated diffusion processes, and to problems with stochastic resetting, have been explored (see [34, 5, 17, 66, 12] and the references therein). We also emphasize that the knowledge of the *mean* FPT does not fully characterize the distribution of this random variable [44, 58]. Ana-

lytical and numerical studies for obtaining the full probability distribution include [107, 59, 105, 88, 27] (see the references therein).

The above stopping condition corresponds to the simplest reaction kinetics when the reaction event occurs certainly and instantly upon the first arrival onto the target. This perfect reaction scenario assumes that the diffusive search is the only limiting factor and thus oversimplifies reaction kinetics that is relevant in many applications [98, 64]. Indeed, a particle that arrives onto the target may not react instantly due to various reasons: (i) a reaction event often requires overcoming an activation energy barrier [120, 67]; (ii) an escape event may involve overcoming an entropic barrier [123, 103, 25]; (iii) a macromolecule may need to be in the proper conformational state to bind its partner [36, 42, 90]; (iv) the target may switch between active and passive states (e.g., an ion channel can be open or closed) [4, 104, 82]; (v) the target may be microscopically inhomogeneous so that the arrival point may be inert [9, 7, 8, 95, 87, 11, 101]. Whatever the microscopic origin is, such *imperfect* targets, generally referred to as *partially reactive*, are often modeled by a Robin boundary condition [33]. For instance, the BVP (1.1) is replaced by

$$-D\Delta\mathcal{T}(\mathbf{X}) = 1\,, \quad \mathbf{X}\in\Omega\,, \tag{1.2a}$$

$$D\partial_n\mathcal{T} + \mathcal{K}\mathcal{T} = 0\,, \quad \mathbf{X}\in\partial\Omega_a\,, \tag{1.2b}$$

$$\partial_n\mathcal{T}(\mathbf{X}) = 0\,, \quad \mathbf{X}\in\partial\Omega_r = \partial\Omega\backslash\partial\Omega_a\,, \tag{1.2c}$$

with the mixed Robin-Neumann boundary condition. The reactivity $\mathcal{K}$, which has units of length per time, characterizes the facility of the reaction event, by ranging from 0 (inert passive target, no reaction) to $+\infty$ (perfect reaction upon the first arrival). If the particle that arrives onto the target fails to react, it is reflected from the target and resumes its diffusion in the domain until the next arrival, and so on. As a consequence, the successful reaction event is generally preceded by a sequence of diffusive excursions in the bulk after each failed reaction attempt, and the mean *first-reaction time* (MFRT), $\mathcal{T}(\mathbf{X})$, satisfying (1.2), can significantly exceed the MFPT $T(\mathbf{X})$ satisfying (1.1). The probabilistic interpretation of the Robin boundary condition and the relation of the reactivity $\mathcal{K}$ to the probability of the reaction event upon each attempt were provided in [51].

The effect of partial reactivity on the efficiency of the diffusive search, which was ignored in most former studies, has recently attracted considerable attention. For instance, the small-patch asymptotic behavior of the MFRT was deduced in [61] by using a constant-flux approximation. In particular, for a circular patch on a spherical boundary, the MFRT was shown to behave as $|\Omega|/(\mathcal{K}|\partial\Omega_a|)$ in the leading order in ϵ, where $|\partial\Omega_a| = \pi\epsilon^2$ is the surface area of the patch. The faster divergence $\mathcal{O}(\epsilon^{-2})$ is reminiscent to the reaction-limited rate, which becomes dominant in the small-patch limit for a finite reactivity $\mathcal{K}$. The change of scaling between diffusion-limited and reaction-limited regimes suggests a nontrivial dependence on the reactivity, especially in the limit $\mathcal{K}\to\infty$. In fact, the limits $\mathcal{K}\to\infty$ and $\epsilon\to 0$ are not interchangeable. This point was further investigated in [65, 22, 56], where the behavior of the MFRT on a small circular patch was inspected for small, intermediate, and large reactivities by different methods. The effect of spatially heterogeneous reactivity was analyzed via a spectral approach [48], whereas the role of target anisotropy onto the MFRT was studied in [23]. The trapping rate of a reflecting plane covered by partially reactive circular patches was estimated by means of boundary homogenization technique [100].

Despite this recent progress, many open questions about partially reactive patches in 3-D remain unsolved. Some key open questions include the following:

(i) Most aforementioned works have dealt with a single patch. Can we develop an asymptotic theory that incorporates the effect of multiple patches that compete with each other for capturing diffusing particles (the so-called diffusional screening [40] or diffusive interactions [116, 117, 6])?

(ii) Many former works focused on the leading-order term, which scales as ϵ^{-2}. However, the expected "correction" terms $\mathcal{O}(\epsilon^{-1})$, $\mathcal{O}(\log \epsilon)$ and $\mathcal{O}(1)$ may provide significant contributions, and their knowledge is required for an accurate estimation of the MFRT in applications, especially if ϵ is not too small. Can we develop a systematic approach to capture these higher-order terms?

(iii) To our knowledge, all previous analyses on partially reactive patches have assumed their *circular* shape. How does the shape of the patch affect the asymptotic behavior of the MFRT?

(iv) What is the impact of the spatial arrangement of patches? This question was addressed for perfectly reactive patches but remains open for partially reactive ones.

(v) Even though the use of the MFRT is a common way to characterize the efficiency of the diffusive search, other quantities may be needed to reveal versatile facets of this phenomenon. For instance, one often employs the splitting probabilities to describe the efficiency of individual patches in their competition for capturing the diffusing particles. What is the asymptotic behavior of the splitting probabilities of partially reactive patches?

(vi) Finally, the Robin boundary condition (1.2b) implements the simplest model of a constant reactivity on the patch. The encounter-based approach [51] allows one to introduce a much more general class of surface reactions that describe, e.g., progressive activation or de-activation of the patch by its interaction with diffusing particles, non-Markovian binding, surface adsorption, etc. [53, 15, 16]. In probabilistic terms, one imposes a more general stopping condition that involves the boundary local time, i.e., a proxy of the number of encounters of the particle with the patch [50, 52]. In turn, the PDE formulation of this framework substitutes the Robin boundary condition by an integral equation on the patch. A natural framework for solving and analyzing such PDEs relies on the Steklov-Neumann problem [56] or the Steklov-Dirichlet-Neumann problem [54] (see §2 for their formulation). These are basic extensions of the conventional Steklov spectral problem that has been thoroughly studied in spectral geometry [84, 43, 32]. To characterize the efficiency of multiple small patches with more sophisticated reaction mechanisms, can we analyze the asymptotic behavior of the eigenvalues and eigenfunctions of the related Steklov problems in the small-patch limit? To our knowledge, this asymptotic problem was not addressed in the past (except for [56] that focused on a single circular patch).

In this paper, we aim at answering all these questions. For this purpose, we combine the method of matched asymptotic expansions, based on strong localized perturbation theory [119], with spectral expansions based on the local exterior Steklov problem on each patch. The use of geodesic normal coordinates is another key tool to access higher-order terms in the asymptotic expansions. In the next section, we formulate four asymptotic problems and summarize our main results.

2. Summary of main results. We consider reflected Brownian motion in a three-dimensional bounded domain Ω, with a smooth boundary $\partial\Omega$, which consists of the union $\partial\Omega_a = \cup_{i=1}^{N} \partial\Omega_i$ of N reactive patches $\partial\Omega_i$ and the remaining reflecting (inert) boundary $\partial\Omega_r$. Each reactive boundary patch $\partial\Omega_i$ of diameter $2L_i$ is assumed to be simply-connected with a smooth boundary, but with an otherwise arbitrary shape. Our asymptotic analysis will exploit an assumed length-scale separation $L/R \ll 1$,

where $L \equiv \max_i\{L_i\}$, and $2R$ is the diameter of the confining domain Ω. The patches are assumed to be well-separated in the sense that $\text{dist}\{\partial\Omega_i, \partial\Omega_j\} \gg L$ for all $i \neq j$. We will study four different problems that can be analyzed with a common theoretical framework. For this reason, we will employ the same notations, e.g., $U(\mathbf{X})$, for formulating and studying these problems.

(I) The mean first-reaction time, $\mathcal{T}(\mathbf{X}) = U(\mathbf{X})$, on the union $\partial\Omega_a$ of partially reactive patches $\partial\Omega_1, \ldots, \partial\Omega_N$ with finite reactivities $\mathcal{K}_1, \ldots, \mathcal{K}_N$, satisfies a Poisson equation with mixed Neumann-Robin boundary conditions, re-formulated from (1.2) as

$$\Delta U = -\frac{1}{D}\,, \quad \mathbf{X} \in \Omega\,, \tag{2.1a}$$

$$D\partial_n U + \mathcal{K}_i U = 0\,, \quad \mathbf{X} \in \partial\Omega_i\,, \quad i = 1, \ldots, N\,, \tag{2.1b}$$

$$\partial_n U = 0\,, \quad \mathbf{X} \in \partial\Omega_r\,. \tag{2.1c}$$

We also consider the volume-averaged MFRT,

$$\overline{U} \equiv \frac{1}{|\Omega|}\int_\Omega U(\mathbf{X})\, d\mathbf{X}\,, \tag{2.2}$$

which corresponds to the average with respect to a uniform distribution of initial points $\mathbf{X} \in \Omega$, where $|\Omega|$ denotes the volume of Ω.

(II) The splitting probability, $U(\mathbf{X})$, to react on the first patch $\partial\Omega_1$, before reacting on the other patches, satisfies

$$\Delta U = 0\,, \quad \mathbf{X} \in \Omega\,, \tag{2.3a}$$

$$D\partial_n U + \mathcal{K}_i U = \delta_{i1}\mathcal{K}_i\,, \quad \mathbf{X} \in \partial\Omega_i\,, \quad i = 1, \ldots, N\,, \tag{2.3b}$$

$$\partial_n U = 0\,, \quad \mathbf{X} \in \partial\Omega_r\,, \tag{2.3c}$$

where $\delta_{11} = 1$ and $\delta_{i1} = 0$ for $i = 2, \ldots, N$. The volume-averaged splitting probability is also given by (2.2).

(III) More sophisticated surface reactions can be formulated in terms of various Steklov spectral problems (cf. [51, 52, 53, 54, 55, 56]). One such problem consists of finding the eigenpairs $\{\Sigma, U\}$ of the mixed Steklov-Dirichlet-Neumann (SDN) problem formulated as

$$\Delta U = 0\,, \quad \mathbf{X} \in \Omega\,, \tag{2.4a}$$

$$\partial_n U = \Sigma U\,, \quad \mathbf{X} \in \partial\Omega_1\,, \tag{2.4b}$$

$$U = 0\,, \quad \mathbf{X} \in \partial\Omega_i\,, \quad i = 2, \ldots, N\,, \tag{2.4c}$$

$$\partial_n U = 0\,, \quad \mathbf{X} \in \partial\Omega_r. \tag{2.4d}$$

These eigenpairs allow one to solve the escape problem when the diffusing particle has to react on the patch $\partial\Omega_1$ before escaping from the domain Ω through any Dirichlet patch $\partial\Omega_j$, for $j = 2, \ldots, N$, which may represent holes or channels on the domain boundary [54].

(IV) Finally, we will consider the mixed Steklov-Neumann (SN) problem that consists of finding the eigenpairs $\{\Sigma, U\}$ satisfying

$$\Delta U = 0\,, \quad \mathbf{X} \in \Omega\,, \tag{2.5a}$$

$$\partial_n U = \Sigma U\,, \quad \mathbf{X} \in \partial\Omega_i\,, \quad i = 1, \ldots, N\,, \tag{2.5b}$$

$$\partial_n U = 0\,, \quad \mathbf{X} \in \partial\Omega_r\,. \tag{2.5c}$$

These eigenpairs can be used to investigate sophisticated surface reactions on multiple patches and their competition. The general spectral properties of mixed Steklov-Neumann problems, known as sloshing or ice-fishing problems in hydrodynamics, were studied previously in [68, 41, 78, 85] (see also the references therein).

For each of these four problems we focus on the spherical domain $\Omega = \{\mathbf{X} \in \mathbb{R}^3 \,|\, |\mathbf{X}| \le R\}$ in order to derive the three-term asymptotic behavior in the limit $\varepsilon = L/R \ll 1$. We emphasize that the leading-order terms in our derived asymptotic results do not depend on the geometry of the confining domain and are thus valid for an arbitrary domain with a smooth boundary. However, our emphasis is on calculating the higher-order terms in the asymptotic expansions, which are often relevant for applications, and are needed for determining the effect of the location of the patches on the surface and for deriving a homogenization result for the MFRT. Although the methodology for deriving the three-term expansions can potentially be extended to arbitrary 3-D domains, we will restrict our analysis to the sphere, where the surface Neumann Green's function is available analytically.

For our analysis, it is convenient to reformulate the four problems in terms of dimensionless variables defined by

$$\mathbf{x} = \frac{\mathbf{X}}{R}\,, \quad L = \max_i L_i\,, \quad \varepsilon = \frac{L}{R}\,, \quad a_i = \frac{L_i}{L}\,, \quad \kappa_i = \frac{L\mathcal{K}_i}{D}\,, \quad \sigma = \Sigma L\,. \tag{2.6}$$

Moreover, the dimensionless MFRT $u(\mathbf{x})$ will be expressed as

$$u(\mathbf{x}) = \frac{D}{R^2} U(\mathbf{x}R)\,. \tag{2.7}$$

Such a rescaling of U is not needed for the splitting probability (which is already dimensionless) nor for the Steklov eigenfunctions, which are defined up to a suitable normalization.

In terms of the new variables (2.6) and (2.7), the dimensionless MFRT $u(\mathbf{x})$ in the unit sphere Ω with partially reactive patches and dimensionless reactivities κ_i satisfies

$$\Delta_{\mathbf{x}} u = -1\,, \quad \mathbf{x} \in \Omega\,, \tag{2.8a}$$

$$\varepsilon \partial_n u + \kappa_i u = 0\,, \quad \mathbf{x} \in \partial\Omega_i^\varepsilon\,, \quad i = 1, \ldots, N\,, \tag{2.8b}$$

$$\partial_n u = 0\,, \quad \mathbf{x} \in \partial\Omega_r = \partial\Omega \backslash \partial\Omega_a\,, \tag{2.8c}$$

where $\Delta_{\mathbf{x}}$ is the Laplacian in $\mathbf{x}$, and ∂_n is again the outward normal derivative to $\partial\Omega$. Each reactive boundary patch $\partial\Omega_i^\varepsilon$, of small diameter $\mathcal{O}(\varepsilon)$, is assumed to be simply-connected with a smooth boundary, but with an otherwise arbitrary shape, and satisfies $\partial\Omega_i^\varepsilon \to \mathbf{x}_i \in \partial\Omega$ as $\varepsilon \to 0$. The patches are assumed to be well-separated in the sense that $|\mathbf{x}_i - \mathbf{x}_j| = \mathcal{O}(1)$ for all $i \neq j$. With respect to a uniform distribution of initial points $\mathbf{x} \in \Omega$ for the reflected Brownian motion, the dimensionless volume-averaged MFRT is

$$\overline{u} \equiv \frac{1}{|\Omega|} \int_\Omega u(\mathbf{x})\, d\mathbf{x}\,, \tag{2.9}$$

where $|\Omega| = 4\pi/3$ is the volume of Ω. The geometry of a confining sphere with reactive patches on its boundary is depicted in Fig. 2.1(a).

In the limit $\varepsilon \to 0$ of small patches, in §4 we will derive an asymptotic expansion for $u(\mathbf{x})$ and $\overline{u}$ for arbitrary $\kappa_i > 0$. The main result is summarized in Proposition

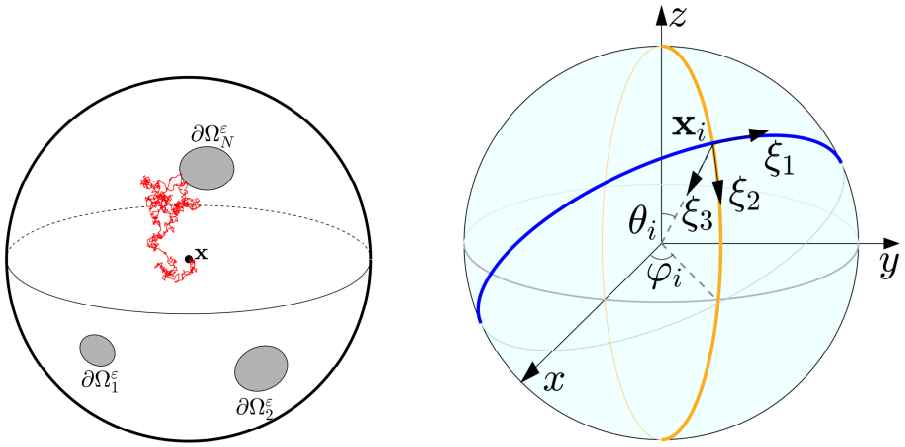

(a) Brownian trajectory in unit sphere **(b)** Geodesic normal coordinates

Fig. 2.1: (a): Sketch of a Brownian trajectory in the unit sphere in $\mathbb{R}^3$ with partially reactive patches $\partial\Omega_1^\varepsilon, \ldots, \partial\Omega_N^\varepsilon$ on the boundary. (b): Geodesic normal coordinates $(\xi_1, \xi_2, \xi_3)^T$ centered at $\mathbf{x}_i \in \partial\Omega$, with the geodesics (orange and blue curves) indicated.

1 of §4. For the special case where $\kappa_i = \infty$ and when the patches are disks, such an analysis has been performed in [30] by expanding spherical coordinates near each patch. In §4 we will use a different and simpler approach than in [30] that relies on geodesic normal coordinates as introduced in §3, which allows us to more readily consider the case of finite κ_i and arbitrary patch shapes. More explicit results will be obtained when the patches are locally circular with radii εa_i for $i = 1, \ldots, N$. Further preliminary results that are the central building blocks for our analysis of the MFRT and for the other three problems are summarized in §3. As a byproduct of this analysis, we also derive in §4.4 a three-term expansion for the principal (lowest) eigenvalue of the Laplace operator with mixed Neumann-Robin boundary conditions.

In a similar way, in terms of (2.6), the splitting probability $u(\mathbf{x})$ for a Brownian particle in the unit sphere Ω to react on a specific target patch on the domain boundary, labeled below by $\partial\Omega_1^\varepsilon$, before reacting on any of the remaining $N-1$, with $N \geq 2$, other boundary patches satisfies

$$\Delta_{\mathbf{x}} u = 0\,, \quad \mathbf{x} \in \Omega\,, \tag{2.10a}$$

$$\varepsilon \partial_n u + \kappa_i u = \delta_{i1}\kappa_i\,, \quad \mathbf{x} \in \partial\Omega_i^\varepsilon\,, \quad i = 1, \ldots, N\,, \tag{2.10b}$$

$$\partial_n u = 0\,, \quad \mathbf{x} \in \partial\Omega_r = \partial\Omega \backslash \partial\Omega_a\,. \tag{2.10c}$$

Here $\delta_{11} = 1$ and $\delta_{i1} = 0$ for $i = 2, \ldots, N$ and we have used the same notation and assumptions on the patches as for the MFRT problem (2.8). The asymptotic analysis of (2.10) is done in §5, with our main result being summarized in Proposition 2.

In terms of (2.6) the dimensionless SDN problem in the unit sphere Ω consists of

finding the eigenpairs $\{\sigma, u\}$ satisfying

$$\Delta_{\mathbf{x}} u = 0\,, \quad \mathbf{x} \in \Omega\,, \tag{2.11a}$$

$$\varepsilon \partial_n u = \sigma u\,, \quad \mathbf{x} \in \partial\Omega_1^{\varepsilon}\,, \tag{2.11b}$$

$$u = 0\,, \quad \mathbf{x} \in \partial\Omega_i^{\varepsilon}\,, \quad i = 2, \ldots, N\,, \tag{2.11c}$$

$$\partial_n u = 0\,, \quad \mathbf{x} \in \partial\Omega_r. \tag{2.11d}$$

In the limit $\varepsilon \to 0$, this problem is analyzed in §6, with the main result summarized in Proposition 3.

In turn, the dimensionless SN problem for (2.5) consists of finding the eigenpairs $\{\sigma, u\}$ satisfying

$$\Delta_{\mathbf{x}} u = 0\,, \quad \mathbf{x} \in \Omega\,, \tag{2.12a}$$

$$\varepsilon \partial_n u = \sigma u\,, \quad \mathbf{x} \in \partial\Omega_i^{\varepsilon}\,, \quad i = 1, \ldots, N\,, \tag{2.12b}$$

$$\partial_n u = 0\,, \quad \mathbf{x} \in \partial\Omega_r\,. \tag{2.12c}$$

This problem is studied in §7, with the main result given in Proposition 4. For a single circular patch, the leading-order asymptotic behavior of the SN problem was thoroughly analyzed in [56]. We will extend this previous analysis for the Steklov eigenvalues by determining a three-term asymptotic result that pertains to multiple well-separated, but arbitrary-shaped, patches. Finally, in §8 we discuss a few open problems.

3. Preliminaries. We first derive some preliminary results that are central for our asymptotic analysis as $\varepsilon \to 0$ of the MFRT, the splitting probability, and the Steklov eigenvalue problems. Our framework will use strong localized perturbation theory [119] based on the method of matched asymptotic expansions. To construct the local expansion near each patch on $\partial\Omega$ it is convenient to introduce geodesic normal coordinates $\xi = (\xi_1, \xi_2, \xi_3)^T \in (-\pi/2, \pi/2) \times (-\pi, \pi) \times [0, 1]$ in $\Omega \cup \partial\Omega$ so that $\xi = 0$ corresponds to $\mathbf{x}_i \in \partial\Omega$, with $\xi_3 > 0$ corresponding to the interior of Ω. Here ξ_2 can be viewed as the polar angle of a spherical coordinate system centered at $\mathbf{x}_i$ on the sphere, but defined on the range $\xi_2 \in (-\pi/2, \pi/2)$ that avoids the usual coordinate singularity of spherical coordinates at the north pole. The curves obtained by setting $\xi_3 = 0$ and fixing either $\xi_1 = 0$ or $\xi_2 = 0$ are geodesics on $\partial\Omega$ (see Fig. 2.1(b)).

In terms of the global transformation $\mathbf{x} = \mathbf{x}(\xi)$ between cartesian and geodesic coordinates, in (A.2) of Appendix A we derive an exact expression for the Laplacian of a generic function $\mathcal{V}(\xi) \equiv u(\mathbf{x}(\xi))$. Then, by introducing the inner, or local variables, $\mathbf{y} = (y_1, y_2, y_3)^T$, defined by

$$\xi_1 = \varepsilon y_1\,, \qquad \xi_2 = \varepsilon y_2\,, \qquad \xi_3 = \varepsilon y_3\,, \tag{3.1}$$

we derive in Appendix A that for $\varepsilon \to 0$, and with $V(\mathbf{y}) = \mathcal{V}(\varepsilon\mathbf{y})$ and $\Delta_{\mathbf{y}} V \equiv V_{y_1 y_2} + V_{y_2 y_2} + V_{y_3 y_3}$, we have

$$\Delta_{\mathbf{x}} u = \varepsilon^{-2} \Delta_{\mathbf{y}} V + \varepsilon^{-1} \left[2 y_3 \left(V_{y_1 y_1} + V_{y_2 y_2} \right) - 2 V_{y_3} \right] + \mathcal{O}(1)\,. \tag{3.2}$$

This two-term inner expansion will be central in our asymptotic analysis.

The leading-order term in our local or inner expansion near $\mathbf{x} = \mathbf{x}_i$ relies on the

canonical solution $w_i = w_i(\mathbf{y};\kappa_i)$ satisfying

$$\Delta_{\mathbf{y}} w_i = 0\,, \quad \mathbf{y} \in \mathbb{R}^3_+\,, \tag{3.3a}$$

$$-\partial_{y_3} w_i + \kappa_i w_i = \kappa_i\,, \quad y_3 = 0\,,\ (y_1,y_2) \in \Gamma_i\,, \tag{3.3b}$$

$$\partial_{y_3} w_i = 0\,, \quad y_3 = 0\,,\ (y_1,y_2) \notin \Gamma_i\,, \tag{3.3c}$$

$$w_i \sim \frac{C_i(\kappa_i)}{|\mathbf{y}|} + \frac{\mathbf{p}_i(\kappa_i)\cdot\mathbf{y}}{|\mathbf{y}|^3} + \cdots\,, \quad \text{as} \quad |\mathbf{y}| \to \infty\,, \tag{3.3d}$$

where the neglected term in (3.3d) is a quadrupole. Here

$$\mathbb{R}^3_+ \equiv \{\mathbf{y} = (y_1,y_2,y_3) \,|\, y_3 > 0\,,\ -\infty < y_1, y_2 < \infty\}$$

is the upper half-space, and $\Gamma_i \asymp \varepsilon^{-1}\partial\Omega_i^\varepsilon$ is the compact flat Robin patch on the horizontal plane $y_3 = 0$, obtained by rescaling and flattening the small patch $\partial\Omega_i^\varepsilon$ on the spherical boundary. In (3.3d), the dipole vector $\mathbf{p}_i = \mathbf{p}_i(\kappa_i)$ has the form $\mathbf{p}_i = (p_{1i}, p_{2i}, 0)^T$ to ensure that the far-field behavior (3.3d) satisfies (3.3c). When Γ_i is symmetric in y_1 and y_2, such as when Γ_i is a disk, we must have $p_{i1} = p_{i2} = 0$ by symmetry, so that the dipole term in the far-field (3.3d) vanishes identically.

3.1. Reactive capacitance. By using the divergence theorem over a large hemisphere, we readily obtain the following identity for $C_i(\kappa_i)$:

$$C_i(\kappa_i) = \frac{1}{\pi}\int_{\Gamma_i} q_i(y_1,y_2;\kappa_i)\,dy_1dy_2\,, \quad \text{where} \quad q_i(y_1,y_2;\kappa_i) \equiv -\frac{1}{2}\partial_{y_3} w_i|_{y_3=0}\,. \tag{3.4}$$

In analogy to electrostatics, $C_i(\kappa_i)$ can be interpreted as a *capacitance* of the partially reactive patch Γ_i with reactivity κ_i, which we will refer to as the *reactive capacitance*. In turn, we will refer to q_i as the *charge density*. Although there is no explicit analytical solution to (3.3) for arbitrary κ_i, in Appendix D we establish a spectral representation (D.9) of w_i in terms of eigenpairs of a suitable exterior *local* Steklov problem (D.1), from which we deduce

$$C_i(\kappa_i) = \frac{\kappa_i}{2\pi}\sum_{k=0}^{\infty}\frac{\mu_{ki}d_{ki}^2}{\mu_{ki}+\kappa_i}\,. \tag{3.5}$$

In (3.5), $\mu_{ki} > 0$ are the Steklov eigenvalues that correspond to nontrivial spectral weights $d_{ki} \neq 0$ defined in (D.8). Both μ_{ki} and d_{ki} depend on the shape of the patch Γ_i. Although their numerical computation is required for a given patch shape, the functional form of $C_i(\kappa_i)$ and its dependence on reactivity κ_i is universal. Moreover, in the important special case where all the patches are of the same shape (but of variable size), such as a collection of disks, the rescaling relations (D.14) imply that

$$C_i(\kappa_i) = a_i\mathcal{C}(\kappa_i a_i), \qquad i = 1,\ldots,N, \tag{3.6}$$

where $\mathcal{C}(\mu)$ is the reactive capacitance of the rescaled patches Γ_i/a_i, which needs to be computed only once for a given patch shape.

For an arbitrary patch shape, we readily calculate from (3.5) that the derivative,

$$C_i'(\kappa_i) \equiv \frac{dC_i(\kappa_i)}{d\kappa_i} = \frac{1}{2\pi}\sum_{k=0}^{\infty}\frac{\mu_{ki}^2 d_{ki}^2}{(\mu_{ki}+\kappa_i)^2} > 0\,, \tag{3.7}$$

is strictly positive for all κ_i (except for the simple poles $\{-\mu_{ki}\}$), so that $C_i(\kappa_i)$ increases monotonically between consecutive poles, and on the positive semi-axis $\kappa_i > 0$. Moreover, in the small-reactivity limit $\kappa_i \to 0$, one can employ the Taylor expansion

$$C_i(\kappa_i) = -a_i \sum_{n=1}^{\infty} c_{ni} \, (-\kappa_i a_i)^n \,, \tag{3.8a}$$

where the coefficients

$$c_{ni} = \frac{1}{2\pi a_i^{n+1}} \sum_{k=0}^{\infty} \frac{d_{ki}^2}{\mu_{ki}^{n-1}} \tag{3.8b}$$

are defined to be invariant under dilations of the patch. In Appendix D, we show that

$$c_{1i} = \frac{|\Gamma_i|}{2\pi a_i^2} \,, \qquad c_{2i} = \frac{1}{2\pi a_i^3} \int_{\Gamma_i} \omega_i(\mathbf{y}) \, d\mathbf{y} \,, \qquad c_{3i} = \frac{1}{2\pi a_i^4} \int_{\Gamma_i} \omega_i^2(\mathbf{y}) \, d\mathbf{y} \,, \tag{3.9}$$

where $\omega_i(\mathbf{y})$ is defined by

$$\omega_i(\mathbf{y}) = \int_{\Gamma_i} \frac{d\mathbf{y}'}{2\pi |\mathbf{y} - \mathbf{y}'|} \,, \qquad \text{for} \quad \mathbf{y} \in \Gamma_i \,. \tag{3.10}$$

To leading order the expansion (3.8a) yields

$$C_i(\kappa_i) \sim \kappa_i \frac{|\Gamma_i|}{2\pi} \,, \qquad \text{as} \quad \kappa_i \to 0 \,. \tag{3.11}$$

In the opposite high-reactivity limit, $C_i(\kappa_i)$ approaches the capacitance $C_i(\infty)$ of the patch Γ_i. After inspecting the spectral representation (3.5), we propose the following heuristic approximation over the entire range of reactivities:

$$C_i(\kappa_i) \approx C_i^{\text{app}}(\kappa_i) = \frac{\kappa_i C_i(\infty)}{\kappa_i + 2\pi C_i(\infty)/|\Gamma_i|} \,, \qquad \text{for} \quad \kappa_i > 0. \tag{3.12}$$

This sigmoidal approximation gives the correct limit as $\kappa_i \to \infty$ and agrees with the leading-order term in the small-reactivity limit $\kappa_i \to 0$ (it is also close to the lower bound (D.46) derived in Appendix D.4). However, this approximation fails to recover the higher-order terms for $\kappa_i \ll 1$, and does not correctly reproduce the asymptotic approach to $C_i(\infty)$ (see (3.19a)). We remark that a similar sigmoidal formula was developed for approximating the principal eigenvalue of the Laplace operator [23] and for studying the boundary local time distribution on small targets [52].

Circular patch. When Γ_i is a disk of radius a_i, the limiting problem with $\kappa_i = \infty$ in (3.3), for which $w_i = 1$ on Γ_i, is the classical problem for the capacitance of a flat disk (cf. [75]), whose solution labeled by $w_i(\mathbf{y}; \infty)$, is (see page 38 of [39])

$$w_i(\mathbf{y}; \infty) = \frac{2}{\pi} \sin^{-1}\left(\frac{a_i}{B(y_3, \rho_0)} \right) \,, \tag{3.13a}$$

where $\rho_0 \equiv (y_1^2 + y_2^2)^{1/2}$ and

$$B(y_3, \rho_0) \equiv \frac{1}{2} \left(\left[(\rho_0 + a_i)^2 + y_3^2 \right]^{1/2} + \left[(\rho_0 - a_i)^2 + y_3^2 \right]^{1/2} \right) \,. \tag{3.13b}$$

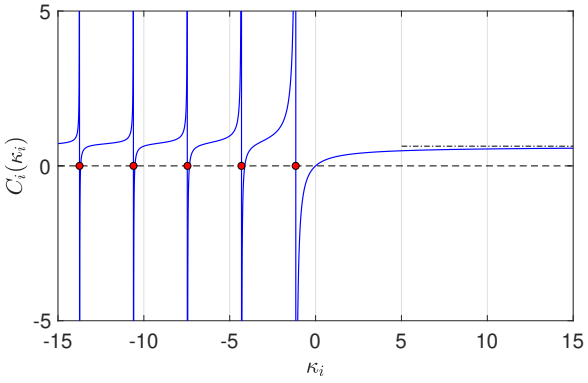

Fig. 3.1: The reactive capacitance $C_i(\kappa_i)$ for a circular patch Γ_i of unit radius ($a_i = 1$), as computed from (3.5). Filled circles presents the poles $\{-\mu_{ki}\}$, all located on the negative axis, at which $C_i(\kappa_i)$ diverges. The dash-dotted horizontal line indicates the asymptotic limit $C_i(\infty) = 2/\pi$.

From this solution, we obtain the far-field behavior

$$w_i(\mathbf{y};\infty) \sim C_i(\infty)\left(\frac{1}{|\mathbf{y}|} + \frac{a_i^2}{6|\mathbf{y}|^5}\left(y_1^2 + y_2^2 - 2y_3^2\right) + \cdots\right), \quad \text{as} \quad |\mathbf{y}| \to \infty, \tag{3.13c}$$

where $C_i(\infty) = 2a_i/\pi$ is the electrostatic capacitance of the circular disk of radius a_i (cf. [75]). Owing to the symmetry of the disk, (3.13c) confirms that there is no dipole term in the far-field. In addition, from (3.13a) and the radial symmetry, we calculate

$$q_i(y_1, y_2;\infty) = q_i(\rho_0;\infty) \equiv -\frac{1}{2}\partial_{y_3} w_i(\mathbf{y};\infty)|_{y_3=0} = \frac{1}{\pi\sqrt{a_i^2 - \rho_0^2}}, \quad 0 \le \rho_0 \le a_i, \tag{3.14}$$

which is needed in our analysis below. We conclude that, in the large-reactivity limit, one has

$$C_i(\kappa_i) \to C_i(\infty) = \frac{2a_i}{\pi}, \quad \text{as} \quad \kappa_i \to \infty. \tag{3.15}$$

However, owing to the edge singularity in (3.14) at $\rho_0 = a_i$, the difference $C_i(\kappa_i) - C_i(\infty)$ is not analytic for $\kappa_i \gg 1$. This difference has been estimated analytically from an integral equation formulation in [65], and in our notation is given explicitly in (D.29) of Appendix D.3 (see also Fig. D.1 and the order estimate in (3.19a)).

For a circular patch, one can use the oblate spheroidal coordinates to efficiently solve the exterior local Steklov problem as in [55] to compute μ_{ki} and d_{ki}. Some of these values are reported in Table D.1 of Appendix D, whereas the function $C_i(\kappa_i)$ is shown in Fig. 3.1. As expected, this function increases monotonically from 0 at $\kappa_i = 0$ to its limit $C_i(\infty) = 2a_i/\pi$ as $\kappa_i \to \infty$. The asymptotic behavior of $C_i(\kappa_i)$ for $\kappa_i \ll 1$ is given by (3.8a), in which the exact values of the first three coefficients c_{ni} are determined in Appendix B (see also Appendix D) as

$$c_{1i} = \frac{1}{2}, \quad c_{2i} = \frac{4}{3\pi} \approx 0.4244, \quad c_{3i} = \frac{4}{\pi^2}\int_0^1 r\,[E(r)]^2\,dr \approx 0.3651, \tag{3.16}$$

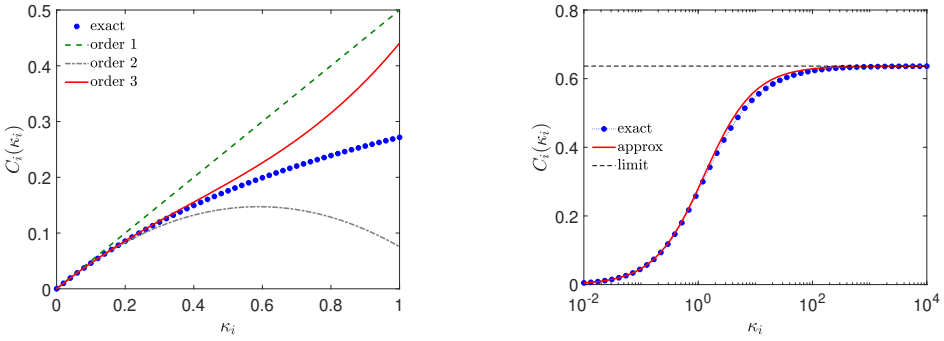

(a) Small κ_i comparison

(b) Sigmoidal approximation

Fig. 3.2: The reactive capacitance $C_i(\kappa_i)$ for the circular patch Γ_i of unit radius ($a_i = 1$). **(a):** A comparison of $C_i(\kappa_i)$ numerically computed from (3.5), with the one-, two-, and three-term approximations obtained from (3.8a) and (3.16), valid for $\kappa_i \ll 1$. **(b):** The sigmoidal approximation (3.17) provides a decent approximation of the numerical result for $C_i(\kappa_i)$ on the full range $\kappa_i > 0$.

where $E(r)$ is the complete elliptic integral of the second kind. In (D.25) of Appendix D we give a fully explicit accurate approximation for all coefficients c_{ni} with $n \geq 2$.

Figure 3.2(a) shows that a three-term small-reactivity series expansion of $C_i(\kappa_i)$ in (3.8a), with the coefficients from (3.16), provides a very close approximation for $C_i(\kappa_i)$ on the range $0 < \kappa_i a_i < 0.45$. Finally, the heuristic formula (3.12), when applied to a disk-shaped patch of radius a_i, reads

$$C_i(\kappa_i) \approx C_i^{\rm app}(\kappa_i) = a_i \mathcal{C}^{\rm app}(\kappa_i a_i)\,, \quad \text{where} \quad \mathcal{C}^{\rm app}(\mu) = \frac{2\mu}{\pi\mu + 4}\,. \tag{3.17}$$

We verified numerically that (3.17) provides a good approximation (see Fig. 3.2(b)), with a maximal relative error of 4%, over the entire range of $\kappa_i > 0$. We summarize the asymptotic results above as follows:

LEMMA 3.1. *When Γ_i is the disk $y_1^2 + y_2^2 \leq a_i^2$, its reactive capacitance is determined by (3.5), as well as by*

$$C_i(\kappa_i) = 2\int_0^{a_i} q_i(\rho_0;\kappa_i)\rho_0\, d\rho_0\,, \qquad q_i(\rho_0;\kappa_i) = -\frac{1}{2} w_{i,y_3}|_{y_3=0}\,, \tag{3.18}$$

where w_i is the solution to (3.3). It has the asymptotics

$$C_i(\kappa_i) \sim C_i(\infty) + \mathcal{O}\left(\frac{\log \kappa_i}{\kappa_i}\right)\,, \quad \textit{as} \quad \kappa_i \to \infty\,, \quad \textit{with} \quad C_i(\infty) = \frac{2a_i}{\pi}\,, \tag{3.19a}$$

$$C_i(\kappa_i) \sim a_i\left[c_{1i}\kappa_i a_i - c_{2i}(\kappa_i a_i)^2 + c_{3i}(\kappa_i a_i)^3 + \mathcal{O}((\kappa_i a_i)^4)\right], \quad \textit{as} \quad \kappa_i \to 0\,, \tag{3.19b}$$

with the coefficients c_{ni} for $n = 1, 2, 3$ given by (3.16). The error estimate in (3.19a) follows from (D.29) of Appendix D.3.

3.2. Monopole from a Higher-Order Inner Solution. Our higher-order asymptotic analysis of each of our four problems (2.8)–(2.12) also involves the monopole coefficient $E_i = E_i(\kappa_i)$, which is defined by the solution to the following inhomogeneous inner problem (see Appendix C):

$$\Delta_{\mathbf{y}}\Phi_{2hi} = 0\,, \quad \mathbf{y} \in \mathbb{R}^3_+\,, \tag{3.20a}$$

$$-\partial_{y_3}\Phi_{2hi} + \kappa_i\Phi_{2hi} = -\kappa_i\mathcal{F}_i\,, \quad y_3 = 0\,,\ (y_1,y_2) \in \Gamma_i\,, \tag{3.20b}$$

$$\partial_{y_3}\Phi_{2hi} = 0\,, \quad y_3 = 0\,,\ (y_1,y_2) \notin \Gamma_i\,, \tag{3.20c}$$

$$\Phi_{2hi} \sim \frac{E_i}{|\mathbf{y}|}\,, \quad \text{as} \quad |\mathbf{y}| \to \infty\,, \tag{3.20d}$$

where $\mathcal{F}_i = \mathcal{F}_i(y_1,y_2;\kappa_i)$ is the unique solution to

$$\mathcal{F}_{i,y_1y_1} + \mathcal{F}_{i,y_2y_2} = q_i(y_1,y_2;\kappa_i)I_{\Gamma_i}\,, \quad I_{\Gamma_i} \equiv \begin{cases} 1\,, & (y_1,y_2) \in \Gamma_i \\ 0\,, & (y_1,y_2) \notin \Gamma_i \end{cases} \tag{3.21a}$$

$$\mathcal{F}_i \sim \frac{C_i}{2}\log\rho_0 + o(1)\,, \quad \text{as} \quad \rho_0 \equiv (y_1^2+y_2^2)^{1/2} \to \infty\,. \tag{3.21b}$$

Here $C_i = C_i(\kappa_i)$ while the charge density $q_i(y_1,y_2;\kappa_i)$ is given in (3.4).

For an arbitrary patch shape, in Appendix C we show that $E_i(\kappa_i)$ is determined by

$$E_i(\kappa_i) = -\frac{1}{2\pi^2}\int_{\Gamma_i}\int_{\Gamma_i} q_i(\mathbf{y};\kappa_i)\,q_i(\mathbf{y}';\kappa_i)\,\log|\mathbf{y}-\mathbf{y}'|\,d\mathbf{y}\,d\mathbf{y}'\,. \tag{3.22}$$

In addition, in the limit $\kappa_i \to 0$, we derive in Appendix C that to leading order

$$E_i(\kappa_i) \sim e_i C_i^2(\kappa_i)\,, \quad \text{with} \quad e_i \equiv -\frac{1}{2|\Gamma_i|^2}\int_{\Gamma_i}\int_{\Gamma_i}\log|\mathbf{y}-\mathbf{y}'|\,d\mathbf{y}\,d\mathbf{y}'\,, \tag{3.23}$$

where $C_i(\kappa_i) \sim \kappa_i|\Gamma_i|/(2\pi)$ for $\kappa_i \ll 1$.

The next result, also proved in Appendix C, characterizes E_i when Γ_i is a disk:

LEMMA 3.2. *When Γ_i is the disk $y_1^2+y_2^2 \le a_i^2$, we have*

$$E_i = E_i(\kappa_i) = -\frac{\log a_i}{2}[C_i(\kappa_i)]^2 + a_i^2\,\mathcal{E}_i(\kappa_i a_i)\,, \tag{3.24}$$

where $C_i(\kappa_i)$ is given by (3.5), and

$$\mathcal{E}_i(\mu) = 2\int_0^1 \frac{1}{\rho_0}\left(\int_0^{\rho_0} a_i q_i(\eta a_i;\mu/a_i)\,\eta\,d\eta\right)^2 d\rho_0 \tag{3.25}$$

corresponds to the unit disk, with $q_i(\rho_0;\kappa_i)$ as given in (3.18). The asymptotic behavior of $E_i(\kappa_i)$ is

$$E_i \sim E_i(\infty) \equiv -\frac{2a_i^2}{\pi^2}\left(\log a_i + \log 4 - \frac{3}{2}\right)\,, \quad \textit{as} \quad \kappa_i \to \infty\,, \tag{3.26a}$$

$$E_i \sim \frac{\kappa_i^2 a_i^4}{8}\left(\frac{1}{4} - \log a_i\right)\,, \quad \textit{as} \quad \kappa_i \to 0\,. \tag{3.26b}$$

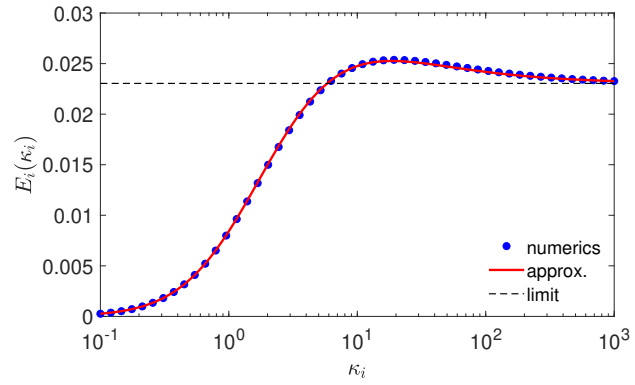

Fig. 3.3: For a circular patch of radius $a_i = 1$, the heuristic approximation $\mathcal{E}^{\text{app}}(\kappa_i)$ (solid line) from (3.27b) is compared with $E_i(\kappa_i) = \mathcal{E}_i(\kappa_i)$ (filled circles) given by (3.24) and computed via the numerical approach in Appendix E. The dashed horizontal line is the asymptotic limiting value $(3 - 4\log 2)/\pi^2$ consistent with (3.26a).

Although there is no explicit formula for $E_i(\kappa_i)$ for arbitrary $\kappa_i > 0$ even when Γ_i is a disk, in Appendix E we show how it can be numerically computed to high precision by expanding the charge density q_i in terms of Steklov eigenfunctions. Moreover, when Γ_i is a disk, we provide the heuristic approximation (see Appendix E)

$$E_i(\kappa_i) \approx E_i^{\text{app}}(\kappa_i) = -\frac{a_i^2 \log a_i}{2} \left[\mathcal{C}^{\text{app}}(\kappa_i a_i)\right]^2 + a_i^2 \mathcal{E}^{\text{app}}(\kappa_i a_i)\,, \qquad \kappa_i > 0\,, \tag{3.27a}$$

where $\mathcal{C}^{\text{app}}(\mu)$ is given by the sigmoidal approximation (3.17), and we define (see (E.6) of Appendix E)

$$\mathcal{E}^{\text{app}}(\mu) = \left[\mathcal{C}^{\text{app}}(\mu)\right]^2 \left(\frac{3}{4} - \log 2 + \frac{1}{\frac{1}{\log 2 - 5/8} + 5.17\,\mu^{0.81}}\right). \tag{3.27b}$$

In Fig. 3.3 we show that, over the full range $\kappa_i > 0$, (3.27a) agrees remarkably well, with only a maximal relative error of 0.7%, with corresponding numerical results as computed using the methodology described in Appendix E. This heuristic approximation also ensures that the required limits from (3.26) as $\kappa_i \to 0$ and $\kappa_i \to \infty$ hold.

3.3. The Surface Neumann Green's Function. The asymptotic solutions at each order in the outer region, defined at $\mathcal{O}(1)$ distances from the surface patches, is represented in terms of the surface Neumann Green's function $G_s(\mathbf{x}; \mathbf{x}_i)$ for the unit sphere Ω, which is the unique solution to

$$\Delta_{\mathbf{x}} G_s = \frac{1}{|\Omega|}\,, \quad \mathbf{x} \in \Omega\,; \quad \partial_n G_s = \delta(\mathbf{x} - \mathbf{x}_i)\,, \quad \mathbf{x} \in \partial\Omega\,; \quad \int_\Omega G_s \, d\mathbf{x} = 0\,, \tag{3.28}$$

with $|\mathbf{x}_i| = 1$. The exact solution to (3.28), as derived in Appendix A of [30], is

$$G_s(\mathbf{x}; \mathbf{x}_i) = \frac{1}{2\pi\,|\mathbf{x} - \mathbf{x}_i|} + \frac{|\mathbf{x}|^2 + 1}{8\pi} + \frac{1}{4\pi} \log\left(\frac{2}{1 - \mathbf{x}\cdot\mathbf{x}_i + |\mathbf{x} - \mathbf{x}_i|}\right) - \frac{7}{10\pi}\,. \tag{3.29}$$

The following result characterizes the local behavior of G_s as $\mathbf{x} \to \mathbf{x}_i$ in terms of the local geodesic coordinates $\mathbf{y}$ defined in (3.1).

LEMMA 3.3. *As* $\mathbf{x} \to \mathbf{x}_i$ *with* $|\mathbf{x}_i| = 1$, *we have*

$$G_s(\mathbf{x};\mathbf{x}_i) \sim \frac{1}{2\pi|\mathbf{x}-\mathbf{x}_i|} - \frac{1}{4\pi}\log\big(|\mathbf{x}-\mathbf{x}_i| + 1 - |\mathbf{x}|\big) + \frac{\log 2}{4\pi} - \frac{9}{20\pi} + o(1)\,. \tag{3.30}$$

In terms of the local geodesic coordinates $\mathbf{y} = \varepsilon^{-1}\mathcal{Q}_i^T(\mathbf{x}-\mathbf{x}_i)$, *where* $\mathcal{Q}_i$ *is the orthogonal matrix from (A.8) of Appendix A, we have that*

$$G_s \sim \frac{1}{2\pi\varepsilon|\mathbf{y}|} - \frac{1}{4\pi}\log\left(\frac{\varepsilon}{2}\right) + \frac{y_3(y_1^2+y_2^2)}{4\pi|\mathbf{y}|^3} - \frac{1}{4\pi}\log(|\mathbf{y}|+y_3) - \frac{9}{20\pi} + o(1)\,. \tag{3.31}$$

Proof. We use the law of cosines with $|\mathbf{x}_i| = 1$ to get $2\mathbf{x}\cdot\mathbf{x}_i = |\mathbf{x}|^2 + 1 - |\mathbf{x}-\mathbf{x}_i|^2$, so that (3.29) becomes

$$G_s(\mathbf{x};\mathbf{x}_i) = \frac{1}{2\pi\,|\mathbf{x}-\mathbf{x}_i|} + \frac{|\mathbf{x}|^2+1}{8\pi} + \frac{1}{4\pi}\log\left(\frac{4}{(|\mathbf{x}-\mathbf{x}_i|+1)^2 - |\mathbf{x}|^2}\right) - \frac{7}{10\pi}\,. \tag{3.32}$$

Upon using $a^2-b^2 = (a-b)(a+b)$, we let $\mathbf{x}\to\mathbf{x}_i$ with $|\mathbf{x}_i| = 1$ to obtain that (3.32) reduces to (3.30). Finally, as $\mathbf{x}\to\mathbf{x}_i$ we use $1-|\mathbf{x}| \sim \varepsilon y_3$ in (3.30), together with (A.7) of Appendix A, to reduce (3.30) to (3.31). ∎

4. The Mean First-Reaction Time. In this section, we investigate the MFRT in the small-patch limit and derive its three-term expansion, which is valid for arbitrary reactivities. We also discuss its asymptotic behavior for fixed reactivities, as well as the homogenization of the spherical boundary. The asymptotic tools developed in this section will be applied for solving the three other problems in the sections below.

We use the method of matched asymptotic expansions to construct solutions to (2.8) in the limit $\varepsilon \to 0$. In the outer region away from the Robin patches we expand the outer solution as

$$u \sim \varepsilon^{-1}U_0 + U_1 + \varepsilon\log\left(\frac{\varepsilon}{2}\right)U_2 + \varepsilon U_3 + \cdots\,, \tag{4.1}$$

where U_0 is a constant to be determined and where U_k for $k \geq 1$ satisfies

$$\Delta_{\mathbf{x}}U_k = -\delta_{k1}\,, \quad \mathbf{x}\in\Omega\,; \quad \partial_n U_k = 0\,, \quad \mathbf{x}\in\partial\Omega\backslash\{\mathbf{x}_1,\ldots,\mathbf{x}_N\}\,. \tag{4.2}$$

Here $\delta_{k1} = 1$ if $k = 1$ and $\delta_{k1} = 0$ for $k > 1$. Our asymptotic analysis below provides singularity behaviors for each U_k as $\mathbf{x}\to\mathbf{x}_i$, for $i = 1,\ldots,N$. The non-analytic term in ε in (4.1) arises from the subdominant logarithmic term in the local behavior (3.31) of the surface Neumann Green's function.

In the inner region near the i-th Robin patch we introduce the local geodesic coordinates (3.1) and expand each inner solution as

$$u \sim \varepsilon^{-1}V_{0i} + \log\left(\frac{\varepsilon}{2}\right)V_{1i} + V_{2i} + \ldots\,. \tag{4.3}$$

Upon substituting (4.3) into (3.2), we obtain that V_{ki} for $k = 0,1,2$ satisfies

$$\Delta_{\mathbf{y}}V_{ki} = \delta_{k2}\left(2y_3V_{0i,y_3y_3} + 2V_{0i,y_3}\right)\,, \quad \mathbf{y}\in\mathbb{R}^3_+\,, \tag{4.4a}$$

$$-\partial_{y_3}V_{ki} + \kappa_i V_{ki} = 0\,, \quad y_3 = 0\,,\ (y_1,y_2)\in\Gamma_i\,, \tag{4.4b}$$

$$\partial_{y_3}V_{ki} = 0\,, \quad y_3 = 0\,,\ (y_1,y_2)\notin\Gamma_i\,, \tag{4.4c}$$

where $\delta_{22} = 1$ and $\delta_{k2} = 0$ if $k = 0,1$.

Since the leading-order matching condition is $V_{0i} \sim U_0$ as $|\mathbf{y}| \to \infty$, we have

$$V_{0i} = U_0\,(1 - w_i)\;, \tag{4.5}$$

where w_i is the solution to (3.3), defined on the tangent plane to the sphere at $\mathbf{x} = \mathbf{x}_i$, which has the far-field behavior (3.3d) in terms of C_i and $\mathbf{p}_i$. The matching condition is that the local behavior of the outer expansion (4.1) as $\mathbf{x} \to \mathbf{x}_i$ must agree with the far-field behavior of the inner expansion (4.3), so that

$$\begin{aligned} &\frac{U_0}{\varepsilon} + U_1 + \varepsilon \log\left(\frac{\varepsilon}{2}\right) U_2 + \varepsilon U_3 + \ldots \\ &\qquad\qquad \sim \frac{U_0}{\varepsilon}\left(1 - \frac{C_i}{|\mathbf{y}|} - \frac{\mathbf{p}_i\cdot\mathbf{y}}{|\mathbf{y}|^3}\right) + \log\left(\frac{\varepsilon}{2}\right) V_{1i} + V_{2i} + \ldots\,. \end{aligned} \tag{4.6}$$

Since $|\mathbf{y}| \sim \varepsilon^{-1}|\mathbf{x} - \mathbf{x}_i|$ from (A.8) of Appendix A, it follows that the outer correction U_1 must satisfy (4.2) with the singular behavior $U_1 \sim -U_0 C_i/|\mathbf{x} - \mathbf{x}_i|$ as $\mathbf{x} \to \mathbf{x}_i$ for $i = 1, \ldots, N$. In this way, U_1 satisfies

$$\Delta_{\mathbf{x}} U_1 = -1\,, \quad \mathbf{x} \in \Omega\,; \quad \partial_n U_1 = 0\,, \quad \mathbf{x} \in \partial\Omega \backslash \{\mathbf{x}_1, \ldots, \mathbf{x}_N\}\,, \tag{4.7a}$$

$$U_1 \sim -\frac{U_0 C_i}{|\mathbf{x} - \mathbf{x}_i|}\,, \quad \text{as} \quad \mathbf{x} \to \mathbf{x}_i \in \partial\Omega\,, \quad i = 1, \ldots, N\,. \tag{4.7b}$$

From the divergence theorem, the solvability condition for (4.7) is that $|\Omega| = 2\pi U_0 \sum_{i=1}^N C_i$, which determines U_0 as

$$U_0 = \frac{|\Omega|}{2\pi \overline{C}}\,, \quad \text{where} \quad \overline{C} \equiv \sum_{j=1}^N C_j\,. \tag{4.8}$$

The solution to (4.7) is represented in terms of the surface Neumann Green's function of (3.29) as

$$U_1 = \overline{U}_1 - 2\pi U_0 \sum_{j=1}^N C_j G_s(\mathbf{x}; \mathbf{x}_j)\,, \quad \text{where} \quad \overline{U}_1 \equiv |\Omega|^{-1} \int_\Omega U_1\, d\mathbf{x}\,. \tag{4.9}$$

We recall that the coefficients $C_i = C_i(\kappa_i)$, defined by (3.3d) and (3.4), have the asymptotic behavior for both small and large κ_i given in Lemma 3.1 for circular Robin patches. As in [30], we need to expand the unknown constant $\overline{U}_1$ in (4.9) as

$$\overline{U}_1 = \overline{U}_{10} \log\left(\frac{\varepsilon}{2}\right) + \overline{U}_{11}\,, \tag{4.10}$$

where $\overline{U}_{10}$ and $\overline{U}_{11}$ are constants independent of ε, which we determine below. We remark that the $\overline{U}_{10} \log(\varepsilon/2)$ term in (4.10) is a "switchback term" [80] and effectively corresponds to inserting a constant term between U_0/ε and U_1 in the outer expansion (4.1).

To proceed to higher order, we expand U_1 as $\mathbf{x} \to \mathbf{x}_i$ by using the local behavior

(3.31) of G_s near the i-th patch. The matching condition (4.6) becomes

(4.11)
$$\frac{U_0}{\varepsilon}\left(1-\frac{C_i}{|\mathbf{y}|}\right)+\left(\frac{U_0C_i}{2}+\overline{U}_{10}\right)\log\left(\frac{\varepsilon}{2}\right)+\frac{U_0C_i}{2}\left(\log(y_3+|\mathbf{y}|)-\frac{y_3(y_1^2+y_2^2)}{|\mathbf{y}|^3}\right)$$
$$+U_0\beta_i+\overline{U}_{11}+\varepsilon\log\left(\frac{\varepsilon}{2}\right)U_2+\varepsilon U_3+\ldots$$
$$\sim\frac{U_0}{\varepsilon}\left(1-\frac{C_i}{|\mathbf{y}|}-\frac{\mathbf{p}_i\cdot\mathbf{y}}{|\mathbf{y}|^3}\right)+\log\left(\frac{\varepsilon}{2}\right)V_{1i}+V_{2i}+\ldots.$$

Here the constant β_i is defined by the i-th component of the matrix-vector product

$$\beta_i=-2\pi\left(\mathcal{G}_s\mathbf{C}\right)_i\,, \tag{4.12}$$

where $\mathbf{C}\equiv(C_1,\ldots,C_N)^T$ and $\mathcal{G}_s$ is the symmetric Green's matrix defined by

$$\mathcal{G}_s\equiv\begin{pmatrix} R_s & G_{12} & \cdots & G_{1N}\\ G_{21} & R_s & \cdots & G_{2N}\\ \vdots & \vdots & \ddots & \vdots\\ G_{N1} & \cdots & G_{N,N-1} & R_s\end{pmatrix},\quad R_s\equiv-\frac{9}{20\pi},\quad G_{ij}\equiv G_s(\mathbf{x}_i;\mathbf{x}_j)\,. \tag{4.13}$$

The matrix entries above can be calculated from (3.29).

Upon comparing the $\mathcal{O}\left(\log\left(\varepsilon/2\right)\right)$ terms on both sides of (4.11) we conclude that we must have $V_{1i}\sim\overline{U}_{10}+U_0C_i/2$ as $|\mathbf{y}|\to\infty$, where V_{1i} satisfies the inner problem (4.4) with $k=1$. This solution is determined in terms of w_i of (3.3) by

$$V_{1i}=\left(\frac{U_0C_i}{2}+\overline{U}_{10}\right)(1-w_i)\,. \tag{4.14}$$

The far-field behavior (3.3d) for w_i yields for $\rho=|\mathbf{y}|\to\infty$ that

$$V_{1i}\sim\left(\frac{U_0C_i}{2}+\overline{U}_{10}\right)\left(1-\frac{C_i}{|\mathbf{y}|}+\cdots\right),\quad\text{as}\quad|\mathbf{y}|\to\infty\,. \tag{4.15}$$

Next, we substitute (4.15) into the matching condition (4.11). We conclude that the solution U_2 to (4.2) has the singular behavior $U_2\sim-\left(\frac{1}{2}U_0C_i+\overline{U}_{10}\right)C_i/|\mathbf{x}-\mathbf{x}_i|$ as $\mathbf{x}\to\mathbf{x}_i$. Therefore, U_2 satisfies

$$\Delta_{\mathbf{x}}U_2=0\,,\quad\mathbf{x}\in\Omega\,;\quad\partial_nU_2=0\,,\quad\mathbf{x}\in\partial\Omega\backslash\{\mathbf{x}_1,\ldots,\mathbf{x}_N\}\,, \tag{4.16a}$$

$$U_2\sim-\left(\frac{U_0C_i}{2}+\overline{U}_{10}\right)\frac{C_i}{|\mathbf{x}-\mathbf{x}_i|}\,,\quad\text{as}\quad\mathbf{x}\to\mathbf{x}_i\in\partial\Omega\,,\quad i=1,\ldots,N\,. \tag{4.16b}$$

By using the divergence theorem, (4.16) is solvable only when $\overline{U}_{10}$ satisfies

$$\frac{\overline{U}_{10}}{U_0}=-\frac{\mathbf{C}^T\mathbf{C}}{2\overline{C}}\,,\quad\text{where}\quad\mathbf{C}^T\mathbf{C}=\sum_{j=1}^{N}C_j^2\,. \tag{4.17}$$

Then, the solution to (4.16) is represented in terms of an unknown constant $\overline{U}_2$ as

$$U_2=\overline{U}_2-2\pi\sum_{j=1}^{N}C_j\left(\frac{U_0C_j}{2}+\overline{U}_{10}\right)G_s(\mathbf{x};\mathbf{x}_j)\,. \tag{4.18}$$

Next, we match the $\mathcal{O}(1)$ terms in (4.11). We obtain that V_{2i} satisfies (4.4) with $k=2$ together with the far-field behavior

$$V_{2i} \sim \beta_i U_0 + \overline{U}_{11} + \frac{U_0 C_i}{2}\left(\log(y_3+|\mathbf{y}|) - \frac{y_3(y_1^2+y_2^2)}{|\mathbf{y}|^3}\right), \quad \text{as} \quad |\mathbf{y}|\to\infty\,. \tag{4.19}$$

Since $V_{0i} = U_0(1-w_i)$ from (4.5), we decompose V_{2i} as

$$V_{2i} = U_0\left(\Phi_{2i} + \left(\beta_i + \frac{\overline{U}_{11}}{U_0}\right)(1-w_i)\right), \tag{4.20}$$

and obtain from (4.4) and (4.19) that Φ_{2i} satisfies

$$\Delta_{\mathbf{y}}\Phi_{2i} = -\left(2y_3 w_{i,y_3y_3} + 2w_{i,y_3}\right), \quad \mathbf{y}\in\mathbb{R}^3_+\,, \tag{4.21a}$$

$$-\partial_{y_3}\Phi_{2i} + \kappa_i\Phi_{2i} = 0\,, \quad y_3 = 0\,,\ (y_1,y_2)\in\Gamma_i\,, \tag{4.21b}$$

$$\partial_{y_3}\Phi_{2i} = 0\,, \quad y_3 = 0\,,\ (y_1,y_2)\notin\Gamma_i\,, \tag{4.21c}$$

$$\Phi_{2i} \sim \frac{C_i}{2}\left(\log(y_3+|\mathbf{y}|) - \frac{y_3(y_1^2+y_2^2)}{|\mathbf{y}|^3}\right), \quad \text{as} \quad |\mathbf{y}|\to\infty\,. \tag{4.21d}$$

In Appendix C we analyze the solution to (4.21) and we determine the monopole term $E_i = E_i(\kappa_i)$ in the refined far-field behavior, defined by the limiting behavior

$$\Phi_{2i} - \frac{C_i}{2}\left(\log(y_3+|\mathbf{y}|) - \frac{y_3(y_1^2+y_2^2)}{|\mathbf{y}|^3}\right) \sim \frac{E_i}{|\mathbf{y}|}, \quad \text{as} \quad |\mathbf{y}|\to\infty\,. \tag{4.22}$$

For an arbitrary patch shape Γ_i, $E_i(\kappa_i)$ is given by (3.22). Some properties of $E_i(\kappa_i)$ were summarized in §3.2. In particular, when Γ_i is a disk, the limiting asymptotics of $E_i(\kappa_i)$ for $\kappa_i \ll 1$ and $\kappa_i \gg 1$ are given in (3.26) of Lemma 3.2. In addition, an accurate heuristic global approximation for E_i was given in (3.27).

Finally, we determine $\overline{U}_{11}$ from a solvability condition for the problem for the outer correction U_3 in (4.1). To do so, we substitute (4.22) into (4.20) and use $w_i \sim C_i/|\mathbf{y}|$ as $|\mathbf{y}|\to\infty$. We conclude that V_{2i} satisfies the refined far-field behavior

$$\begin{aligned} V_{2i} \sim{}& \beta_i U_0 + \overline{U}_{11} + \frac{U_0 C_i}{2}\left(\log(y_3+|\mathbf{y}|) - \frac{y_3(y_1^2+y_2^2)}{|\mathbf{y}|^3}\right) \\ &+ \frac{U_0 E_i}{|\mathbf{y}|} - \left(\beta_i U_0 + \overline{U}_{11}\right)\frac{C_i}{|\mathbf{y}|}, \quad \text{as} \quad |\mathbf{y}|\to\infty\,. \end{aligned} \tag{4.23}$$

The second line in (4.23) is the first of two terms that needs to be accounted for by U_3 in the matching condition (4.11). The second term is the dipole term in (4.11), which arises from (3.3d). This term is written in terms of outer variables using (A.8) of Appendix A.

In this way, we conclude from (4.2), (4.11) and (4.23) that U_3 must satisfy

$$\Delta_{\mathbf{x}} U_3 = 0\,, \quad \mathbf{x}\in\Omega\,; \quad \partial_n U_3 = 0\,, \quad \mathbf{x}\in\partial\Omega\backslash\{\mathbf{x}_1,\ldots,\mathbf{x}_N\}\,, \tag{4.24a}$$

$$U_3 \sim \frac{\left[U_0 E_i - \left(\beta_i U_0 + \overline{U}_{11}\right)C_i\right]}{|\mathbf{x}-\mathbf{x}_i|} - U_0\frac{\mathbf{p}_i\cdot\mathcal{Q}_i^T(\mathbf{x}-\mathbf{x}_i)}{|\mathbf{x}-\mathbf{x}_i|^3}, \quad \text{as} \quad \mathbf{x}\to\mathbf{x}_i\in\partial\Omega\,, \quad i=1,\ldots,N\,, \tag{4.24b}$$

where the orthogonal matrix $\mathcal{Q}_i$ is defined in (A.8) in terms of the basis vectors of the geodesic coordinate system and $\mathbf{p}_i$ is the dipole vector in (3.3d). By using the divergence theorem, (4.24) has a solution if and only if $\overline{U}_{11}$ satisfies

$$\frac{\overline{U}_{11}}{U_0} = \frac{1}{\overline{C}} \left(\sum_{j=1}^{N} E_j - \sum_{j=1}^{N} \beta_j C_j \right) , \tag{4.25}$$

where we find that the contribution from the dipole term vanishes identically by symmetry since $\mathbf{p}_i$ has the form $\mathbf{p}_i = (p_{1i}, p_{2i}, 0)^T$. Finally, by using (4.12) for β_i, we get

$$\frac{\overline{U}_{11}}{U_0} = \frac{2\pi}{\overline{C}} \mathbf{C}^T \mathcal{G}_s \mathbf{C} + \frac{\overline{E}}{\overline{C}} , \quad \text{where} \quad \overline{E} = \sum_{j=1}^{N} E_j . \tag{4.26}$$

We summarize our main result for the dimensionless MFRT $u(\mathbf{x})$ and the volume-averaged MFRT $\overline{u}$ in the small-patch limit in the following proposition. We also provide the corresponding dimensional result for (2.1), based on the scalings (2.6) and (2.7).

PROPOSITION 1. *For $\varepsilon \to 0$, the asymptotic solution to (2.8) in the unit sphere Ω is given in the outer region $|\mathbf{x} - \mathbf{x}_i| \gg \mathcal{O}(\varepsilon)$ for $i = 1, \ldots, N$ by*

$$\begin{aligned} u(\mathbf{x}) \sim \frac{U_0}{\varepsilon} \Bigg[1 + \varepsilon \log\left(\frac{\varepsilon}{2}\right) \frac{\overline{U}_{10}}{U_0} + \varepsilon \left(\frac{\overline{U}_{11}}{U_0} - 2\pi \sum_{j=1}^{N} C_j G_s(\mathbf{x}; \mathbf{x}_j) \right) \\ + \varepsilon^2 \log\left(\frac{\varepsilon}{2}\right) \left(\frac{\overline{U}_2}{U_0} - 2\pi \sum_{j=1}^{N} C_j \left(\frac{C_j}{2} + \frac{\overline{U}_{10}}{U_0} \right) G_s(\mathbf{x}; \mathbf{x}_j) \right) + \mathcal{O}(\varepsilon^2) \Bigg] . \end{aligned} \tag{4.27}$$

The volume-averaged MFRT $\overline{u}$, defined by (2.9), satisfies

$$\overline{u} \sim \frac{U_0}{\varepsilon} \left[1 + \varepsilon \log\left(\frac{\varepsilon}{2}\right) \frac{\overline{U}_{10}}{U_0} + \varepsilon \frac{\overline{U}_{11}}{U_0} + \mathcal{O}\left(\varepsilon^2 \log \varepsilon\right) \right] . \tag{4.28}$$

In (4.27) and (4.28), U_0, $\overline{U}_{10}$ and $\overline{U}_{11}$ are determined in terms of $\mathbf{C} = (C_1, \ldots, C_N)^T$, $\overline{C} = \sum_{j=1}^{N} C_j$, $\overline{E} = \sum_{j=1}^{N} E_j$, and the Green's matrix $\mathcal{G}_s$ from (4.13) and (3.29) by

$$U_0 = \frac{2}{3\overline{C}} , \qquad \frac{\overline{U}_{10}}{U_0} = -\frac{\mathbf{C}^T \mathbf{C}}{2\overline{C}} , \qquad \frac{\overline{U}_{11}}{U_0} = \frac{2\pi}{\overline{C}} \mathbf{C}^T \mathcal{G}_s \mathbf{C} + \frac{\overline{E}}{\overline{C}} . \tag{4.29}$$

For a single patch, where $N = 1$, we have

$$U_0 = \frac{2}{3C_1} , \qquad \frac{\overline{U}_{10}}{U_0} = -\frac{C_1}{2} , \qquad \frac{\overline{U}_{11}}{U_0} = -\frac{9}{10} C_1 + \frac{E_1}{C_1} . \tag{4.30}$$

In terms of the dimensional variables, we use (2.6) and (2.7) to conclude for a sphere of radius R and for a collection of Robin patches with maximum diameter L that

$$\overline{U} \sim \frac{R^2}{D} \overline{u} . \tag{4.31}$$

Here in calculating $\overline{u}$ in (4.28) we set $C_i = C_i(L\mathcal{K}_i/D)$ and $E_i = E_i(L\mathcal{K}_i/D)$ in (4.29) and evaluate the Green's matrix $\mathcal{G}_s$ at $\mathbf{x}_i = \mathbf{X}_i/R$.

Although in (4.27) the coefficient $\overline{U}_2$ can only be determined at higher order, the spatial dependence of the $\varepsilon^2 \log(\varepsilon/2)$ correction term is completely specified up to this unknown constant. In (4.27) and (4.28), $C_i = C_i(\kappa_i)$ is determined by the solution to (3.3), while $E_i = E_i(\kappa_i)$ is given by (3.22) for an arbitrary shaped patch and by (3.24) when the Robin patches are disks. Their asymptotic behaviors when Γ_i is a disk are given for small and large reactivities in Lemmas 3.1 and 3.2.

We emphasize several features of our main result for the MFRT:

(i) The coefficient $\overline{U}_{11}$ in (4.28) depends on the spatial configuration $\{\mathbf{x}_1, \ldots, \mathbf{x}_N\}$ of the centers of the Robin patches on the surface of the unit sphere via the Green's matrix $\mathcal{G}_s$, defined in (4.13) and (3.29). Therefore, the effect of the location of the patches is only revealed at the third order in the asymptotic expansion.

(ii) To numerically calculate the asymptotic result (4.28) for the volume-averaged MFRT, we need only numerically compute $C_i(\kappa_i)$ from a PDE solution of (3.3) and $E_i(\kappa_i)$ from the quadrature in (3.22). However, by using the heuristic, but accurate, approximations (3.12) and (3.27) that closely predict respectively C_i and E_i for all $\kappa_i > 0$, the coefficients in the asymptotic expansion of the volume-averaged MFRT (4.29) can be explicitly estimated when Γ_i is a disk.

(iii) We observe from Lemmas 3.1 and 3.2 that both $\overline{U}_{10}/U_0$ and $\overline{U}_{11}/U_0$ are $\mathcal{O}(\kappa_i)$ as $\kappa_i \to 0$ for $i = 1, \ldots, N$. As a result, the expansion (4.28) in ε remains uniformly valid in the limit $\kappa_i \to 0$ for each Robin patch.

(iv) Proposition 1 extends the previous result from [30] that dealt with the special case of N perfectly reactive ($\kappa_i = \infty$) disk-shape patches.

For the special case of N *identical* patches, we have $\overline{C} = NC_1$, $\overline{E} = NE_1$, $U_0 = 2/(3NC_1)$, $\overline{U}_{10}/U_0 = -C_1/2$, $\overline{U}_{11}/U_0 = 2\pi C_1(\mathbf{e}^T\mathcal{G}_s\mathbf{e})/N + E_1/C_1$, with $\mathbf{e} = (1, \ldots, 1)^T$, so that the asymptotic expansion (4.28) applied to the dimensional volume-averaged MFRT in (4.31) yields

$$\overline{U} \sim \frac{|\Omega|}{2\pi DNR}\left(\frac{1}{\varepsilon C_1} + \frac{1}{2}\log(2/\varepsilon) + \frac{2\pi}{N}(\mathbf{e}^T\mathcal{G}_s\mathbf{e}) + \frac{E_1}{C_1^2} + \mathcal{O}(\varepsilon\log\varepsilon)\right), \tag{4.32}$$

where $|\Omega| = 4\pi R^3/3$. For instance, for N circular perfectly reactive patches of radius εR, we have $C_1 = 2/\pi$ and $E_1 = (3-4\log 2)/\pi^2$ from (3.19a) and (3.26a), respectively, so that (4.32) reduces to

$$\overline{U} \sim \frac{|\Omega|}{4DNR}\left(\frac{1}{\varepsilon} + \frac{1}{\pi}\log(1/\varepsilon) + \frac{4}{N}(\mathbf{e}^T\mathcal{G}_s\mathbf{e}) + \frac{3}{2\pi} - \frac{\log 2}{\pi} + \mathcal{O}(\varepsilon\log\varepsilon)\right). \tag{4.33}$$

This expression corrects and extends, with its inclusion of the $\mathcal{O}(1)$ term, the seminal result by Singer *et al.* [114] that was obtained for a single circular patch (note that the factor $1/\pi$ in front of the logarithmic term was missing in [114]).

4.1. Expansion for Moderate Reactivities. The crucial advantage of our asymptotic analysis is that the expansions (4.27) and (4.28) remain valid for any reactivities κ_i, even in the limit $\kappa_i \to \infty$ of perfectly reactive patches. In contrast, former approaches usually fixed *finite* reactivities $\mathcal{K}_i$ and then analyzed the limit $\varepsilon \to 0$ such that $\kappa_i = \varepsilon R\mathcal{K}_i/D \to 0$ according to (2.6). In this limit, one can use the asymptotic behaviors of $C_i(\kappa_i)$ and $E_i(\kappa_i)$ as $\kappa_i \to 0$ to derive more explicit expansions. Throughout this subsection, we aim to express the volume-averaged MFRT in terms of finite reactivities $\mathcal{K}_i$ and the small parameter ε.

We first rewrite the Taylor expansion (3.8a) for the reactive capacitance in terms of dimensional parameters. Upon using $a_i = L_i/(\varepsilon R)$ from (2.6) together with (3.9)

for c_{1i}, we obtain

$$C_i = \frac{1}{2\pi\varepsilon RD}\left(|\partial\Omega_i|\mathcal{K}_i - 2\pi c_{2i}\frac{L_i^3\mathcal{K}_i^2}{D} + 2\pi c_{3i}\frac{L_i^4\mathcal{K}_i^3}{D^2} + \dots\right). \tag{4.34}$$

Here the dimensionless coefficients c_{2i} and c_{3i} are given in (3.9) for arbitrary patch shapes, while their exact values for circular patches are given in (3.16). We emphasize that they depend only on the shape of the i-th patch, not on its size. As a consequence, we get for $\overline{C} = \sum_{j=1}^N C_j$ that

$$\overline{C} = \frac{|\partial\Omega|}{2\pi\varepsilon RD}\left(\overline{\mathcal{K}}^{(1)} - \overline{\mathcal{K}}^{(2)} + \overline{\mathcal{K}}^{(3)} + \mathcal{O}(\varepsilon^5)\right), \tag{4.35}$$

where $|\partial\Omega| = 4\pi R^2$ is the surface area of the sphere and where we introduced the weighted reactivities defined by

$$\overline{\mathcal{K}}^{(1)} \equiv \frac{1}{|\partial\Omega|}\sum_{i=1}^N |\partial\Omega_i|\mathcal{K}_i = \sum_{i=1}^N K_i \equiv \overline{K}\,, \quad \text{with} \quad K_i \equiv \mathcal{K}_i\frac{|\partial\Omega_i|}{|\partial\Omega|}\,, \tag{4.36a}$$

$$\overline{\mathcal{K}}^{(n)} \equiv \frac{2\pi}{D^{n-1}|\partial\Omega|}\sum_{i=1}^N c_{ni}L_i^{n+1}\mathcal{K}_i^n\,, \quad \text{for} \quad n = 2, 3, \dots\,. \tag{4.36b}$$

Since $L_i \sim \mathcal{O}(\varepsilon)$ and $|\partial\Omega_i| \sim \mathcal{O}(\varepsilon^2)$, we have $\overline{\mathcal{K}}^{(n)} \sim \mathcal{O}(\varepsilon^{n+1})$ for $n \geq 1$.

Substitution of the expansion (4.35) into (4.29), while using the binomial approximation, yields

$$U_0 = \frac{4\pi\varepsilon RD}{3|\partial\Omega|\overline{K}}\left(1 + \frac{\overline{\mathcal{K}}^{(2)}}{\overline{K}} + \frac{[\overline{\mathcal{K}}^{(2)}]^2 - \overline{\mathcal{K}}^{(3)}\overline{K}}{\overline{K}^2} + \mathcal{O}(\varepsilon^5)\right). \tag{4.37}$$

We also derive from (4.29) that

$$\frac{\overline{U}_{10}}{U_0} = -\frac{1}{2\overline{C}}\sum_{i=1}^N C_i^2 = -\frac{|\partial\Omega|}{4\pi\varepsilon DR\overline{K}}\sum_{i=1}^N K_i^2 + \mathcal{O}(\varepsilon^2)\,. \tag{4.38}$$

To estimate $\overline{U}_{11}/U_0$ in (4.29), we first use $E_i \sim C_i^2 e_i$ from (3.23) to obtain to leading order that

$$\frac{\overline{E}}{\overline{C}} = \frac{|\partial\Omega|}{2\pi\varepsilon RD\overline{K}}\sum_{i=1}^N e_i K_i^2 + \mathcal{O}(\varepsilon^2)\,. \tag{4.39}$$

In this way, we obtain in terms of $\mathbf{K} = (K_1, \dots, K_N)^T$ that

$$\frac{\overline{U}_{11}}{U_0} = \frac{|\partial\Omega|}{2\pi\varepsilon RD\overline{K}}\left(2\pi(\mathbf{K}^T\mathcal{G}_s\mathbf{K}) + \sum_{i=1}^N e_i K_i^2\right) + \mathcal{O}(\varepsilon^2)\,. \tag{4.40}$$

Substituting the expansions (4.37), (4.38), and (4.40) into (4.28) and (4.31), we finally obtain the following *four-term* expansion for the dimensional volume-averaged

MFRT:

$$\overline{U} \sim \frac{|\Omega|}{|\partial\Omega|}\Bigg(\underbrace{\frac{1}{\overline{K}}}_{\propto\varepsilon^{-2}} + \underbrace{\frac{\overline{\mathcal{K}}^{(2)}}{\overline{K}^2}}_{\propto\varepsilon^{-1}} + \underbrace{\log(2/\varepsilon)\frac{|\partial\Omega|(\mathbf{K}^T\mathbf{K})}{4\pi DR\overline{K}^2}}_{\propto\log(\varepsilon)} + \underbrace{\frac{[\overline{\mathcal{K}}^{(2)}]^2 - \overline{\mathcal{K}}^{(3)}\overline{K}}{\overline{K}^3}}_{\propto 1} + \underbrace{\frac{|\partial\Omega|}{2\pi RD\overline{K}^2}\left(2\pi(\mathbf{K}^T\mathcal{G}_s\mathbf{K}) + \sum_{i=1}^{N} e_i K_i^2\right)}_{\propto 1} + o(1)\Bigg). \tag{4.41}$$

This is the main result of this subsection. Several comments are in order:

(i) The first (leading-order) term in (4.41) depends only on the reactivities and surface areas of the patches. The second and the third terms, providing the contributions $\mathcal{O}(\varepsilon^{-1})$ and $\mathcal{O}(\log\varepsilon)$, also depend on the shape of the patches (via the coefficients c_{2i} and c_{3i}). Finally, the last term in (4.41) of order $\mathcal{O}(1)$ incorporates the details on the spatial arrangement of patches via the Green's matrix $\mathcal{G}_s$.

(ii) For N identical patches of a common reactivity $\mathcal{K}$ and surface area $|\partial\Omega_1|$, (4.41) reduces, with $\mathbf{e} = (1,\dots,1)^T$, to

$$\overline{U} \sim \frac{|\Omega|}{N}\left(\frac{1}{\mathcal{K}|\partial\Omega_1|} + 2\pi c_{21}\frac{L_1^3}{D|\partial\Omega_1|^2} + \frac{\log(2/\varepsilon)}{4\pi DR} + \frac{1}{2\pi RD}\left(e_1 + \frac{2\pi}{N}(\mathbf{e}^T\mathcal{G}_s\mathbf{e})\right) + \frac{2\pi\mathcal{K}L_1^6}{D^2|\partial\Omega_1|^3}\left(2\pi c_{21}^2 - c_{31}\frac{|\partial\Omega_1|}{L_1^2}\right) + o(1)\right). \tag{4.42}$$

Interestingly, the second and the third terms do not depend on the reactivity $\mathcal{K}$. One might thus naively expect that these terms remain valid even in the limit $\mathcal{K}\to\infty$. However, this is not true, as revealed by comparison of these terms with the first two terms of the expansion (4.32), which is valid for any $\mathcal{K}$. One sees that the logarithmic terms are indeed the same. However, the coefficients in front of the contribution $\mathcal{O}(\varepsilon^{-1})$ are in general different (e.g., for circular patches, the second term in (4.42) is $8/(3\pi^2 DR\varepsilon)$, whereas the first term in (4.33) is $1/(4DR\varepsilon)$). This distinction originates from the singular character of the limit $\mathcal{K}\to\infty$. In fact, the expansions (4.41) and (4.42) are based on the asymptotic behavior of $C_i(\kappa_i)$ as $\kappa_i\to 0$, which is not applicable when $\kappa_i = \infty$.

(iii) For N identical circular patches of radius $\varepsilon R = L_1$, we have $c_2 = 4/(3\pi)$ and $c_3 \approx 0.3651$ as given in (3.16). Moreover, since $E_1 \sim C_1^2/8$ as $\kappa_i\to 0$ from (3.26b), we identify from (3.23) that $e_1 = 1/8$. In this way, (4.42) yields the explicit result

$$\overline{U} \sim \frac{|\Omega|}{N\pi}\left(\frac{1}{\mathcal{K}R^2\varepsilon^2} + \frac{8}{3\pi RD\varepsilon} + \frac{1}{4DR}\log(2/\varepsilon) + \left(\frac{64}{9\pi^2} - 2c_3\right)\frac{\mathcal{K}}{D^2} + \frac{1}{2RD}\left(\frac{1}{8} + \frac{2\pi}{N}(\mathbf{e}^T\mathcal{G}_s\mathbf{e})\right) + o(1)\right). \tag{4.43}$$

First, we compare this expansion with an approximate expansion that was derived in [61] for a single circular patch by using a constant-flux approximation. Despite the approximate character of the expansion from [61], its first three terms turn out to be identical with those in our exact expansion (4.43). Secondly, the expansion (4.43) also agrees with the expansion (5.22) from [56], which was obtained for a single circular patch by a different method.

We conclude this subsection with two comments:

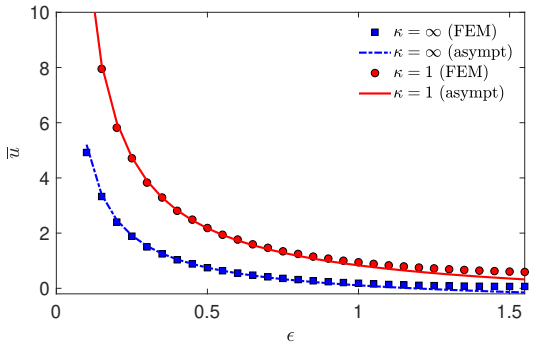

Fig. 4.1: Dimensionless volume-averaged MFRT $\overline{u}$ from (4.28) to two identical circular patches of angle ϵ (with $a_1 = a_2 = 1$), located at the north and south poles of the unit sphere, with $\kappa_1 = \kappa_2 = \infty$ (squares) or $\kappa_1 = \kappa_2 = 1$ (circles). The curves present the asymptotic formula (4.28) with $\varepsilon = 2\sin(\epsilon/2)$, whereas symbols indicate the FEM solution with the maximal meshsize $h_{\max} = 0.0025$.

(i) To leading order, the volume-averaged MFRT behaves as $\overline{U} \sim |\Omega|/(|\partial\Omega|\overline{K})$, so that the trapping effect of small patches is analogous to a parallel connection of wires, whose resistances are inversely proportional to wire cross-sectional areas $|\partial\Omega_i|$ and charge career's mobilities (here $\mathcal{K}_i$) in electrostatics. Diffusion screening between patches (i.e., their competition for diffusing particles) appears only at higher orders.

(ii) The volume-averaged MFRT scales as ε^{-2}, i.e., as the surface area of the patches, which is drastically different from the case of perfectly reactive patches, for which $\overline{U}$ scales as ε^{-1}. This crucial distinction between perfectly and partially reactive patches was emphasized in [61] (see also [58]).

4.2. Numerical Comparison. We aim at validating the asymptotic results by comparison with a numerical solution of the original PDE (2.8). Different numerical methods are available for this purpose, including a hierarchical, fast multipole method [76], spectral expansions [48], finite-element methods [31], Monte Carlo methods [100, 122]. However, most of these methods are either specifically designed for perfectly reactive patches (i.e., Dirichlet boundary condition), or limited to not-too-small partially reactive patches. For our validation purposes, we resort to a basic finite-element method (FEM) implemented in Matlab and focus on the unit sphere with two patches centered at the north and south poles. The symmetry of this setting allows one to reduce the original 3-D problem to a planar one that can be solved with less numerical efforts.

Figure 4.1 illustrates the volume-averaged MFRT $\overline{u}$ (4.28) on two identical circular patches of angle ϵ on the unit sphere (since $\varepsilon = 2\sin(\epsilon/2)$, one has $\varepsilon \approx \epsilon$ for small patches). While the asymptotic results were derived in the limit $\varepsilon \to 0$, the volume-averaged MFRT was computed numerically for a broad range of ϵ, up to $\pi/2$, when one patch covers a hemisphere, whereas two patches cover the whole sphere. Remarkably, Fig. 4.1 reveals that the asymptotic formula (4.28) remains accurate up to $\epsilon \simeq 1$, i.e., far beyond its expected range of applicability. We remark that the minor deviations at small ϵ can be attributed to the inaccuracy of the FEM solution.

4.3. Effective Reactivity in the Homogenized Limit. We now derive a scaling law that characterizes the (dimensionless) effective reactivity k_{eff} corresponding to a large number of identical circular patches, with a common radius ε and reactivity κ, that are uniformly distributed on the surface on the unit sphere. A similar analysis has been done for the case of Dirichlet patches in [31].

For this homogenized limit we define $u_{\text{eff}} = u_{\text{eff}}(|\mathbf{x}|)$ as the radially symmetric solution to

$$\Delta_{\mathbf{x}} u_{\text{eff}} = -1\,, \quad 0 \le |\mathbf{x}| < 1\,; \qquad \partial_n u_{\text{eff}} + k_{\text{eff}} u_{\text{eff}} = 0\,, \quad |\mathbf{x}| = 1\,. \tag{4.44}$$

The solution to (4.44) and the homogenized volume-averaged MFRT, defined as $\overline{u}_{\text{eff}} \equiv |\Omega|^{-1} \int_\Omega u_{\text{eff}}\, d\mathbf{x}$, are

$$u_{\text{eff}} = \frac{1}{6}\left(1 - |\mathbf{x}|^2\right) + \frac{1}{3k_{\text{eff}}} \qquad \text{and} \qquad \overline{u}_{\text{eff}} = \frac{1}{15} + \frac{1}{3k_{\text{eff}}}\,. \tag{4.45}$$

Since the reactive patches are all disks with radius ε and reactivity κ, we set $C_i = C(\kappa)$ and $E_i = E(\kappa)$ in (4.28) and (4.29) to obtain that

$$\overline{u} \sim \frac{2}{3N\varepsilon C}\left[1 + \frac{\varepsilon C}{2}\log\left(2/\varepsilon\right) + \varepsilon C\left(\frac{P}{N} + \frac{E}{C^2}\right)\right]\,, \tag{4.46}$$

where $P = P(\mathbf{x}_1, \ldots, \mathbf{x}_N) \equiv 2\pi \mathbf{e}^T \mathcal{G}_s \mathbf{e}$ with $\mathbf{e} = (1, \ldots, 1)^T$. Upon using the entries of the Green's matrix $\mathcal{G}_s$ in (4.13), as can be calculated from (3.29), we obtain that

$$P = -\frac{9N^2}{10} + N(N-1)\log 2 + 2\mathcal{H}(\mathbf{x}_1, \ldots, \mathbf{x}_N)\,, \tag{4.47}$$

where the discrete energy $\mathcal{H}$ on the unit sphere is defined by

$$\mathcal{H}(\mathbf{x}_1, \ldots, \mathbf{x}_N) = \sum_{i=1}^{N}\sum_{j=i+1}^{N}\left(\frac{1}{|\mathbf{x}_i - \mathbf{x}_j|} - \frac{1}{2}\log|\mathbf{x}_i - \mathbf{x}_j| - \frac{1}{2}\log\left(2 + |\mathbf{x}_i - \mathbf{x}_j|\right)\right)\,. \tag{4.48}$$

For our homogenized limit, we require $\overline{u} = \overline{u}_{\text{eff}}$. By using (4.45), and in terms of $\mathcal{H}$, we obtain after a little algebra that (4.46) determines k_{eff} as

$$\frac{1}{k_{\text{eff}}} \sim \frac{2}{N\varepsilon C}\left[1 + \frac{\varepsilon C}{2}\log\left(2/\varepsilon\right) + \varepsilon C\left(\frac{E}{C^2} - N + (N-1)\log 2 + \frac{2\mathcal{H}}{N}\right)\right]\,. \tag{4.49}$$

As derived formally in Appendix of [31] (see also §4 of [30]), for a large collection of uniformly distributed patches with centers at $\mathbf{x}_i$ for $i = 1, \ldots, N$, we have for $N \to \infty$ that

$$\mathcal{H} \sim \frac{N^2}{2}\left(1 - \log 2\right) + b_1 N^{3/2} + b_2 N \log N + b_3 N + \mathcal{O}\left(N^{1/2}\right)\,, \tag{4.50a}$$

with coefficients

$$b_1 = -\frac{1}{2}\,, \quad b_2 = -\frac{1}{8}\,, \quad b_3 = \frac{1}{2}\left(\log 2 - \frac{1}{4}\right)\,. \tag{4.50b}$$

To derive our scaling law for k_{eff} we substitute (4.50) into (4.49) and write the result in terms of the surface fraction of patches, defined by $f \equiv N\pi\varepsilon^2/(4\pi)$. For the dilute fraction limit $f \ll 1$, we obtain after some algebra that (4.49) reduces to

$$k_{\text{eff}} \sim \frac{2fC}{\varepsilon}\left[1 + 4b_1 C\sqrt{f} + \varepsilon C\left(\frac{E}{C^2} - \frac{1}{4} - \frac{1}{4}\log f\right)\right]^{-1}, \tag{4.51}$$

with $b_1 = -1/2$. We remark that, as shown in [87] for a related problem, the estimate $b_1 \approx -0.5523$ should be slightly better than using $b_1 = -1/2$ as it accounts for the small defects from the uniformly distributed patch assumption. Such defects will always occur when tiling on a sphere. Related homogenization results, but valid only for $\kappa = \infty$, have been derived in [31] and in [87] for the interior and exterior problems, respectively.

This main result characterizes k_{eff} in terms of both C and E, which depend on the common local reactivity κ of the patches. In particular, for $\kappa \to \infty$, we set $a_i = 1$ in (3.19a) and (3.26a) to obtain $C \sim 2/\pi$ and $E/C^2 \sim (3 - 4\log 2)/(2\pi)$, so that (4.51) becomes

$$k_{\text{eff}} \sim \frac{4f}{\pi\varepsilon}\left[1 + \frac{8b_1}{\pi}\sqrt{f} + \frac{\varepsilon}{\pi}\left(1 - \log 4 - \frac{1}{2}\log f\right)\right]^{-1}, \quad \text{for} \quad \kappa \gg 1\,. \tag{4.52}$$

Alternatively, for $\kappa \to 0$, (3.19b) and (3.26b) with $a_i = 1$ yield that $C \sim \kappa/2$ and $E \sim \kappa^2/32$ so that (4.51) becomes

$$k_{\text{eff}} \sim \frac{f\kappa}{\varepsilon}\left[1 + 2b_1\kappa\sqrt{f} - \frac{\varepsilon\kappa}{16}(1 + 2\log f)\right]^{-1}, \quad \text{for} \quad \kappa \ll 1\,. \tag{4.53}$$

In order to obtain an explicit approximation for k_{eff} valid for all $\kappa > 0$, one can use in (4.51) the heuristic approximations for C and E from §3. Upon setting $a_i = 1$, we can use $C(\kappa) \approx \mathcal{C}^{\text{app}}(\kappa)$ and $E(\kappa) \approx \mathcal{E}^{\text{app}}(\kappa)$, where the explicit functions $\mathcal{C}^{\text{app}}(\kappa)$ and $\mathcal{E}^{\text{app}}(\kappa)$ are given by (3.17) and (3.27), respectively.

Finally, we reformulate the homogenized result for the dimensional problem (2.1) in a sphere of radius R, covered by circular patches of a common radius $L \ll R$ and common dimensional reactivity $\mathcal{K}_i = \mathcal{K}$ for $i = 1, \ldots, N$. Upon recalling (2.6) and $\varepsilon = L/R$, we use (4.51) to identify that

$$\mathcal{K}_{\text{eff}} = \frac{D}{L}k_{\text{eff}} \sim \frac{2DR}{L^2}fC\left[1 + 4b_1 C\sqrt{f} + \varepsilon C\left(\frac{E}{C^2} - \frac{1}{4} - \frac{1}{4}\log f\right)\right]^{-1}, \tag{4.54}$$

where $C = C\,(L\mathcal{K}/D)$ and $E = E\,(L\mathcal{K}/D)$, and $\mathcal{K}_{\text{eff}}$ has units of length/time. This result for $\mathcal{K}_{\text{eff}}$ pertains to the low patch area fraction $f = N\,(L/R)^2/4 \ll 1$.

4.4. Laplacian Eigenvalue Problem with Reactive Patches. In this subsection, we briefly consider the following eigenvalue problem for the Robin Laplacian in the unit sphere Ω:

$$\Delta_{\mathbf{x}}\phi + \lambda\phi = 0\,, \quad \mathbf{x} \in \Omega\,; \qquad \int_\Omega \phi^2\, d\mathbf{x} = 1\,, \tag{4.55a}$$

$$\varepsilon\partial_n\phi + \kappa_i\phi = 0\,, \quad \mathbf{x} \in \partial\Omega_i^\varepsilon\,, \quad i = 1, \ldots, N\,, \tag{4.55b}$$

$$\partial_n\phi = 0\,, \quad \mathbf{x} \in \partial\Omega_r = \partial\Omega\backslash\partial\Omega_a\,. \tag{4.55c}$$

In §3 of [30], a three-term expansion for the principal (lowest) eigenvalue λ_0 of (4.55) was derived for a collection of well-separated perfectly reactive ($\kappa_i = \infty$) locally

circular patches Ω_i^ε. We now derive the corresponding result for partially reactive and arbitrary-shaped patches. Instead of repeating an inner-outer expansion analysis similar to that done for the MFRT and in §3 of [30], we derive our result primarily from an eigenfunction expansion solution of (2.8).

Labeling $\lambda_j = \lambda_j(\varepsilon)$ and $\phi_j = \phi_j(\mathbf{x};\varepsilon)$ for $j \geq 0$ to be the eigenpairs of (4.55), for which $\lambda_0 \to 0$ as $\varepsilon \to 0$ and $\lambda_j = \mathcal{O}(1)$ as $\varepsilon \to 0$, we represent the solution to (2.8) as $u = \sum_{j=0}^{\infty} \lambda_j^{-1}\phi_j \left(\int_\Omega \phi_j \, d\mathbf{x}\right)$. By calculating the average $\overline{u} \equiv |\Omega|^{-1}\int_\Omega u \, d\mathbf{x}$, we conclude that

$$\overline{u} = \frac{\left(\int_\Omega \phi_0 \, d\mathbf{x}\right)^2}{|\Omega|\lambda_0} + \sum_{j=1}^{\infty} \frac{\left(\int_\Omega \phi_j \, d\mathbf{x}\right)^2}{|\Omega|\lambda_j}\,, \tag{4.56}$$

where a three-term expansion for $\overline{u}$ was given in (4.28) of Proposition 1.

As in [30], the principal eigenvalue λ_0 and the corresponding eigenfunction ϕ_0 in the outer region have the expansion

$$\begin{aligned} \lambda_0 &= \varepsilon\lambda_{00} + \varepsilon^2 \log\left(\frac{\varepsilon}{2}\right)\lambda_{01} + \varepsilon^2\lambda_{02} + \mathcal{O}(\varepsilon^3\log\varepsilon)\,, \\ \phi_0 &= \phi_{00} + \varepsilon\phi_{01} + \varepsilon^2\log\left(\frac{\varepsilon}{2}\right)\phi_{02} + \varepsilon^2\phi_{03} + \ldots\,. \end{aligned} \tag{4.57}$$

By substituting the expansion for ϕ_0 into the normalization condition in (4.55a), collecting powers of ε, and ignoring negligible $\mathcal{O}(\varepsilon^3)$ contributions from the inner regions near the patches, we obtain that $\phi_{00} = 1/|\Omega|^{1/2}$, $\int_\Omega \phi_{01}\, d\mathbf{x} = 0$, $\int_\Omega \phi_{02}\, d\mathbf{x} = 0$, and $\int_\Omega \phi_{03}\, d\mathbf{x} \neq 0$. As a result, we estimate that

$$\left(\int_\Omega \phi_0 \, d\mathbf{x}\right)^2 \sim \left(|\Omega|^{1/2} + \mathcal{O}(\varepsilon^2)\right)^2 \sim \Omega + \mathcal{O}(\varepsilon^2)\,. \tag{4.58}$$

Next, by the orthogonality property $\int_\Omega \phi_j\phi_0 \, d\mathbf{x} = 0$ for $j \geq 1$, we use (4.57) to estimate

$$0 = \int_\Omega \phi_j\phi_0 \, d\mathbf{x} \sim \frac{1}{|\Omega|^{1/2}}\int_\Omega \phi_j \, d\mathbf{x} + \varepsilon\int_\Omega \phi_j\phi_{0j} \, d\mathbf{x}\,, \tag{4.59}$$

which yields that $\left(\int_\Omega \phi_j \, d\mathbf{x}\right)^2 = \mathcal{O}(\varepsilon^2)$ for $j \geq 1$. By using this estimate and (4.58) in (4.56), we conclude that $\overline{u} \sim \lambda_0^{-1}\left[1 + \mathcal{O}(\varepsilon^2)\right] + \mathcal{O}(\varepsilon^2)$, which yields

$$\lambda_0 \sim \frac{1 + \mathcal{O}(\varepsilon^2)}{\overline{u} - \mathcal{O}(\varepsilon^2)}\,. \tag{4.60}$$

By using the expansion (4.28) for $\overline{u}$ in (4.60) it follows that we can neglect the $\mathcal{O}(\varepsilon^2)$ terms in (4.60), so that

$$\lambda_0 \sim \frac{\varepsilon}{U_0}\left(1 + \varepsilon\log\left(\frac{\varepsilon}{2}\right)\frac{\overline{U}_{10}}{U_0} + \varepsilon\frac{\overline{U}_{11}}{U_0} + \varepsilon^2\log\varepsilon\right)^{-1}\,. \tag{4.61}$$

Then, by using $(1+y)^{-1} \sim 1 - y$, we obtain the expansion (4.57) for λ_0 in which $\lambda_{01} = 1/U_0$, $\lambda_{02} = -\overline{U}_{10}/U_0^2$ and $\lambda_{03} = -\overline{U}_{11}/U_0^2$. Finally, by using (4.29), we obtain our main result that

$$\lambda_0 \sim \frac{2\pi\varepsilon\overline{C}}{|\Omega|} + \varepsilon^2\log\left(\frac{\varepsilon}{2}\right)\frac{\pi\mathbf{C}^T\mathbf{C}}{|\Omega|} - \frac{2\pi\varepsilon^2}{|\Omega|}\left(2\pi\mathbf{C}^T\mathcal{G}_s\mathbf{C} + \overline{E}\right) + \mathcal{O}(\varepsilon^3\log\varepsilon)\,, \tag{4.62}$$

where $|\Omega| = 4\pi/3$, $\mathbf{C} = (C_1, \ldots, C_N)^T$, $\overline{C} = \sum_{i=1}^N C_i$, $\overline{E} = \sum_{i=1}^N E_i$, and $\mathcal{G}_s$ is the surface Neumann Green's matrix, which depends on the patch locations.

For the special case of perfectly reactive locally circular patches for which $C_i = 2a_i/\pi$ and $E_i = E_i(\infty)$ is given in (3.26a), we readily observe that (4.62) agrees with the result in Proposition 3.1 of [30]. For circular patches, by using our heuristic approximations in (3.17) and (3.27) for C_i and E_i, (4.62) gives an explicit three-term approximation for λ_0 over the full range $\kappa_i > 0$ of reactivities.

5. The Splitting Probability. We use the method of matched asymptotic expansions to approximate solutions to (2.10) as $\varepsilon \to 0$. Since the MFRT and splitting probability problems have a similar structure, our asymptotic analysis for (2.10) relies heavily on that done in §4.

5.1. Asymptotic Analysis. In the outer region, we expand

$$u \sim U_0 + \varepsilon U_1 + \varepsilon^2 \log\left(\frac{\varepsilon}{2}\right) U_2 + \varepsilon^2 U_3 + \cdots , \tag{5.1}$$

where U_0 is a constant to be determined and where U_k for $k \geq 1$ satisfies

$$\Delta_{\mathbf{x}} U_k = 0 , \quad \mathbf{x} \in \Omega ; \quad \partial_n U_k = 0 , \quad \mathbf{x} \in \partial\Omega \backslash \{\mathbf{x}_1, \ldots, \mathbf{x}_N\} . \tag{5.2}$$

The singularity behavior for U_k as $\mathbf{x} \to \mathbf{x}_i$ will be found by matching.

To construct the inner solution we introduce local geodesic coordinates near each $\mathbf{x}_i \in \partial\Omega$ to obtain (3.2) with $-\partial_{y_3} V + \kappa_i V = \delta_{i1}\kappa_i$ on $y_3 = 0$ and $(y_1, y_2) \in \Gamma_i$. In the inner region near the i-th Robin patch we expand the inner solution as

$$u \sim V_{0i} + \varepsilon \log\left(\frac{\varepsilon}{2}\right) V_{1i} + \varepsilon V_{i2} + \ldots . \tag{5.3}$$

Owing to the different boundary condition on the target $\partial\Omega_1^\varepsilon$, we find that V_{0i} satisfies

$$\Delta_{\mathbf{y}} V_{0i} = 0 , \quad \mathbf{y} \in \mathbb{R}^3_+ , \tag{5.4a}$$

$$-\partial_{y_3} V_{0i} + \kappa_i V_{0i} = \delta_{i1}\kappa_i , \quad y_3 = 0 , \, (y_1, y_2) \in \Gamma_i , \tag{5.4b}$$

$$\partial_{y_3} V_{0i} = 0 , \quad y_3 = 0 , \, (y_1, y_2) \notin \Gamma_i . \tag{5.4c}$$

Moreover, for $k = 1, 2$, we have that V_{ki} satisfies

$$\Delta_{\mathbf{y}} V_{ki} = \delta_{k2} \left(2y_3 V_{0i,y_3 y_3} + 2V_{0i,y_3}\right) , \quad \mathbf{y} \in \mathbb{R}^3_+ , \tag{5.5a}$$

$$-\partial_{y_3} V_{ki} + \kappa_i V_{ki} = 0 , \quad y_3 = 0 , \, (y_1, y_2) \in \Gamma_i , \tag{5.5b}$$

$$\partial_{y_3} V_{ki} = 0 , \quad y_3 = 0 , \, (y_1, y_2) \notin \Gamma_i . \tag{5.5c}$$

In terms of $w_i = w_i(\mathbf{y}; \kappa_i)$, which satisfies (3.3), the solution to (5.4) is

$$V_{0i} = U_0 + (\delta_{i1} - U_0)\, w_i , \quad \text{for} \quad i = 1, \ldots, N . \tag{5.6}$$

By using the far-field behavior (3.3d) for w_i, we have

$$V_{0i} \sim U_0 + (\delta_{i1} - U_0) \left(\frac{C_i}{|\mathbf{y}|} + \frac{\mathbf{p}_i \cdot \mathbf{y}}{|\mathbf{y}|^3} + \cdots \right) , \quad \text{as} \quad |\mathbf{y}| \to \infty .$$

The matching condition as $\mathbf{x} \to \mathbf{x}_i$ and $|\mathbf{y}| \to \infty$ is that

$$
\begin{aligned}
&U_0 + \varepsilon U_1 + \varepsilon^2 \log\left(\frac{\varepsilon}{2}\right) U_2 + \varepsilon^2 U_3 + \dots \\
&\qquad \sim U_0 + (\delta_{i1} - U_0)\left(\frac{C_i}{|\mathbf{y}|} + \frac{\mathbf{p}_i \cdot \mathbf{y}}{|\mathbf{y}|^3}\right) + \varepsilon \log\left(\frac{\varepsilon}{2}\right) V_{1i} + \varepsilon V_{2i} + \dots .
\end{aligned} \tag{5.7}
$$

Upon using $|\mathbf{y}| \sim \varepsilon^{-1}|\mathbf{x} - \mathbf{x}_i|$, (5.7) gives the singularity behavior for $U_1(\mathbf{x})$ as $\mathbf{x} \to \mathbf{x}_i$.

At order $\mathcal{O}(\varepsilon)$ in the outer expansion (5.1) we obtain that $U_1(\mathbf{x})$ satisfies

$$
\Delta_{\mathbf{x}} U_1 = 0\,, \quad \mathbf{x} \in \Omega\,; \quad \partial_n U_1 = 0\,, \quad \mathbf{x} \in \partial\Omega \backslash \{\mathbf{x}_1, \dots, \mathbf{x}_N\}\,, \tag{5.8a}
$$

$$
U_1 \sim -\frac{(U_0 - \delta_{i1})\, C_i}{|\mathbf{x} - \mathbf{x}_i|}\,, \quad \text{as} \quad \mathbf{x} \to \mathbf{x}_i \in \partial\Omega\,, \quad i = 1, \dots, N\,. \tag{5.8b}
$$

The solvability condition for (5.8) determines U_0 as

$$
U_0 = \frac{C_1}{\overline{C}}\,, \quad \text{where} \quad \overline{C} \equiv \sum_{j=1}^{N} C_j\,. \tag{5.9}
$$

In terms of the surface Neumann Green's function G_s, given in (3.29), the solution to (5.8) is

$$
U_1 = \overline{U}_1 - 2\pi \sum_{j=1}^{N} (U_0 - \delta_{j1})\, C_j G_s(\mathbf{x}; \mathbf{x}_j)\,, \quad \text{where} \quad \overline{U}_1 \equiv |\Omega|^{-1} \int_{\Omega} U_1 \, d\mathbf{x}\,. \tag{5.10}
$$

As similar to that for the MFRT problem in §4, we expand $\overline{U}_1$ as

$$
\overline{U}_1 = \overline{U}_{10} \log\left(\frac{\varepsilon}{2}\right) + \overline{U}_{11}\,, \tag{5.11}
$$

where $\overline{U}_{10}$ and $\overline{U}_{11}$ are constants independent of ε, which are to be determined.

Next, we expand U_1 in (5.10) as $\mathbf{x} \to \mathbf{x}_i$ to obtain, after some algebra, that

$$
\begin{aligned}
U_1 \sim &-(U_0 - \delta_{i1})\frac{C_i}{\varepsilon|\mathbf{y}|} + \left(\overline{U}_{10} + \frac{(U_0 - \delta_{i1})\, C_i}{2}\right) \log\left(\frac{\varepsilon}{2}\right) + \gamma_i + \overline{U}_{11} \\
&+ \frac{(U_0 - \delta_{i1})\, C_i}{2}\left(\log(y_3 + |\mathbf{y}|) - \frac{y_3(y_1^2 + y_2^2)}{|\mathbf{y}|^3}\right)\,,
\end{aligned} \tag{5.12}
$$

where γ_i is the i-th component of the vector $\boldsymbol{\gamma}$ defined by

$$
\boldsymbol{\gamma} \equiv 2\pi C_1 \mathbf{g} - 2\pi U_0 \mathcal{G}_s \mathbf{C}\,, \quad \text{where} \quad \mathbf{g} \equiv (R_s, G_{12}, \dots, G_{1N})^T\,. \tag{5.13}
$$

Here $R_s = -9/(20\pi)$, $G_{1j} = G_s(\mathbf{x}_1; \mathbf{x}_j)$, and $\mathcal{G}_s$ is the Green's matrix of (4.13).

Upon substituting (5.12) into the matching condition (5.7), we conclude that the dominant $\mathcal{O}\left(\varepsilon \log\left(\varepsilon/2\right)\right)$ terms determine the far-field behavior for the inner correction V_{1i} in (5.3). In particular, we find that V_{1i} satisfies (5.5) with $k = 1$ subject to $V_{1i} \sim \overline{U}_{10} + (U_0 - \delta_{i1})\, C_i/2$ as $|\mathbf{y}| \to \infty$. In terms of w_i, satisfying (3.3), we obtain that V_{1i} is given by

$$
V_{1i} = \left(\overline{U}_{10} + \frac{(U_0 - \delta_{i1})\, C_i}{2}\right)(1 - w_i)\,. \tag{5.14}
$$

We substitute (5.14) into the matching condition (5.7), where we use $w_i \sim C_i/|\mathbf{y}|$ as $|\mathbf{y}| \to \infty$ from (3.3d). This provides the required singularity behavior of the outer correction U_2 in (5.1). In this way, we find that U_2 satisfies

$$\Delta_{\mathbf{x}} U_2 = 0\,, \quad \mathbf{x} \in \Omega\,; \quad \partial_n U_2 = 0\,, \quad \mathbf{x} \in \partial\Omega \backslash \{\mathbf{x}_1, \ldots, \mathbf{x}_N\}\,, \tag{5.15a}$$

$$U_2 \sim -\left(\overline{U}_{10} + \frac{(U_0 - \delta_{i1})\, C_i}{2}\right) \frac{C_i}{|\mathbf{x} - \mathbf{x}_i|}\,, \quad \text{as} \quad \mathbf{x} \to \mathbf{x}_i \in \partial\Omega\,, \quad i = 1, \ldots, N\,. \tag{5.15b}$$

From the divergence theorem we find that (5.15) is solvable only when $\overline{U}_{10}$ satisfies $2\overline{U}_{10} \sum_{j=1}^N C_j = -\sum_{j=1}^N C_j^2\,(U_0 - \delta_{j1})$. Upon using (5.9) for U_0, we obtain in terms of $\mathbf{C} = (C_1, \ldots, C_N)^T$ and $\overline{C} = \sum_{j=1}^N C_j$ that

$$\frac{\overline{U}_{10}}{U_0} = -\frac{1}{2\overline{C}}\left(\mathbf{C}^T\mathbf{C} - \overline{C}C_1\right)\,. \tag{5.16}$$

Then, the solution to (5.15) is written in terms of an unknown constant $\overline{U}_2$ as

$$U_2 = \overline{U}_2 - 2\pi \sum_{j=1}^N \left(\overline{U}_{10} + \frac{(U_0 - \delta_{j1})\, C_j}{2}\right) C_j G_s(\mathbf{x}; \mathbf{x}_j)\,. \tag{5.17}$$

Next, we continue our expansion to higher order by substituting (5.12) into (5.7). We conclude that V_{2i} satisfies (5.5) with $k = 2$ subject to the far-field behavior

$$V_{2i} \sim \frac{(U_0 - \delta_{i1})\, C_i}{2}\left(\log(y_3 + |\mathbf{y}|) - \frac{y_3(y_1^2 + y_2^2)}{|\mathbf{y}|^3}\right) + \gamma_i + \overline{U}_{11}\,, \quad \text{as} \quad |\mathbf{y}| \to \infty\,. \tag{5.18}$$

Since $V_{0i} = U_0 + (\delta_{i1} - U_0)\, w_i$ from (5.6), we decompose V_{2i} as

$$V_{2i} = (U_0 - \delta_{i1})\left[\Phi_{2i} + \frac{\left(\gamma_i + \overline{U}_{11}\right)}{U_0 - \delta_{i1}}(1 - w_i)\right]\,. \tag{5.19}$$

We conclude from (5.5) with $k = 2$ and (5.18) that Φ_{2i} satisfies (4.21) of §4. As a result, the refined far-field behavior of Φ_{2i} is given by (4.22) in terms of $E_i = E_i(\kappa_i)$, which is determined by the far-field behavior of (3.20) (see also Appendix C).

To determine $\overline{U}_{11}$ we will impose a solvability condition on the problem for the outer correction U_3 in (5.1). To obtain the singularity behavior for U_3 as $\mathbf{x} \to \mathbf{x}_i$, we substitute (4.22) and $w_i \sim C_i/|\mathbf{y}|$ as $|\mathbf{y}| \to \infty$ into (5.19) to conclude that V_{2i} satisfies the refined far-field behavior

$$\begin{aligned} V_{2i} \sim \gamma_i + \overline{U}_{11} + \frac{(U_0 - \delta_{i1})\, C_i}{2}\left(\log(y_3 + |\mathbf{y}|) - \frac{y_3(y_1^2 + y_2^2)}{|\mathbf{y}|^3}\right) \\ + \frac{E_i\,(U_0 - \delta_{i1})}{|\mathbf{y}|} - \frac{\left(\gamma_i + \overline{U}_{11}\right) C_i}{|\mathbf{y}|}\,, \quad \text{as} \quad |\mathbf{y}| \to \infty\,. \end{aligned} \tag{5.20}$$

The second line in (5.20) is one of the two terms that provides the singularity behavior for U_3 in the matching condition (5.7). The other term is the dipole term given in (5.7), which is written in terms of outer variables using (A.8) of Appendix A.

In this way, upon substituting (5.20) into the matching condition (5.7), we conclude that U_3 in the outer expansion (5.1) must satisfy

$$\Delta_{\mathbf{x}} U_3 = 0\,, \quad \mathbf{x}\in\Omega\,; \quad \partial_n U_3 = 0\,, \quad \mathbf{x}\in\partial\Omega\backslash\{\mathbf{x}_1,\ldots,\mathbf{x}_N\}\,, \tag{5.21a}$$

$$U_3 \sim \frac{E_i\,(U_0-\delta_{i1})}{|\mathbf{x}-\mathbf{x}_i|} - \frac{\left(\gamma_i+\overline{U}_{11}\right)C_i}{|\mathbf{x}-\mathbf{x}_i|} + (\delta_{i1}-U_0)\,\frac{\mathbf{p}_i\cdot\mathcal{Q}_i^T(\mathbf{x}-\mathbf{x}_i)}{|\mathbf{x}-\mathbf{x}_i|^3}\,, \quad \text{as} \quad \mathbf{x}\to\mathbf{x}_i\in\partial\Omega\,, \quad i=1,\ldots,N\,. \tag{5.21b}$$

From the divergence theorem, (5.21) has a solution if and only if $\sum_{j=1}^N E_j\,(U_0-\delta_{j1}) = \sum_{j=1}^N\left(\gamma_j+\overline{U}_{11}\right)C_j$, where we observe that the contribution from the dipole term again vanishes identically. By using (5.13) for γ_i, we solve for $\overline{U}_{11}$ as

$$\overline{U}_{11}\overline{C} = U_0\sum_{j=1}^N E_j - E_1 + 2\pi U_0\mathbf{C}^T\mathcal{G}_s\mathbf{C} - 2\pi C_1\left(\mathcal{G}_s\mathbf{C}\right)_1\,,$$

which yields

$$\overline{U}_{11} = \frac{U_0\sum_{j=1}^N E_j}{\overline{C}} - \frac{E_1}{\overline{C}} + \frac{2\pi C_1}{\overline{C}}\left(\frac{\mathbf{C}^T\mathcal{G}_s\mathbf{C}}{\overline{C}} - \left(\mathcal{G}_s\mathbf{C}\right)_1\right)\,. \tag{5.22}$$

We summarize our main result for the splitting probability $u(\mathbf{x})$ and the volume-averaged splitting probability $\overline{u} = |\Omega|^{-1}\int_\Omega u(\mathbf{x})\,d\mathbf{x}$ in the small-patch limit as follows:

PROPOSITION 2. *For $\varepsilon\to 0$, the asymptotic solution to (2.10) is given in the outer region $|\mathbf{x}-\mathbf{x}_i|\gg\mathcal{O}(\varepsilon)$ for $i=1,\ldots,N$ by*

$$u(\mathbf{x}) \sim U_0\left[1+\varepsilon\log\left(\frac{\varepsilon}{2}\right)\frac{\overline{U}_{10}}{U_0} + \varepsilon\left(\frac{\overline{U}_{11}}{U_0} + 2\pi\sum_{j=1}^N\frac{(\delta_{j1}-U_0)}{U_0}C_jG_s(\mathbf{x};\mathbf{x}_j)\right)\right.$$
$$\left.+\varepsilon^2\log\left(\frac{\varepsilon}{2}\right)\left(\frac{\overline{U}_2}{U_0} + 2\pi\sum_{j=1}^N C_j\left(\frac{C_j\,(\delta_{j1}-U_0)}{2U_0} - \frac{\overline{U}_{10}}{U_0}\right)G_s(\mathbf{x};\mathbf{x}_j)\right) + \mathcal{O}(\varepsilon^2)\right]\,. \tag{5.23}$$

The volume-averaged splitting probability $\overline{u}$ satisfies

$$\overline{u} \sim U_0\left[1+\varepsilon\log\left(\frac{\varepsilon}{2}\right)\frac{\overline{U}_{10}}{U_0} + \varepsilon\frac{\overline{U}_{11}}{U_0} + \mathcal{O}\left(\varepsilon^2\log\varepsilon\right)\right]\,. \tag{5.24}$$

In (5.23) and (5.24), U_0, $\overline{U}_{10}$ and $\overline{U}_{11}$ are determined in terms of $\mathbf{C}=(C_1,\ldots,C_N)^T$, $\overline{C}=\sum_{j=1}^N C_j$, $\overline{E}=\sum_{j=1}^N E_j$, and the Green's matrix $\mathcal{G}_s$ from (4.13) by

$$U_0 = \frac{C_1}{\overline{C}}\,, \qquad \frac{\overline{U}_{10}}{U_0} = -\frac{1}{2\overline{C}}\left(\mathbf{C}^T\mathbf{C} - C_1\overline{C}\right)\,,$$
$$\frac{\overline{U}_{11}}{U_0} = \left(\frac{\overline{E}}{\overline{C}} - \frac{E_1}{C_1}\right) + 2\pi\left(\frac{\mathbf{C}^T\mathcal{G}_s\mathbf{C}}{\overline{C}} - \left(\mathcal{G}_s\mathbf{C}\right)_1\right)\,. \tag{5.25}$$

In (5.23), $\overline{U}_2$ can only be found at higher order, $C_i=C_i(\kappa_i)$ is obtained from (3.3), while $E_i=E_i(\kappa_i)$ is given by (3.22) for arbitrary-shaped patches and by (3.24) when

the patches are disks. Their asymptotic behaviors for small and large reactivities are given in Lemmas 3.1 and 3.2. When the patches are disks, heuristic approximations for C_i and E_i valid for all $\kappa_i > 0$ are given in (3.17) and (3.27).

To obtain the corresponding result in terms of dimensional variables, we use (2.6) to conclude that we need only replace $C_i = C_i\,(L\mathcal{K}_i/D)$ and $E_i = E_i\,(L\mathcal{K}_i/D)$ in (5.24) and (5.25), while evaluating the Green's matrix $\mathcal{G}_s$ at $\mathbf{x}_i = \mathbf{X}_i/R$.

We remark that in the limit $\kappa_i \to 0$ for $i = 1, \ldots, N$, it follows from Lemma 3.1 and Lemma 3.2 that $C_i \sim \kappa_i a_i^2/2$ and $E_i = \mathcal{O}(\kappa_i^2)$. In this limit, we obtain from (5.25) that $U_0 = \mathcal{O}(1)$, while both $\overline{U}_{10}/U_0$ and $\overline{U}_{11}/U_0$ are $\mathcal{O}(\kappa_i)$ as $\kappa_i \to 0$. As a result, we conclude that the asymptotic expansions in (5.23) and (5.24) remain well-ordered in ε in the limit $\kappa_i \to 0$ for $i = 1, \ldots, N$. Moreover, since

$$U_0 \approx \frac{\kappa_1 a_1^2}{\kappa_1 a_1^2 + \cdots + \kappa_N a_N^2}\,, \quad \text{for} \quad \kappa_i \ll 1\,, \quad i = 1, \ldots, N\,, \tag{5.26}$$

we observe that the leading-order splitting probability is determined by the relative reactive surface $\kappa_1 a_1^2$ of the first patch as compared to other patches. When all reactivities $\mathcal{K}_i$ are finite and fixed, one has $\kappa_i = \varepsilon \mathcal{K}_i R/D \to 0$ as $\varepsilon \to 0$, so that

$$\overline{U} \sim U_0 \approx \frac{|\partial\Omega_1|\mathcal{K}_1}{|\partial\Omega_1|\mathcal{K}_1 + \cdots + |\partial\Omega_N|\mathcal{K}_N}\,, \tag{5.27}$$

to leading order in ε. This shows that to leading-order the trapping capacity of the i-th patch is simply the product of its reactivity and surface area. We emphasize that this approximate relation is not valid if at least one reactivity is infinite (see a numerical example in the next subsection).

5.2. Numerical Example. As an example, we consider two circular patches located at the north and south poles of the unit sphere. Figure 5.1 illustrates how the volume-averaged splitting probability $\overline{u}$ depends on the reactivity $\kappa_1 = \kappa$ of the first patch, where the second patch is assumed to be perfectly reactive ($\kappa_2 = \infty$). We consider two scenarios: two patches of the same radius (i.e., $a_1 = a_2 = 1$), and two patches of different radii ($0.5 = a_2 < a_1 = 1$). In both cases, the asymptotic result (5.24) is in very close agreement with the FEM solution of the BVP (2.10) over a broad interval of reactivities, ranging from 10^{-2} to 10^2. When two patches are of the same radius, the splitting probability approaches $1/2$ in the limit $\kappa \to \infty$. Curiously, even for a weak reactivity (e.g., $\kappa = 0.1$), the first patch has a non-negligible chance of capturing the particle.

6. The Steklov-Dirichlet-Neumann (SDN) Eigenvalue Problem. Next, we analyze the SDN eigenvalue problem (2.11) in the unit sphere Ω, where we refer to $\partial\Omega_1^\varepsilon$ as the Steklov patch and to $\partial\Omega_i^\varepsilon$ for $i = 2, \ldots, N$ as Dirichlet patches. As previously, each boundary patch $\partial\Omega_i^\varepsilon$ having diameter $\mathcal{O}(\varepsilon) \ll 1$ is assumed to be simply-connected with a smooth boundary, but with an otherwise arbitrary shape and satisfies $\partial\Omega_i^\varepsilon \to \mathbf{x}_i \in \partial\Omega$. For convenience, in our analysis below we will normalize the Steklov eigenfunctions of (2.11) by

$$\int_{\partial\Omega_1^\varepsilon} u^2\, d\mathbf{s} = 1\,, \tag{6.1}$$

where the surface area element on the unit sphere in geodesic coordinates is $d\mathbf{s} = \cos(\xi_1) d\xi_1 d\xi_2$ (see Appendix A).

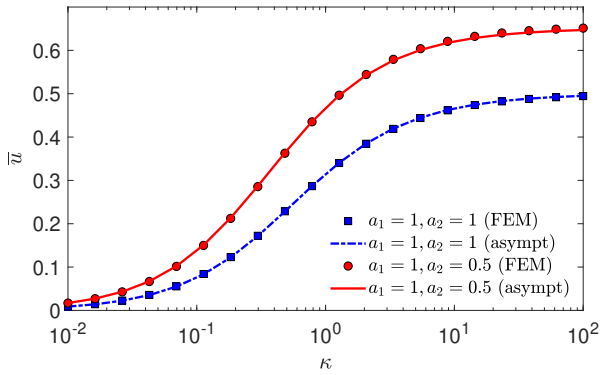

Fig. 5.1: The volume-averaged splitting probability $\overline{u}$ to the first circular patch of reactivity $\kappa_1 = \kappa$ in the presence of the second circular patch of infinite reactivity ($\kappa_2 = \infty$). Two patches are located at the north and south poles of the unit sphere. Two configurations are considered: (i) patches of equal radii ($a_1 = a_2 = 1$, $\varepsilon = 0.2$) and (ii) patches of different radii ($a_1 = 1$, $a_2 = 0.5$, $\varepsilon = 0.4$). The curves present the asymptotic formula (5.24), while the symbols indicate a FEM solution with the maximal meshsize $h_{\max} = 0.0025$.

As in §4 and §5, the dependence of the inner solution near the Steklov patch Γ_1 on the spectral parameter σ at each order in ε will rely on properties of the parameterized solution $w_1 \equiv w_1(\mathbf{y}; -\sigma)$ to the canonical problem (3.3). Here the dependences of the monopole term C_1 and the dipole term $\mathbf{p}_1$ on σ are obtained by setting $\kappa_1 = -\sigma$ in (3.3). However, the "negative reactivity" $\kappa_1 < 0$ presents the crucial difference with respect to the previously considered problems in §4 and §5. In fact, from the Steklov spectral representation (3.5), it follows that $C_1(-\sigma)$ has simple poles at the eigenvalues μ_{k1}, with $k \geq 0$, of the local Steklov eigenvalue problem (D.1), which is defined near the patch Γ_1, with nontrivial spectral weights $d_{k1} \neq 0$ (see Appendix D for details; we also recall Fig. 3.1 where the poles of C_1 were shown for a circular patch of unit radius). We label this resonant set as

$$\mathcal{P}_1 \equiv \bigcup_{k=0}^{\infty} \{\mu_{k1} \mid \text{if } d_{k1} \neq 0\} \ , \tag{6.2}$$

(i.e., this set includes only the indices k for which $d_{k1} \neq 0$). As an eigenvalue $\sigma = \sigma(\varepsilon)$ of the SDN problem (2.11) depends on ε, a small-ε expansion of $w_1(\mathbf{y}; -\sigma(\varepsilon))$ would naturally lead to $w_1(\mathbf{y}; -\sigma_0)$, where $\sigma_0 = \lim_{\varepsilon \to 0} \sigma(\varepsilon)$. However, the solution $w_1(y; -\sigma_0)$ exists only when $\sigma_0 \notin \mathcal{P}_1$. This preliminary consideration clarifies the need to distinguish between two cases in our analysis below:

(I) $\sigma_0 \notin \mathcal{P}_1$, in which case an eigenpair $\{\sigma, u\}$ is called *non-resonant*;

(II) $\sigma_0 \in \mathcal{P}_1$, in which case an eigenpair $\{\sigma, u\}$ is called *near-resonant*.

In the next subsection, we will determine the asymptotic behavior of the non-resonant SDN eigenvalues. In turn, in §6.4, we will show that near-resonant eigenvalues do not exist for the SDN problem (2.11) with a single Steklov patch. In other words, the near-resonant case is not possible for this SDN problem. In contrast, this case will re-appear in our analysis in §7 for the SN problem (2.12) with multiple Steklov patches.

Before undertaking our asymptotic analysis, we outline an important auxiliary result related to the Steklov patch. When $\sigma \notin \mathcal{P}_1$, we observe upon substituting $\kappa_1 = -\sigma$ into (3.3) and differentiating it with respect to σ that

$$w_{c1} = w_{c1}(\mathbf{y}; -\sigma) \equiv \partial_\sigma w_1(\mathbf{y}; -\sigma) \tag{6.3}$$

satisfies

$$\Delta_{\mathbf{y}} w_{c1} = 0\,, \quad \mathbf{y} \in \mathbb{R}^3_+\,, \tag{6.4a}$$

$$\partial_{y_3} w_{c1} + \sigma w_{c1} = 1 - w_1\,, \quad y_3 = 0\,,\ (y_1, y_2) \in \Gamma_1\,, \tag{6.4b}$$

$$\partial_{y_3} w_{c1} = 0\,, \quad y_3 = 0\,,\ (y_1, y_2) \notin \Gamma_1\,, \tag{6.4c}$$

$$w_{c1} \sim -\frac{C_1'(-\sigma)}{|\mathbf{y}|} - \frac{\mathbf{p}_1'(-\sigma)\cdot\mathbf{y}}{|\mathbf{y}|^3} + \cdots\,, \quad \text{as} \quad |\mathbf{y}| \to \infty\,, \tag{6.4d}$$

where we have defined

$$C_1'(-\sigma) \equiv \left(\frac{dC_1(\kappa)}{d\kappa}\right)\Big|_{\kappa=-\sigma} \qquad \text{and} \qquad \mathbf{p}_1'(-\sigma) \equiv \left(\frac{d\mathbf{p}_1(\kappa)}{d\kappa}\right)\Big|_{\kappa=-\sigma}\,. \tag{6.4e}$$

The identification of this problem satisfied by w_{c1} is key for solving the different inner problems at each order of the inner expansion near the Steklov patch Γ_1. A general spectral representation (D.11) for w_{c1} is established in Appendix D.

6.1. Asymptotic Analysis. In the outer region, we expand the solution to (2.11) away from all the patches as

$$u \sim U_0 + \varepsilon U_1 + \varepsilon^2 \log\left(\frac{\varepsilon}{2}\right) U_2 + \varepsilon^2 U_3 + \cdots\,. \tag{6.5}$$

We will initially seek a solution where $U_0 \neq 0$ is a constant. This non-zero leading-order outer solution will be used below to satisfy the normalization condition (6.1). In Remark 2 below we will briefly discuss whether one can find SDN eigenpairs for the case where $U_0 = 0$.

Upon substituting (6.5) into (2.11) and (6.1) we obtain that U_j for $j = 1, 2, 3$ satisfies the outer problems

$$\Delta_{\mathbf{x}} U_j = 0\,, \quad \mathbf{x} \in \Omega\,; \qquad \partial_n U_j = 0\,, \quad \mathbf{x} \in \partial\Omega \backslash \{\mathbf{x}_1, \ldots, \mathbf{x}_N\}\,. \tag{6.6}$$

Our analysis below provides singularity behaviors for each U_j as $\mathbf{x} \to \mathbf{x}_i$.

The novel feature of our analysis of (2.11) is that each Steklov eigenvalue $\sigma = \sigma(\varepsilon)$ must be expanded as

$$\sigma = \sigma(\varepsilon) = \sigma_0 + \varepsilon \log\left(\frac{\varepsilon}{2}\right) \sigma_1 + \varepsilon \sigma_2 + \ldots\,. \tag{6.7}$$

The coefficients σ_j for $j = 0, 1, 2$, which are independent of ε, will be determined below by ensuring that the outer problems are solvable at each order. We emphasize that by using (6.7) in (2.11b) we will obtain distinct boundary conditions on the Steklov patch at each order of the inner expansion.

In the inner region near the i-th patch we introduce the local geodesic coordinates (3.1) and expand each inner solution as

$$u \sim V_{0i} + \varepsilon \log\left(\frac{\varepsilon}{2}\right) V_{1i} + \varepsilon V_{i2} + \ldots\,. \tag{6.8}$$

For each Dirichlet patch with $i = 2, \ldots, N$, we readily obtain that V_{ji} for $j = 0, 1, 2$ satisfies

$$\Delta_{\mathbf{y}} V_{ji} = \delta_{j2} \left(2y_3 V_{0i,y_3y_3} + 2V_{0i,y_3} \right) , \quad \mathbf{y} \in \mathbb{R}^3_+ , \tag{6.9a}$$

$$V_{ji} = 0 , \quad y_3 = 0 , \, (y_1, y_2) \in \Gamma_i , \tag{6.9b}$$

$$\partial_{y_3} V_{ji} = 0 , \quad y_3 = 0 , \, (y_1, y_2) \notin \Gamma_i , \tag{6.9c}$$

where $\delta_{22} = 1$, $\delta_{j2} = 0$ if $j = 0, 1$, and $\Gamma_i \asymp \varepsilon^{-1} \partial\Omega_i^\varepsilon$. In contrast, on the re-scaled Steklov patch $\Gamma_1 \asymp \varepsilon^{-1} \partial\Omega_1^\varepsilon$, we obtain that V_{j1} for $j = 0, 1, 2$ satisfies

$$\Delta_{\mathbf{y}} V_{j1} = \delta_{j2} \left(2y_3 V_{01,y_3y_3} + 2V_{01,y_3} \right) , \quad \mathbf{y} \in \mathbb{R}^3_+ , \tag{6.10a}$$

$$\partial_{y_3} V_{j1} + \sigma_0 V_{j1} = -(1 - \delta_{j0}) \sigma_j V_{01} , \quad y_3 = 0 , \, (y_1, y_2) \in \Gamma_1 , \tag{6.10b}$$

$$\partial_{y_3} V_{j1} = 0 , \quad y_3 = 0 , \, (y_1, y_2) \notin \Gamma_1 . \tag{6.10c}$$

Since the leading-order matching condition between inner and outer solutions is that $V_{0i} \sim U_0$ as $|\mathbf{y}| \to \infty$, the leading-order inner solution, obtained from (6.9) and (6.10), is

$$V_{0i} = U_0 \left(1 - w_{0i} \right) . \tag{6.11}$$

In (6.11), $w_{0i}(\mathbf{y})$ is defined in terms of the solution $w_i(\mathbf{y}; \kappa_i)$ to (3.3) by

$$w_{0i}(\mathbf{y}) \equiv \begin{cases} w_1 \left(\mathbf{y}; -\sigma_0 \right) , & i = 1, \\ w_i(\mathbf{y}; \infty) , & i = 2, \ldots, N. \end{cases} \tag{6.12}$$

Our assumption $\sigma_0 \notin \mathcal{P}_1$ implies that $C_1(-\sigma_0)$ and $w_1(\mathbf{y}; -\sigma_0)$ are well-defined.

Upon using (3.3d) to obtain the far-field behavior for w_{0i}, we match the inner and outer expansions to conclude that the outer correction U_1 in (6.5) satisfies

$$\Delta_{\mathbf{x}} U_1 = 0 , \quad \mathbf{x} \in \Omega ; \qquad \partial_n U_1 = 0 , \quad \mathbf{x} \in \partial\Omega \backslash \{ \mathbf{x}_1, \ldots, \mathbf{x}_N \} , \tag{6.13a}$$

$$U_1 \sim - \frac{C_1 \left(-\sigma_0 \right) U_0}{|\mathbf{x} - \mathbf{x}_1|} , \quad \text{as} \quad \mathbf{x} \to \mathbf{x}_1 \in \partial\Omega , \tag{6.13b}$$

$$U_1 \sim - \frac{C_i(\infty) U_0}{|\mathbf{x} - \mathbf{x}_i|} , \quad \text{as} \quad \mathbf{x} \to \mathbf{x}_i \in \partial\Omega , \quad i = 2, \ldots, N . \tag{6.13c}$$

The solvability condition for (6.13), together with the assumption that $U_0 \neq 0$, provides the following nonlinear algebraic equation for the leading-order term σ_0 in the expansion (6.7) of a Steklov eigenvalue:

$$C_1 \left(-\sigma_0 \right) = \mathcal{N} \equiv - \sum_{i=2}^{N} C_i(\infty) . \tag{6.14}$$

Since $C_i(\infty) > 0$, we conclude that $\mathcal{N} < 0$. The spectral expansion (3.5) ensures that, for any $\mathcal{N} < 0$, (6.14) has infinitely many solutions that we denote as $\sigma_0^{(k)}$, with $k = 0, 1, \ldots$. Moreover, since $C_1(-\sigma_0)$ decreases monotonically in σ_0 between its poles in $\mathcal{P}_1$, each solution $\sigma_0^{(k)}$ is simple and lies between two consecutive poles. In our analysis below, we will determine the next-order corrections $\sigma_1^{(k)}$ and $\sigma_2^{(k)}$ to the dominant contribution $\sigma_0^{(k)}$. As our asymptotic analysis is applicable to any k, we omit the superscript $^{(k)}$ for brevity.

With σ_0 determined by (6.14), the solution to (6.13) is represented in terms of an unknown constant $\overline{U}_1$ as

(6.15)
$$U_1(\mathbf{x}) = \overline{U}_1 - 2\pi U_0 \sum_{j=1}^{N} C_j G_s(\mathbf{x};\mathbf{x}_j)\,, \quad \text{where} \quad C_j \equiv \begin{cases} C_1(-\sigma_0)\,, & j=1 \\ C_j(\infty)\,, & j=2,\ldots,N\,. \end{cases}$$

Here G_s is the surface Neumann Green's function for the sphere given in (3.29).

To proceed to higher order, we expand $U_1(\mathbf{x})$ in (6.15) as $\mathbf{x}\to\mathbf{x}_i$ to obtain in terms of local geodesic coordinates that

$$U_1 \sim -\frac{C_i U_0}{|\mathbf{y}|} + \frac{U_0 C_i}{2}\log\left(\frac{\varepsilon}{2}\right) + \frac{U_0 C_i}{2}\left(\log(y_3+|\mathbf{y}|) - \frac{y_3(y_1^2+y_2^2)}{|\mathbf{y}|^3}\right) + U_0\beta_i + \overline{U}_1\,, \tag{6.16}$$

where β_i is the i-th component of the vector $\boldsymbol{\beta}$ defined by

$$\boldsymbol{\beta} \equiv -2\pi\mathcal{G}_s\mathbf{C}\,, \qquad \text{where} \qquad \mathbf{C} = (C_1,\ldots,C_N)^T\,. \tag{6.17}$$

Here C_i for $i=1,\ldots,N$ is defined in (6.15) and $\mathcal{G}_s$ is the Green's matrix in (4.13).

Upon matching the inner and outer expansions for the $\varepsilon\log(\varepsilon/2)$ terms, we conclude that the inner correction V_{1i} in (6.8) must satisfy $V_{1i}\sim U_0C_i/2$ as $|\mathbf{y}|\to\infty$. As a result, we seek a solution to (6.9) and (6.10) for $k=1$ in the form

$$V_{1i} = \frac{U_0 C_i}{2}\left(1 - w_{1i}\right)\,, \quad \text{for} \quad i=1,\ldots,N\,. \tag{6.18}$$

By using the problem (6.4) satisfied by $w_{c1}(\mathbf{y};-\sigma_0)$ to account for the inhomogeneous term in (6.10b) on the Steklov patch, we use superposition to get that

$$V_{1i} = \frac{U_0 C_i(\infty)}{2}\left(1 - w_i(\mathbf{y};\infty)\right)\,, \quad i=2,\ldots,N\,, \tag{6.19a}$$

$$V_{11} = -U_0\sigma_1 w_{c1}(\mathbf{y};-\sigma_0) + \frac{U_0 C_1(-\sigma_0)}{2}\left(1 - w_1(\mathbf{y};-\sigma_0)\right)\,. \tag{6.19b}$$

Then, by using the far-field behaviors in (3.3d) and (6.4d), we find for $|\mathbf{y}|\to\infty$ that

$$V_{1i} \sim \frac{U_0 C_i(\infty)}{2}\left(1 - \frac{C_i(\infty)}{|\mathbf{y}|}\right) + \cdots\,, \quad i=2,\ldots,N\,, \tag{6.20a}$$

$$V_{11} \sim U_0\sigma_1\frac{C_1'(-\sigma_0)}{|\mathbf{y}|} + \frac{U_0 C_1(-\sigma_0)}{2}\left(1 - \frac{C_1(-\sigma_0)}{|\mathbf{y}|}\right) + \cdots\,, \tag{6.20b}$$

where the neglected higher-order terms are dipole contributions.

Upon matching the monopole terms in the far-field behavior (6.20) to the outer correction U_2 in (6.5), we obtain from (6.6) that U_2 satisfies

$$\Delta_{\mathbf{x}} U_2 = 0\,, \quad \mathbf{x}\in\Omega\,; \qquad \partial_n U_2 = 0\,, \quad \mathbf{x}\in\partial\Omega\backslash\{\mathbf{x}_1,\ldots,\mathbf{x}_N\}\,, \tag{6.21a}$$

(6.21b)
$$U_2 \sim -\frac{U_0}{2}\frac{C_i^2}{|\mathbf{x}-\mathbf{x}_i|} + U_0\sigma_1\delta_{i1}\frac{C_1'(-\sigma_0)}{|\mathbf{x}-\mathbf{x}_i|}\,, \quad \text{as} \quad \mathbf{x}\to\mathbf{x}_i\in\partial\Omega\,, \quad i=1,\ldots,N\,,$$

where C_i for $i = 1, \ldots, N$ is defined in (6.15) and $\delta_{i1} = 1$ if $i = 1$ and $\delta_{i1} = 0$ for $i = 2, \ldots, N$. The solvability condition for (6.21) yields $U_0 \sum_{i=1}^{N} C_i^2 = 2U_0\sigma_1 C_1'(-\sigma_0)$. For $U_0 \neq 0$, this expression determines the coefficient σ_1 in (6.7) as

$$\sigma_1 = \frac{1}{2C_1'(-\sigma_0)} \left([C_1(-\sigma_0)]^2 + \sum_{i=2}^{N} [C_i(\infty)]^2 \right), \tag{6.22}$$

where σ_0 is a root of (6.14). Upon using (6.14) directly in (6.22), we can write σ_1 equivalently as

$$\sigma_1 = \frac{1}{2C_1'(-\sigma_0)} \left(\left[\sum_{i=2}^{N} C_i(\infty) \right]^2 + \sum_{i=2}^{N} [C_i(\infty)]^2 \right). \tag{6.23}$$

From (3.7) we recall that $C_1(\kappa)$ increases monotonically in κ between its poles so that $C_1'(\kappa)$, evaluated at $\kappa = -\sigma_0$, is strictly positive. As a result, the denominator in (6.23) never vanishes, and σ_1 is well-defined and strictly positive. Then, the solution to (6.21) is represented in terms of an unknown constant $\overline{U}_2$ as

$$U_2(\mathbf{x}) = \overline{U}_2 - 2\pi U_0 \sum_{j=1}^{N} \left(\frac{C_j^2}{2} - \sigma_1 C_1'(-\sigma_0)\delta_{j1} \right) G_s(\mathbf{x}; \mathbf{x}_j). \tag{6.24}$$

Finally, we calculate the eigenvalue correction σ_2 in (6.7). To do so, we observe from the matching condition between inner and outer solutions that the $\mathcal{O}(1)$ terms in (6.16) provide the following far-field behavior for the inner correction V_{2i} in (6.8):

$$V_{2i} \sim \frac{U_0 C_i}{2} \left(\log(y_3 + |\mathbf{y}|) - \frac{y_3(y_1^2 + y_2^2)}{|\mathbf{y}|^3} \right) + U_0\beta_i + \overline{U}_1, \quad \text{as} \quad |\mathbf{y}| \to \infty. \tag{6.25}$$

For the Dirichlet patches, and as similar to the analysis for the MFRT and splitting probability problems, the solution to (6.9) with $k = 2$ subject to (6.25) is

$$V_{2i} = U_0\Phi_{2i} + \left(U_0\beta_i + \overline{U}_1\right)(1 - w_i(\mathbf{y}; \infty)), \quad \text{for} \quad i = 2, \ldots, N, \tag{6.26}$$

where Φ_{2i} satisfies (4.21) with $\kappa_i = \infty$ so that $\Phi_{2i} = 0$ on Γ_i. As a result, by using (4.22) for the far-field behavior of Φ_{2i}, we conclude for $i = 2, \ldots, N$ that V_{2i} has the refined far-field behavior

$$\begin{aligned} V_{2i} \sim U_0\beta_i + \overline{U}_1 + \frac{U_0 C_i(\infty)}{2} \left(\log(y_3 + |\mathbf{y}|) - \frac{y_3(y_1^2 + y_2^2)}{|\mathbf{y}|^3} \right) \\ + \left[E_i(\infty) - \left(\beta_i + \frac{\overline{U}_1}{U_0} \right) C_i(\infty) \right] \frac{U_0}{|\mathbf{y}|}, \quad \text{as} \quad |\mathbf{y}| \to \infty. \end{aligned} \tag{6.27}$$

For an arbitrarily-shaped patch, $E_i(\infty)$ is obtained by setting $\kappa_i = \infty$ in (3.22), while for a locally circular patch it is given in (3.24) of Lemma 3.2. The second line in (6.27) is one of the two terms that needs to be accounted for by the outer correction U_3 in the matching condition. The other term is the dipole contribution from (3.3d) and (6.11).

In contrast, for the Steklov patch, we use superposition to determine that the solution to (6.10) with $k = 2$ subject to (6.25) is

$$V_{21} = U_0\Phi_{21} + \left(U_0\beta_1 + \overline{U}_1\right)(1 - w_1(\mathbf{y}; -\sigma_0)) - U_0\sigma_2 w_{c1}(\mathbf{y}; -\sigma_0), \tag{6.28}$$

where Φ_{21} satisfies (4.21) in which we set $\kappa_1 = -\sigma_0$ and $C_1 = C_1(-\sigma_0)$. As a result, the refined far-field behavior of V_{21} is

(6.29)
$$V_{21} \sim U_0\beta_1 + \overline{U}_1 + \frac{U_0 C_1(-\sigma_0)}{2}\left(\log(y_3+|\mathbf{y}|) - \frac{y_3(y_1^2+y_2^2)}{|\mathbf{y}|^3}\right) + \left[E_1(-\sigma_0) - \left(\beta_1 + \frac{\overline{U}_1}{U_0}\right)C_1(-\sigma_0) + \sigma_2 C_1'(-\sigma_0)\right]\frac{U_0}{|\mathbf{y}|}, \quad \text{as} \quad |\mathbf{y}|\to\infty\,.$$

Here $E_1(-\sigma_0)$ is calculated by setting $\kappa_i = -\sigma_0$ in (3.22).

The monopole terms in the far-field behaviors (6.29) and (6.27) together with the dipole terms from the leading order inner solutions V_{0i} in (6.11) provide the required singularity behavior for the outer correction U_3 in (6.5). In this way, we obtain from (6.6) that U_3 satisfies

$$\begin{aligned} &\Delta_{\mathbf{x}} U_3 = 0\,, \quad \mathbf{x}\in\Omega\,; \qquad \partial_n U_3 = 0\,, \quad \mathbf{x}\in\partial\Omega\backslash\{\mathbf{x}_1,\ldots,\mathbf{x}_N\}\,,\\ &U_3 \sim \left[E_i - \left(\beta_i + \frac{\overline{U}_1}{U_0}\right)C_i + \sigma_2 C_1'(-\sigma_0)\delta_{i1}\right]\frac{U_0}{|\mathbf{x}-\mathbf{x}_i|}\\ &\qquad - U_0\frac{\mathbf{p}_i\cdot\mathcal{Q}_i^T(\mathbf{x}-\mathbf{x}_i)}{|\mathbf{x}-\mathbf{x}_i|^3}\,, \quad \text{as} \quad \mathbf{x}\to\mathbf{x}_i\in\partial\Omega\,, \quad i=1,\ldots,N\,, \end{aligned} \tag{6.30}$$

where the orthogonal matrix $\mathcal{Q}_i$ is defined in (A.8) in terms of the basis vectors of the geodesic coordinate system. In (6.30) we have defined E_i and $\mathbf{p}_i$ for $i = 1,\ldots,N$ by

$$E_i \equiv \begin{cases} E_1(-\sigma_0)\,, & i=1,\\ E_i(\infty)\,, & i=2,\ldots,N\,, \end{cases} \qquad \mathbf{p}_i \equiv \begin{cases} \mathbf{p}_1(-\sigma_0)\,, & i=1,\\ \mathbf{p}_i(\infty)\,, & i=2,\ldots,N. \end{cases} \tag{6.31}$$

Here both $\mathbf{p}_i(\infty)$ and $\mathbf{p}_i(-\sigma_0)$ are defined by (3.3d).

In deriving the solvability condition for (6.30), we observe that the dipole terms again do not contribute and we obtain

$$U_0\sum_{i=1}^N E_i - U_0\sum_{i=1}^N \beta_i C_i - \overline{U}_1\sum_{i=1}^N C_i + U_0\sigma_2 C_1'(-\sigma_0) = 0\,, \tag{6.32}$$

where $\sum_{i=1}^N C_i = 0$ from the leading-order result (6.14) for σ_0. As a result, (6.32) shows that σ_2 is independent of the constant $\overline{U}_1$. This term is determined by a higher-order evaluation of the normalization condition for the Steklov eigenfunction.

Then, by using (6.17) for β_i, we solve (6.32) to determine σ_2 as

$$\sigma_2 = -\frac{1}{C_1'(-\sigma_0)}\left[2\pi\mathbf{C}^T\mathcal{G}_s\mathbf{C} + \sum_{i=1}^N E_i\right], \quad \text{where} \quad \mathbf{C}\equiv(C_1,\ldots,C_N)^T\,, \tag{6.33}$$

where $\mathcal{G}_s$ is the Green's matrix in (4.13). Through this Green's matrix, it follows that σ_2 depends on the spatial configuration of the Steklov and Dirichlet patches. We summarize our result as follows:

PROPOSITION 3. *For $\varepsilon\to 0$, there are eigenvalues $\sigma = \sigma(\varepsilon)$ of the Steklov-Dirichlet-Neumann problem (2.11) that have the three-term asymptotics*

$$\sigma = \sigma_0 + \varepsilon\log\left(\frac{\varepsilon}{2}\right)\sigma_1 + \varepsilon\sigma_2 + \mathcal{O}(\varepsilon^2\log\varepsilon)\,, \tag{6.34a}$$

where σ_0, σ_1 and σ_2 are respectively given by (6.14), (6.23) and (6.33). The corresponding eigenfunctions, restricted to Γ_1, have the three-term asymptotics

$$u|_{\Gamma_1} = V_{01} + \varepsilon \log\left(\frac{\varepsilon}{2}\right) V_{11} + \varepsilon V_{21} + \mathcal{O}(\varepsilon^2 \log \varepsilon)\,, \tag{6.34b}$$

where V_{01}, V_{11} and V_{21} are respectively given by (6.11), (6.19b) and (6.28). Here $u|_{\Gamma_1}$ is given up to normalization constants $U_0 \neq 0$ and $\overline{U}_1$ for the eigenfunction, while its spatial behavior is determined by the functions $w_1(\mathbf{y}; -\sigma_0)$ and $w_{c1}(\mathbf{y}; -\sigma_0)$, which admit the spectral expansions (D.9) and (D.11), respectively. For a circular patch, these expansions allow for their efficient numerical computation (see Appendix D).

We emphasize that with our assumption $U_0 \neq 0$, the Steklov eigenfunction is not solely concentrated on the Steklov patch. Instead it has a long-range extension into the outer region as a result of the presence of the other small Dirichlet patches. To determine U_0 we substitute $u \sim V_{01} = U_0\,(1 - w_1(\mathbf{y}; -\sigma_0))$ into the normalization condition (6.1). Upon using $d\mathbf{s} = \cos(\xi_1) d\xi_1 d\xi_2 = \varepsilon^2 \cos(\varepsilon\xi_1) dy_1 dy_2 \sim \varepsilon^2 dy_1 dy_2$, we calculate that

$$U_0 \sim \varepsilon^{-1} \left[\int_{\Gamma_1} \left[1 - w_1(\mathbf{y}; -\sigma_0)\right]^2 d\mathbf{y} \right]^{-1/2}\,. \tag{6.35}$$

REMARK 1. *Proposition 3 offers a straightforward numerical procedure to construct three-term asymptotic expansions of the SDN eigenpairs in the small patch limit when $U_0 \neq 0$. Moreover, since (6.14) has infinitely many solutions, one can construct SDN eigenvalues on any desired, but large enough, interval $(\sigma_{\min}, \sigma_{\max})$. To characterize the associated eigenfunctions on the Steklov patch Γ_1, we use $V_{01} = U_0\,[1 - w_1(y; -\sigma_0)]$ to leading order, together with the divergence theorem applied to the problem (3.3) for w_1, to obtain for $U_0 \neq 0$ that*

$$C_1(-\sigma_0) = -\frac{\sigma_0}{2\pi} \int_{\Gamma_1} (1 - w_1)\, dy_1 dy_2 = -\frac{\sigma_0}{2\pi U_0} \int_{\Gamma_1} V_{01}\, dy_1 dy_2\,. \tag{6.36}$$

Since we must have $C_1(-\sigma_0) \neq 0$ from (6.14), we conclude that to leading order all non-resonant SDN eigenfunctions in Proposition 3 are such that $\int_{\Gamma_1} V_{01}\, dy_1 dy_2 \neq 0$. For a circular patch Γ_1, this implies that these SDN eigenfunctions must be axially symmetric on the patch.

REMARK 2. *If we remove our requirement that $U_0 \neq 0$, so that the bulk solution is now asymptotically small, we can construct an SDN eigenpair where the Dirichlet patches now have only a very weak influence on the SDN eigenvalue. In this situation, the SDN eigenfunction is concentrated on the Steklov patch, and to leading-order is unaffected by the presence of the Dirichlet patches, as if they were absent. The asymptotic behavior for a single circular Steklov patch was studied in [56]. For an arbitrary patch, to construct such a solution, we let $\mu_{k1}^N > 0$ and Ψ_{k1}^N for $k \geq 1$ be the eigenpairs of the local Steklov problem (D.30) near Γ_1 that satisfies, up to a normalization condition, the local boundary value problem*

$$\Delta_{\mathbf{y}} \Psi_{k1}^N = 0\,, \quad \mathbf{y} \in \mathbb{R}^3_+\,, \tag{6.37a}$$

$$\partial_{y_3} \Psi_{k1}^N + \mu_{k1}^N \Psi_{k1}^N = 0\,, \quad y_3 = 0\,,\ (y_1, y_2) \in \Gamma_1\,, \tag{6.37b}$$

$$\partial_{y_3} \Psi_{k1}^N = 0\,, \quad y_3 = 0\,,\ (y_1, y_2) \notin \Gamma_1\,, \tag{6.37c}$$

$$\Psi_{k1}^N(\mathbf{y}) \sim \mathcal{O}(|\mathbf{y}|^{-2})\,, \quad \textit{as} \quad |\mathbf{y}| \to \infty\,, \tag{6.37d}$$

where there is no monopole behavior in the far-field (6.37d). Then, a leading-order SDN eigenpair for (2.11) is obtained by taking $\sigma_0 = \mu_{k1}^N$ *for some index* $k \geq 1$*, and by choosing* $V_{01} = \Psi_{k1}^N$ *as the leading-order inner solution near the Steklov patch* Γ_1*, and* $V_{0i} = 0$ *as the leading-order inner solution near the Dirichlet patches* Γ_i *for* $i = 2, \ldots, N$*. Owing to the fast-decay (6.37d), the outer (bulk) solution away from the patches is* $\mathcal{O}(\varepsilon^2)$ *smaller than that of the SDN eigenfunction evaluated on the Steklov patch. For this leading-order construction, we find by applying the divergence theorem to (6.37) that* $\int_{\Gamma_1} V_{01}\, dy_1 dy_2 = 0$*. As a result, when* Γ_1 *is a circular patch, all of the non-axially symmetric eigenfunctions on the patch will satisfy this condition. It is an open problem to asymptotically construct a higher-order approximation for these SDN eigenpairs.*

6.2. Example of Identical Circular Dirichlet Patches. Our main result can be simplified considerably for the special case of $N-1$ identical locally circular Dirichlet patches $\partial\Omega_i^\varepsilon$, each of radius εa (i.e., $a_i = a$ for $i = 2, \ldots, N$). For this situation, we have $C_i(\infty) = 2a/\pi$ for $i = 2, \ldots, N$, so that from (6.14) σ_0 is a root of the nonlinear algebraic equation

$$C_1(-\sigma_0) = -\frac{2a(N-1)}{\pi}\,. \tag{6.38}$$

In addition, we reduce the expression (6.23) for σ_1 to

$$\sigma_1 = \frac{2a^2}{\pi^2 C_1'(-\sigma_0)} N(N-1)\,. \tag{6.39}$$

Moreover, we can use (6.38) together with (3.26a) for $E_i(\infty)$, so that to determine σ_2 in (6.33) we need only set

$$\mathbf{C} = \frac{2a}{\pi}\,(1-N, 1, \ldots, 1)^T\;; \quad E_i = -\frac{2a^2}{\pi^2}\left(\log a + \log 4 - \frac{3}{2}\right), \quad i = 2, \ldots, N\,. \tag{6.40}$$

In this way, the numerical evaluation of the three-term expansion for σ in (6.34a) only involves first solving the root-finding problem (6.38) for σ_0 and then calculating $E_1(-\sigma_0)$ and $C_1'(-\sigma_0)$ numerically. To calculate $E_1(-\sigma_0)$ for a circular Steklov patch, we use the decomposition (E.1) of Appendix E together with the numerical results shown in Fig. E.2.

To qualitatively illustrate our theory, we consider a Steklov patch of arbitrary shape and examine the limit $a \to 0$ with a fixed N. In this limit, the right-hand side of (6.38) vanishes, and σ_0 is determined by solving $C_1(-\sigma_0) = 0$. These solutions correspond to the eigenvalues μ_{k1}^N of another *local* exterior Steklov problem defined by (D.30) of Appendix D.4 near the Steklov patch Γ_1, with a Neumann-like boundary condition (D.30d) at infinity (see [56] for details; in particular, Table 1 from [56] reports μ_{ki}^N for a circular Steklov patch). Indeed, as the Dirichlet patches vanish, one recovers the conventional Steklov problem with a single Steklov patch (see Remark 2.) In particular, the principal eigenvalue $\sigma^{(0)}$ of the SDN problem should approach 0 for a Steklov patch of arbitrary shape. Substituting the asymptotic relation (3.11) into the left-hand side of (6.38), we obtain to leading-order in a and ε that

$$\sigma^{(0)} \approx \sigma_0^{(0)} \approx \frac{4a(N-1)}{|\Gamma_1|}\,, \quad \text{as} \quad a \to 0\,. \tag{6.41}$$

ε	$h_{\max}$	0.01	0.005	0.0025	0.002	asympt.
0.1	$\sigma^{(0)}$	0.5902	0.5719	0.5636	0.5620	0.5561
	$\sigma^{(1)}$	4.617	4.315	4.215	4.198	4.146
	$\sigma^{(2)}$	8.887	7.818	7.512	7.467	7.338
0.2	$\sigma^{(0)}$	0.5540	0.5460	0.5422	0.5414	0.5286
	$\sigma^{(1)}$	4.252	4.156	4.120	4.112	4.088
	$\sigma^{(2)}$	7.722	7.440	7.346	7.330	7.282

Table 6.1: The first three SDN eigenvalues (that correspond to axially symmetric eigenfunctions) for the unit sphere with two circular patches of radius ε (with $a_1 = a_2 = 1$), located at the north and south poles. Columns 3-6 present the numerical results by FEM with different maximal meshsizes $h_{\max}$. The last column indicates the three-term asymptotic relation (6.34a), which is seen to compare very favorably with the numerical result on the most refined mesh.

6.3. Numerical Comparison. A numerical solution of the SDN spectral problem was obtained via a finite-element method (FEM) described in [24, 57]. For an accurate computation, one needs to ensure that a tetrahedral mesh of the domain is sufficiently refined near small patches, which requires a numerical diagonalization of very large matrices. To avoid these technical issues, we restrict our analysis to two circular patches ($N = 2$), located at the north and south poles. The axial symmetry of this setting reduces the original three-dimensional setting to a planar one. Since our analysis leading to Proposition 3 does not access the asymptotic behavior of non-axially-symmetric eigenfunctions (see Remarks 1 and 2), we restrict the numerical comparison exclusively to the eigenvalues that correspond to axially symmetric eigenfunctions.

Table 6.1 illustrates the accuracy of the three-term asymptotic formula (6.34a) by comparing its predictions (last column) to FEM solutions with different maximal meshsizes $h_{\max}$, with smaller meshsizes yielding more accurate solutions. Even though the obtained numerical values of $\sigma^{(k)}$ did not fully converge to the true eigenvalues, further refinement of the mesh yielded matrices that are too large to be treated on our laptop. Nevertheless, the numerical values reported in the 6th column are very close to the predictions from our three-term asymptotic formula given in the last column. This example serves as a numerical validation of the asymptotic formula (6.34a). Further analysis of the SDN problem and its applications will be reported elsewhere.

6.4. Near-Resonant Case. Next, we inspect whether there may exist a near-resonant SDN eigepair for the spectral problem (2.12) for which the limiting value $\sigma_0 = \lim_{\varepsilon\to 0} \sigma(\varepsilon)$ belongs to $\mathcal{P}_1$ (see (6.2)). More specifically, let us assume that there exists an index $k' \geq 0$ such that $\sigma_0 = \mu_{k'1}$ for some *simple* eigenvalue $\mu_{k'1}$ of the local Steklov eigenvalue problem (D.1) of Appendix D for which $d_{k'1} \neq 0$ (see also Remark 3 below). We normalize the corresponding local Steklov eigenfunction $\tilde{\Psi}_{k'1}$ to be the

unique solution of

$$\Delta_{\mathbf{y}}\tilde{\Psi}_{k'1} = 0\,, \quad \mathbf{y} \in \mathbb{R}^3_+\,, \tag{6.42a}$$

$$\partial_{y_3}\tilde{\Psi}_{k'1} + \sigma_0\tilde{\Psi}_{k'1} = 0\,, \quad y_3 = 0\,,\ (y_1, y_2) \in \Gamma_1\,, \tag{6.42b}$$

$$\partial_{y_3}\tilde{\Psi}_{k'1} = 0\,, \quad y_3 = 0\,,\ (y_1, y_2) \notin \Gamma_1\,, \tag{6.42c}$$

$$\tilde{\Psi}_{k'1}(\mathbf{y}) \sim \frac{1}{|\mathbf{y}|} + \mathcal{O}\left(|\mathbf{y}|^{-2}\right) \quad \text{as} \quad |\mathbf{y}| \to \infty\,, \tag{6.42d}$$

where $\sigma_0 = \mu_{k'1}$ and $\Gamma_1 \asymp \varepsilon^{-1}\partial\Omega_1^\varepsilon$. Here the tilde symbol highlights that this normalization is different from the conventional one used in Appendix D.

With $\sigma_0 = \mu_{k'1}$ we again expand the outer solution, the eigenvalue $\sigma(\varepsilon)$, and the inner solutions as in (6.5), (6.7) and (6.8), respectively. However, in place of (6.11) and (6.12), the leading-order inner solutions near the Steklov patch and the Dirichlet patches are now

$$V_{01} = A_1\tilde{\Psi}_{k'1}(\mathbf{y})\,; \qquad V_{0i} = U_0\left(1 - w_i(\mathbf{y};\infty)\right)\,, \quad i = 2, \ldots, N\,, \tag{6.43}$$

where A_1 is a constant to be determined. Since $V_{01} \to 0$ as $|\mathbf{y}| \to \infty$, we can only match the far-field behaviors of the inner solutions to a leading-order constant outer solution U_0 when $U_0 = 0$. As a result, since $U_0 = 0$, we must have $V_{0i} = 0$ for $i = 2, \ldots, N$. In this way, in place of (6.13) the outer correction U_1 must now satisfy

$$\Delta_{\mathbf{x}}U_1 = 0\,, \quad \mathbf{x} \in \Omega\,; \qquad \partial_n U_1 = 0\,, \quad \mathbf{x} \in \partial\Omega\backslash\{\mathbf{x}_1\}\,, \tag{6.44a}$$

$$U_1 \sim \frac{A_1}{|\mathbf{x} - \mathbf{x}_1|}\,, \quad \text{as} \quad \mathbf{x} \to \mathbf{x}_1 \in \partial\Omega\,. \tag{6.44b}$$

The solvability condition for (6.44) yields that $A_1 = 0$. As a result, $V_{01} = 0$, and we must have $U_1 = \overline{U}_1$ in Ω, where $\overline{U}_1$ is an unknown constant.

Proceeding to higher order it is readily established that $\overline{U}_1 = 0$. We conclude that one cannot construct a *nontrivial* solution to (2.11) with limiting behavior $\sigma_0 = \mu_{k'1}$. As a consequence, there is no near-resonant eigenpair of the SDN problem (2.12) with a single Steklov patch.

REMARK 3. *From the beginning of §6.4, we restricted our analysis to the near-resonant cases, for which $\sigma_0 = \mu_{k'1} \in \mathcal{P}_1$ such that $\mu_{k'1}$ is simple. As a consequence, our statement that there is no near-resonant eigenpair of the SDN problem (2.12) is established only under the assumption that all eigenvalues in the resonant set $\mathcal{P}_1$ are simple. For a circular patch numerical evidence suggests that this assumption does hold, but its rigorous validation presents an interesting open problem. For an arbitrary patch, however, the assumption on the simplicity of eigenvalues from $\mathcal{P}_1$ may not hold. However, we expect that this assumption can be relaxed, i.e., one can use any nontrivial element of the eigenspace associated to $\mu_{k'1}$ in the analysis above. A proof of this statement is beyond the scope of this paper.*

7. The Steklov-Neumann (SN) Eigenvalue Problem. Finally, we address the SN eigenvalue problem (2.12) in the unit sphere Ω, with $N \geq 1$ Steklov patches $\partial\Omega_i^\varepsilon$. We impose the normalization condition

$$\int_{\partial\Omega_a} u^2\, d\mathbf{s} = \sum_{i=1}^{N} \int_{\partial\Omega_i^\varepsilon} u^2 d\mathbf{s} = 1\,. \tag{7.1}$$

This spectral problem has a discrete spectrum, with a countable set of nonnegative eigenvalues $\{\sigma^{(m)}(\varepsilon)\}$ that are enumerated by an integer index $m = 0, 1, 2, \ldots$ that accumulates to infinity [84]. Since the principal eigenvalue, which corresponds to a constant eigenfunction, is $\sigma^{(0)}(\varepsilon) = 0$, independently of ε, we exclude it from our analysis below. Owing to the orthogonality of the Steklov eigenfunctions, or more simply by applying the divergence theorem to (2.12), we must have for any other Steklov eigenvalue $\sigma^{(m)}(\varepsilon) > 0$ with $m = 1, 2, \ldots$ that the corresponding eigenfunction $u^{(m)}$ satisfies

$$\int_{\partial\Omega_a} u^{(m)}\, d\mathbf{s} = \frac{\varepsilon}{\sigma^{(m)}(\varepsilon)} \sum_{i=1}^{N} \int_{\partial\Omega_i^\varepsilon} \partial_n u^{(m)}\, d\mathbf{s} = 0\,. \tag{7.2}$$

For convenience, in our analysis below we omit the superscript $^{(m)}$ to highlight that our asymptotic analysis is not specific to a particular value of m.

In analogy with the SDN problem studied in §6, we need to consider both non-resonant and near-resonant cases. While the near-resonant case was not possible for the SDN problem with a single Steklov patch, it will present one of the challenging features of the SN analysis here.

We introduce the resonant set

$$\mathcal{P} \equiv \bigcup_{i=1}^{N} \mathcal{P}_i\,, \quad \text{where} \quad \mathcal{P}_i \equiv \bigcup_{k=0}^{\infty} \{\mu_{ki} \mid d_{ki} \neq 0\}\,, \tag{7.3}$$

where μ_{ki} with $k = 0, 1, \ldots$ are the eigenvalues of the *local* Steklov problem (D.1) near the i-th Steklov patch Γ_i for $i = 1, \ldots, N$, with nontrivial spectral weights $d_{ki} \neq 0$ (see of Appendix D for details). We distinguish two situations according to the limiting value $\sigma_0 = \lim_{\varepsilon\to 0} \sigma(\varepsilon)$ of a SN eigenvalue $\sigma = \sigma(\varepsilon)$:

(I) If $\sigma_0 \notin \mathcal{P}$, the eigenpair $\{\sigma, u\}$ is called non-resonant. In this case, both $C_i(-\sigma_0)$ and $w_i(\mathbf{y}; -\sigma_0)$ are well-defined for each $i = 1, \ldots, N$. The analysis for this non-resonant case, which is similar to that done in §6.1 for the SDN problem, will be performed in §7.1.

(II) If $\sigma_0 \in \mathcal{P}$, the eigenpair $\{\sigma, u\}$ is called near-resonant. In this case, some $w_i(\mathbf{y}; -\sigma_0)$ may be undefined and thus must be replaced by suitable eigenfunctions of the local Steklov problem (D.1), associated to σ_0. Even though the asymptotic analysis of the near-resonant case is feasible to undertake in more generality, we will restrict our attention below to one relevant setting. More specifically, we assume that $N \geq 2$ and that there are exactly M *identical* patches, with $2 \leq M \leq N$, which we relabel by $\partial\Omega_1^\varepsilon = \ldots = \partial\Omega_M^\varepsilon \equiv \partial\Omega_c^\varepsilon$. For these identical patches, with a common patch shape $\Gamma_c \asymp \varepsilon^{-1}\partial\Omega_c^\varepsilon$, there is a common spectrum μ_{kc} with $k \geq 0$ of the local Steklov problem (D.1) of Appendix D. In §7.3 we will show that the global SN problem (2.12) admits $M - 1$ *near-resonant* eigenvalues (counting multiplicity) such that $\sigma_0 \in \mathcal{P}$. The corresponding eigenfunctions will be shown to concentrate on the M near-resonant patches. We will also derive a three-term asymptotic behavior for these global SN eigenvalues.

REMARK 4. *We remark that for this setting, it is essential that $M > 1$. In fact, if the near-resonant condition occurs on only one patch, i.e. if $\sigma_0 = \mu_{ki}$ for some simple eigenvalue μ_{ki} of (D.1) of a unique patch $i \in \{1, \ldots, N\}$ with $d_{ki} \neq 0$, it is readily shown, as similar to that done in §6.4, that the SN problem (2.12) only admits the trivial solution (see also Remark 3). Hence, for $M = 1$, there is no SN eigenpair*

for (2.12) with such limiting asymptotics σ_0. We emphasize that when there are two or more identical patches the analysis for the non-resonant case will only capture a subset of the SN eigenvalues for the global problem (2.12). The remaining global SN eigenvalues will be in near-resonance with eigenvalues of the local Steklov problem (D.1) on the identical patches. The corresponding eigenfunctions will concentrate on these identical patches. We remark that more intricate near-resonant cases are possible for specific non-generic situations such as when there are two patch indices i_1 and i_2 and two eigenvalue indices k_1 and k_2 for which $\mu_{k_1 i_1} = \mu_{k_2 i_2}$. Although the construction of a SN eigenpair for which $\sigma_0 = \mu_{k_1 i_1} = \mu_{k_2 i_2}$ can be done in a similar way as for the identical patch case undertaken in §7.3, we will not consider this special case.

7.1. Non-Resonant Case. Since the analysis for the SN problem (2.12) in the non-resonant case is very similar to that done in §6.1 for the SDN problem (2.11), we will only briefly outline the analysis to determine $\sigma(\varepsilon)$. As for the SDN problem, we seek to construct eigenpairs of (2.12) for which the leading-order outer solution U_0 is non-vanishing (i.e. $U_0 \neq 0$).

In the outer region, we expand u as in (6.5) to obtain (6.6) at each order of the expansion. In addition, each nontrivial Steklov eigenvalue is expanded as in (6.7). In the inner region near each Steklov patch, we expand the inner solution in terms of geodesic coordinates as in (6.8), to derive that V_{ji} for $j = 0, 1, 2$, and for each $i = 1, \ldots, N$, satisfies

$$\Delta_{\mathbf{y}} V_{ji} = \delta_{j2} \left(2 y_3 V_{0i,y_3 y_3} + 2 V_{0i,y_3} \right) , \quad \mathbf{y} \in \mathbb{R}^3_+ , \tag{7.4a}$$

$$\partial_{y_3} V_{ji} + \sigma_0 V_{ji} = -(1 - \delta_{j0}) \sigma_j V_{0i} , \quad y_3 = 0 , \, (y_1, y_2) \in \Gamma_i , \tag{7.4b}$$

$$\partial_{y_3} V_{ji} = 0 , \quad y_3 = 0 , \, (y_1, y_2) \notin \Gamma_i . \tag{7.4c}$$

For each Steklov patch, we set $w_i = w_i(\mathbf{y}; -\sigma)$ as the solution of (3.3), where the dependence of w_i, C_i and $\mathbf{p}_i$ on σ is obtained by setting $\kappa_i = -\sigma$ in (3.3). As similar to the analysis of the SDN problem in §6, we define

$$w_{ci} = w_{ci}(\mathbf{y}; -\sigma) \equiv \partial_\sigma w_i(\mathbf{y}; -\sigma), \tag{7.5}$$

which satisfies, for each $i = 1, \ldots, N$, the following inner problem:

$$\Delta_{\mathbf{y}} w_{ci} = 0 , \quad \mathbf{y} \in \mathbb{R}^3_+ , \tag{7.6a}$$

$$\partial_{y_3} w_{ci} + \sigma w_{ci} = 1 - w_i , \quad y_3 = 0 , \, (y_1, y_2) \in \Gamma_i , \tag{7.6b}$$

$$\partial_{y_3} w_{ci} = 0 , \quad y_3 = 0 , \, (y_1, y_2) \notin \Gamma_i , \tag{7.6c}$$

$$w_{ci} \sim -\frac{C_i'(-\sigma)}{|\mathbf{y}|} - \frac{\mathbf{p}_i'(-\sigma) \cdot \mathbf{y}}{|\mathbf{y}|^3} + \cdots , \quad \text{as} \quad |\mathbf{y}| \to \infty . \tag{7.6d}$$

Since $\sigma_0 \notin \mathcal{P}$, it follows that $C_i(-\sigma_0)$ and $w_i(\mathbf{y}; -\sigma_0)$ are well-defined. Then, in terms of the constant leading-order outer solution U_0, which will be found below by the normalization condition (7.1), the leading order inner solution for each $i = 1, \ldots, N$, as obtained by setting $j = 0$ in (7.4), is

$$V_{0i} = U_0 \left(1 - w_i(\mathbf{y}; -\sigma_0) \right) . \tag{7.7}$$

Upon matching the far-field of V_{0i} to the outer solution, we find that U_1 satisfies

$$\Delta_{\mathbf{x}} U_1 = 0\,, \quad \mathbf{x} \in \Omega\,; \quad \partial_n U_1 = 0\,, \quad \mathbf{x} \in \partial\Omega \backslash \{\mathbf{x}_1, \ldots, \mathbf{x}_N\}\,, \tag{7.8a}$$

$$U_1 \sim -\frac{C_i\,(-\sigma_0)\,U_0}{|\mathbf{x}-\mathbf{x}_i|}\,, \quad \text{as} \quad \mathbf{x} \to \mathbf{x}_i \in \partial\Omega\,, \quad i = 1, \ldots, N\,. \tag{7.8b}$$

The solvability condition for (7.8) is that

$$U_0 \sum_{i=1}^{N} C_i(-\sigma_0) = 0\,. \tag{7.9}$$

For $U_0 \neq 0$, we conclude that the leading-order Steklov eigenvalue σ_0 is a root of the following nonlinear algebraic equation:

$$\mathcal{N}(\sigma_0) = 0\,, \quad \text{where} \quad \mathcal{N}(\sigma_0) \equiv \sum_{i=1}^{N} C_i\,(-\sigma_0)\,. \tag{7.10}$$

The spectral expansion (3.5) ensures that $\mathcal{N}(\sigma_0)$ increases monotonically between its consecutive poles so that (7.10) has infinitely many solutions that we denote as $\sigma_0^{(k)}$. These solutions lie between consecutive poles but finding their explicit locations is in general more difficult than for the SDN problem with a single Steklov patch. As earlier, we omit the superscript $^{(k)}$ for brevity.

With σ_0 determined in this way, the solution to (7.8) for U_1 is written in terms of the surface Neumann Green's function G_s and an unknown constant $\overline{U}_1$ as

$$U_1(\mathbf{x}) = \overline{U}_1 - 2\pi U_0 \sum_{j=1}^{N} C_j(-\sigma_0) G_s(\mathbf{x}; \mathbf{x}_j)\,. \tag{7.11}$$

To proceed to higher order, we expand U_1 as $\mathbf{x} \to \mathbf{x}_i$ to derive (6.16), where we label $C_i = C_i(-\sigma_0)$ for $i = 1, \ldots, N$. Upon matching to the inner solution we conclude that $V_{1i} \sim U_0 C_i/2$ as $|\mathbf{y}| \to \infty$ for $i = 1, \ldots, N$. Upon solving the problem (7.4) for V_{1i} with this limiting behavior, we obtain that

$$V_{1i} = -U_0 \sigma_1 w_{ci}(\mathbf{y}; -\sigma_0) + \frac{U_0 C_i(-\sigma_0)}{2}\left(1 - w_i(\mathbf{y}; -\sigma_0)\right)\,, \quad i = 1, \ldots, N\,. \tag{7.12}$$

The far-field behavior for V_{1i} as $|\mathbf{y}| \to \infty$ is

$$V_{1i} \sim U_0 \sigma_1 \frac{C_i'(-\sigma_0)}{|\mathbf{y}|} + \frac{U_0 C_i(-\sigma_0)}{2}\left(1 - \frac{C_i(-\sigma_0)}{|\mathbf{y}|}\right) + \cdots\,, \tag{7.13}$$

where the neglected higher-order far-field terms are dipole contributions.

The monopole terms in (7.13) provide the singularity behavior for the outer correction U_2 in (6.5). In this way, we find that U_2 satisfies (6.21a) subject to

$$U_2 \sim -\frac{U_0}{2}\frac{\left[C_i(-\sigma_0)\right]^2}{|\mathbf{x}-\mathbf{x}_i|} + U_0\sigma_1 \frac{C_i'(-\sigma_0)}{|\mathbf{x}-\mathbf{x}_i|}\,, \quad \text{as} \quad \mathbf{x} \to \mathbf{x}_i \in \partial\Omega\,, \quad i = 1, \ldots, N\,. \tag{7.14}$$

The solvability condition for this problem for U_2 is that

$$-\frac{U_0}{2}\sum_{i=1}^{N}\left[C_i(-\sigma_0)\right]^2 + U_0\sigma_1 \sum_{i=1}^{N} C_i'(-\sigma_0) = 0\,. \tag{7.15}$$

Under the condition that $U_0 \neq 0$, (7.15) determines σ_1 as

$$\sigma_1 = \frac{1}{2} \frac{\sum_{i=1}^N [C_i(-\sigma_0)]^2}{\sum_{i=1}^N C_i'(-\sigma_0)}, \tag{7.16}$$

where σ_0 is a root of (7.10). From (3.7), it follows that C_i increases monotonically between its poles so that $C_i'(-\sigma_0) \neq 0$. As a result the denominator in (6.22) never vanishes, and σ_1 is well-defined and strictly positive. With σ_1 determined in this way, the solution to (6.21a) with (7.14) is given in terms of an unknown constant $\overline{U}_2$ by

$$U_2(\mathbf{x}) = \overline{U}_2 - 2\pi U_0 \sum_{j=1}^N \left(\frac{[C_j(-\sigma_0)]^2}{2} - \sigma_1 C_j'(-\sigma_0) \right) G_s(\mathbf{x}; \mathbf{x}_j). \tag{7.17}$$

Finally, we determine σ_2. We readily obtain (6.25) for the far-field behavior for the inner correction V_{2i}, which satisfies (7.4) with $k = 2$. In analogy with (6.28), we determine V_{2i} for $i = 1, \ldots, N$ as

$$V_{2i} = U_0 \Phi_{2i} + \left(U_0 \beta_i + \overline{U}_1 \right) (1 - w_i(\mathbf{y}; -\sigma_0)) - U_0 \sigma_2 w_{ci}(\mathbf{y}; -\sigma_0), \tag{7.18}$$

where Φ_{2i} satisfies (4.21) in which we set $\kappa_i = -\sigma_0$ and $C_i = C_i(-\sigma_0)$. As a result, the refined far-field behavior of V_{2i} for each $i = 1, \ldots, N$ is

$$\begin{aligned} V_{2i} \sim\ & U_0 \beta_i + \overline{U}_1 + \frac{U_0 C_i(-\sigma_0)}{2} \left(\log(y_3 + |\mathbf{y}|) - \frac{y_3(y_1^2 + y_2^2)}{|\mathbf{y}|^3} \right) \\ & + \left[E_i(-\sigma_0) - \left(\beta_i + \frac{\overline{U}_1}{U_0} \right) C_i(-\sigma_0) + \sigma_2 C_i'(-\sigma_0) \right] \frac{U_0}{|\mathbf{y}|}, \quad \text{as} \quad |\mathbf{y}| \to \infty. \end{aligned} \tag{7.19}$$

Here $E_i(-\sigma_0)$ is obtained by setting $\kappa_i = -\sigma_0$ in (3.22).

As similar to the analysis of the SDN problem in §6.1, the monopole terms in the far-field behavior (7.19), together with dipole term in the far-field of V_{0i}, provide the singularity behavior for the outer correction U_3. In this way, we get that U_3 satisfies

$$\begin{aligned} & \Delta_{\mathbf{x}} U_3 = 0, \quad \mathbf{x} \in \Omega; \quad \partial_n U_3 = 0, \quad \mathbf{x} \in \partial\Omega \backslash \{\mathbf{x}_1, \ldots, \mathbf{x}_N\}, \\ & U_3 \sim \left[E_i(-\sigma_0) - \left(\beta_i + \frac{\overline{U}_1}{U_0} \right) C_i(-\sigma_0) + \sigma_2 C_i'(-\sigma_0) \right] \frac{U_0}{|\mathbf{x} - \mathbf{x}_i|} \\ & \qquad - U_0 \frac{\mathbf{p}_i(-\sigma_0) \cdot \mathcal{Q}_i^T (\mathbf{x} - \mathbf{x}_i)}{|\mathbf{x} - \mathbf{x}_i|^3}, \quad \text{as} \quad \mathbf{x} \to \mathbf{x}_i \in \partial\Omega, \quad i = 1, \ldots, N, \end{aligned} \tag{7.20}$$

where the orthogonal matrix $\mathcal{Q}_i$ is defined in (A.8) in terms of the basis vectors of the geodesic coordinate system. The solvability condition for (7.20) is that

$$U_0 \left(\sum_{i=1}^N E_i(-\sigma_0) - \sum_{i=1}^N \beta_i C_i(-\sigma_0) + \sigma_2 \sum_{i=1}^N C_i'(-\sigma_0) \right) - \overline{U}_1 \sum_{i=1}^N C_i(-\sigma_0) = 0, \tag{7.21}$$

which determines σ_2. Since σ_0 satisfies $\sum_{i=1}^N C_i(-\sigma_0) = 0$ when $U_0 \neq 0$, as seen from (7.10) and (7.9), we observe that σ_2 is independent of the unknown normalization constant $\overline{U}_1$. As a result, upon recalling that $\beta_i = -2\pi (\mathcal{G}_s \mathbf{C})_i$ from (6.17), we conclude from (7.21) that, when $U_0 \neq 0$, σ_2 is given by

$$\sigma_2 = -\frac{1}{\sum_{i=1}^N C_i'(-\sigma_0)} \left(2\pi \mathbf{C}^T \mathcal{G}_s \mathbf{C} + \sum_{i=1}^N E_i(-\sigma_0) \right), \tag{7.22}$$

where $\mathcal{G}_s$ is the Green's matrix and $\mathbf{C} = (C_1(-\sigma_0), \ldots, C_N(-\sigma_0))^T$. We summarize our result as follows:

PROPOSITION 4. *For $\varepsilon \to 0$, consider the eigenvalues $\sigma = \sigma(\varepsilon)$ of the Steklov-Neumann problem (2.12), for which $\sigma(\varepsilon) \to \sigma_0 \notin \mathcal{P}$, where the resonant set $\mathcal{P}$ is defined by (7.3). These Steklov eigenvalues and the associated eigenfunctions, restricted to Γ_i, have the three-term asymptotics*

$$\sigma = \sigma_0 + \varepsilon \log\left(\frac{\varepsilon}{2}\right)\sigma_1 + \varepsilon\sigma_2 + \mathcal{O}(\varepsilon^2 \log\varepsilon)\,, \tag{7.23a}$$

$$u|_{\Gamma_i} = V_{0i} + \varepsilon \log\left(\frac{\varepsilon}{2}\right) V_{1i} + \varepsilon V_{2i} + \mathcal{O}(\varepsilon^2 \log\varepsilon)\,, \quad i = 1, \ldots, N\,, \tag{7.23b}$$

where σ_0, σ_1 and σ_2 are respectively determined by (7.10), (7.16) and (7.22). Moreover, V_{0i}, V_{1i} and V_{2i} for each $i = 1, \ldots, N$ are respectively given by (7.7), (7.12), and (7.18). Here $u|_{\Gamma_i}$ is given up to a normalization constants $U_0 \neq 0$ and U_1 for the eigenfunction, whereas its spatial behavior is determined by the functions $w_i(\mathbf{y}; -\sigma_0)$ and $w_{ci}(\mathbf{y}; -\sigma_0)$, which admit the spectral expansions (D.9) and (D.11), respectively. For a circular patch, these expansions can be readily calculated numerically, as shown in Appendix D.

By using the normalization condition (7.1), together with the leading-order inner solutions (7.7), we can determine U_0 as

$$U_0 \sim \varepsilon^{-1}\left[\sum_{i=1}^{N}\int_{\Gamma_i}\left[1 - w_i(\mathbf{y}; -\sigma_0)\right]^2 d\mathbf{y}\right]^{-1/2}. \tag{7.24}$$

Since $U_0 \neq 0$, the class of SN eigenpairs given in Proposition 4 results from a global interaction of the Steklov patches through the outer (bulk) solution.

REMARK 5. *In analogy with the SDN eigenvalue problem analysis (see Remarks 1 and 2), the analysis leading to Proposition 4 does not give access to* all *SN eigenpairs. In particular, as for the SDN problem there are eigenpairs for which the leading-order bulk solution U_0 vanishes. For circular Steklov patches, this situation will always occur for eigenfunctions that are not axially symmetric on the patches. To leading order, these SN eigenvalues have limiting behavior $\sigma_0 = \mu_{ki}^N$, for some index $k \geq 1$ and patch index $i \in \{1, \ldots, N\}$, where $\mu_{ki}^N > 0$ is an eigenvalue of the local Steklov problem (6.37) in which Γ_1 is replaced by Γ_i. The corresponding eigenfunction concentrates on the i-th patch and is only weakly influenced by the other patches. In addition, other SN eigenvalues corresponding to the near-resonant case will be recovered in §7.3.*

7.2. Numerical Comparison. In §4.2, §5.2 and §6.3, we used a finite-element method for validating the asymptotic formulas. However, obtaining accurate numerical results by this method for small patches requires using very fine meshes, which typically results in prohibitively long computations. To achieve a more accurate computation of the SN eigenvalues for a single patch or for two antipodal patches on a sphere, in Appendix F we outline an alternative method, based on [48], which exploits properties of axially symmetric harmonic functions. Using this more refined numerical approach we now give two examples to illustrate our main result (7.23a).

Example I: For a single circular patch $\partial\Omega_1^\varepsilon$ of radius ε (i.e., $N = 1$ and $a_1 = 1$), the condition (7.10) for σ_0 reads as $C_1(-\sigma_0) = 0$. The spectral expansion (3.5) of $C_1(\kappa_1)$ implies that it has infinitely many nontrivial zeros, which we denote as $-\mu_{k1}^N$ with $k = 1, 2, \ldots$ (see Fig. 3.1). As shown in Lemma D.3 of Appendix D.4,

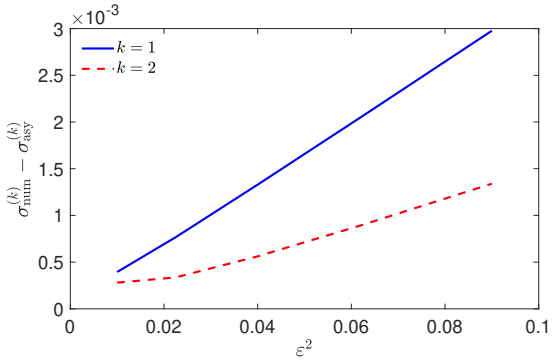

Fig. 7.1: Asymptotic behavior of the first two SN eigenvalues (that correspond to axially-symmetric eigenfunctions) for a single circular patch of radius ε on the unit sphere. Each curve shows the difference between the numerical value $\sigma^{(k)}_{\rm num}$, computed using the methodology in Appendix F, and its asymptotic value $\sigma^{(k)}_{\rm asy}$ given in (7.25a). This difference is shown as a function of ε^2 to highlight the order of the error estimate in (7.25a).

these roots μ^N_{k1} are in fact eigenvalues of a local Steklov eigenvalue problem (D.30) defined near the patch Γ_1, for which the corresponding eigenfunctions satisfy a far-field Neumann-like condition (D.30d). These zeros determine the leading-order behavior of the associated SN eigenvalues for the global SN problem (2.12) as $\sigma^{(k)}_0 = \mu^N_{k1}$. This leading-order behavior was studied in [56], and the numerical values of μ^N_{k1} were reported in Table I of [56]. In turn, the asymptotic formula (7.23a) gives the next-order corrections as $\sigma_1 = 0$ from (7.16) and $\sigma_2 = -E_1(-\sigma_0)/C_1'(-\sigma_0)$ from (7.22). In this way, from (7.23a), the first four SN eigenvalues (that correspond to axially symmetric eigenfunctions) are predicted to have the two-term asymptotic behavior

(7.25a)
$$\sigma^{(1)}_{\rm asy} \sim 4.121 - 0.573\,\varepsilon + \mathcal{O}(\varepsilon^2 \log \varepsilon)\,, \quad \sigma^{(2)}_{\rm asy} \sim 7.342 - 0.552\,\varepsilon + \mathcal{O}(\varepsilon^2 \log \varepsilon)\,,$$
(7.25b)
$$\sigma^{(3)}_{\rm asy} \sim 10.517 - 0.542\,\varepsilon + \mathcal{O}(\varepsilon^2 \log \varepsilon)\,, \quad \sigma^{(4)}_{\rm asy} \sim 13.677 - 0.535\,\varepsilon + \mathcal{O}(\varepsilon^2 \log \varepsilon)\,.$$

In Fig. 7.1 we plot the difference between the numerically computed values $\sigma^{(k)}_{\rm num}$ of the first two SN eigenvalues and their asymptotic approximations in (7.25a), as a function of ε^2. The observed linear dependence on ε^2 indicates that: (i) the first two terms of (7.25a) are correct, and (ii) the next-order term is $\mathcal{O}(\varepsilon^2)$ as the coefficient of the error term $\mathcal{O}(\varepsilon^2 \log \varepsilon)$ seems to vanish.

Example II: Next, we consider the special case of N circular Steklov patches of distinct radii $a_i > 0$, for $i = 1, \ldots, N$, so that $a_i \neq a_j$ for $i \neq j$. Then, using the scaling law (3.6), we obtain from (7.10) that $\sigma^{(k)}_0$ are the roots of $\mathcal{N}(\sigma_0) = 0$, where

$$\mathcal{N}(\sigma_0) = \sum_{i=1}^{N} a_i \mathcal{C}(-\sigma_0 a_i)\,. \tag{7.26}$$

Here $\mathcal{C}(\mu)$ is readily computed via the spectral expansion (3.5) for any rescaled patch Γ_i/a_i. Owing to the monotonicity of $\mathcal{N}(\sigma_0)$ between consecutive poles, which readily

follows from the monotonicity of $\mathcal{C}(\mu)$ established in (3.7), we conclude that between any two consecutive poles of $\mathcal{N}(\sigma_0)$ the function $\mathcal{N}(\sigma_0) = 0$ must have a unique root. For each such root, the asymptotic result (7.23a) can then be used to determine a three-term asymptotic expansion for this particular SN eigenvalue.

To illustrate this result, we numerically compute the eigenvalues of the SN problem (2.12) for two circular patches of radii $a_1\varepsilon$ and $a_2\varepsilon$ (with $a_2 = 1$), located at the north and south poles of the unit sphere (note that the trivial principal eigenvalue $\sigma^{(0)} = 0$ will be excluded from our discussion; we also focus on the eigenvalues that correspond to axially symmetric eigenfunctions). Figure 7.2(a) shows an excellent agreement between the asymptotic result in (7.23a) and the numerically computed eigenvalues as the radius a_1 of the smaller patch is varied on $(0, 1)$. We observe that as $a_1 \to 0$, we recover the eigenvalues, written in the form μ^N_{k2}, for the SN problem with a single Steklov patch Γ_2. The observed behavior of the eigenvalues allows us to push the analogy to a single Steklov patch even further. When ε is small, one might expect that the two well-separated patches do not almost "feel" each other. This (over-)simplified picture suggests that, to leading order, the spectrum of the SN problem with two patches would be the union of the spectra of the two SN problems with a single patch, either Γ_1, or Γ_2. In Fig. 7.2(b), four thin horizontal lines present the asymptotic values $\sigma^{(k)}_{\rm asy}$ from (7.25) of the first four eigenvalues for a single Steklov patch Γ_2 (as if Γ_1 was absent). In turn, the thick solid and dashed lines present the asymptotic values $\sigma^{(k)}_{\rm asy}/a_1$ from (7.25) of the first two eigenvalues for a single Steklov patch Γ_1 (as if Γ_2 was absent). For comparison, symbols show the numerically computed eigenvalues of the SN problem with two patches; these symbols are identical with those shown in Fig. 7.2(a) but just colored differently. One observes an excellent agreement between symbols and curves that *partly* validates the intuitive idea of the patches not feeling each other. However, there are points (shown by triangles) that are not captured by either of the asymptotic relations for single patches. To outline their dependence on a_1, we added the dashed curve $0.95/a_1$, in which the prefactor 0.95 was obtained from fitting, i.e., it does not correspond to any limiting eigenvalue μ^N_{ki}. The presence of such points highlights that the interaction between two patches is still relevant but it mainly affects the smallest (nontrivial) eigenvalue.

Let us now consider the limit $a_1 \to 1$, which corresponds to the setting of two identical patches. Figure 7.2(a) shows that the asymptotic theory of §7.1 does not account for the closely spaced SN eigenvalues that are computed numerically, and instead accurately captures only one of these two eigenvalues. To qualitatively explain this discrepancy for two identical patches, we observe that the poles of $\mathcal{N}(\sigma_0)$, as characterized by the resonant set $\mathcal{P}$ in (7.3) with $N = 2$, are no longer all distinct. In addition, the leading-order SN eigenvalue for two identical patches with $a_1 = a_2 = 1$ reduces from (7.26) to simply finding the roots of $\mathcal{C}(-\sigma_0) = 0$. As a result, our asymptotic theory when applied to two identical patches would predict that, for each $k = 1, 2, \ldots$, there is a *unique* leading-order approximation $\sigma^{(k)}_0 = \mu^N_{k1} (= \mu^N_{k2})$ for the SN eigenvalue, satisfying $C_1(-\mu^N_{k1}) = 0$. We emphasize that these are simply the leading-order SN eigenvalues for a single patch. In particular, the asymptotic result (7.23a) of §7.1 would erroneously predict that the two smallest SN eigenvalues have the *same* two-term asymptotics $\sigma^{(k)}_{\rm asy} \sim \mu^N_{k1} + \varepsilon E_1(-\mu^N_{k1})/C_1'(-\mu^N_{k1})$. This is precisely the asymptotic result given in (7.25a) for a single Steklov patch. These results are shown by the limiting values of the green and black dashed curves at the right endpoint in Fig. 7.2(a). However, our asymptotic theory fails to account for the additional nearby SN eigenvalue at the right end of the red curve in Fig. 7.2(a), as well as a further

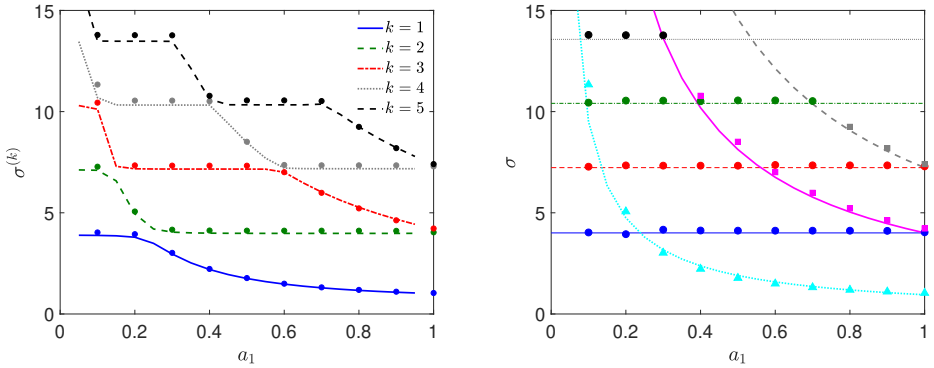

(a) Comparison with asymptotics (7.23a) **(b)** Comparison with asymptotics (7.25)

Fig. 7.2: **(a)** The first five SN eigenvalues $\sigma^{(k)}$ (that correspond to axially symmetric eigenfunctions) for two circular patches Γ_i of radii a_1 and $a_2 = 1$, with $0 < a_1 < 1$, located at the north and south poles of the unit sphere, with $\varepsilon = 0.2$. Symbols illustrate the numerical values computed by the method in Appendix F with truncation order $n_{\max} = 1000$, whereas thick lines indicate the asymptotic formula (7.23a). **(b)** Symbols show the same eigenvalues computed numerically but colored differently, along with the shown curves: the thin horizontal lines present $\sigma^{(k)}_{\text{asy}}/a_2$ with $k = 1, 2, 3, 4$ from (7.25); thick solid and dashed curves present $\sigma^{(k)}_{\text{asy}}/a_1$ with $k = 1, 2$ from (7.25); thick dotted line presents $0.95/a_1$.

closely spaced SN eigenvalue near the right end of the black dashed curve. Moreover, the asymptotic analysis of §7.1 does not predict the lowest SN eigenvalue at the right end of the lower blue curve in Fig. 7.2(a). Indeed, the first line of Table 7.1 reports the first five nontrivial SN eigenvalues for two identical patches with $\varepsilon = 0.2$ that were calculated by the accurate numerical methodology outlined in Appendix F, and which we consider as benchmarks. These results are the SN eigenvalues at the right ends of the curves in Fig. 7.2(a). For comparison, the second line of Table 7.1 yields the first two SN eigenvalues for two identical patches as predicted by the asymptotic theory of §7.1 as obtained by setting $\varepsilon = 0.2$ in (7.25a). As a result, we conclude that when applied to the case of identical patches, the asymptotic theory of §7.1 only accounts for a subset of the true SN eigenvalues. We now remedy this deficiency by refining our asymptotic theory to treat the setting of multiple identical patches.

7.3. Near-Resonant Case. We now give a specific nontrivial illustration of the near-resonant case that will always occur when there are M identical patches, with $2 \le M \le N$. With a suitable relabeling of the patch indices, we label the common patch shape as $\partial\Omega_c^\varepsilon = \partial\Omega_i^\varepsilon$ (with $a_i = a_c$) for $i = 1, \ldots, M$. On these identical patches, there is a common spectrum, labeled by μ_{kc} for $k \ge 0$, for the local Steklov problem (D.1) of Appendix D.

We assume that $\sigma_0 = \lim_{\varepsilon \to 0} \sigma(\varepsilon) = \mu_{k'c}$ for some simple eigenvalue $\mu_{k'c}$ of (D.1) for which $d_{k'c} \neq 0$. The corresponding local Steklov eigenfunction from (D.1), labeled by

k	1	2	3	4	5
Accurate numerics	1.0305	4.0080	4.1950	7.2325	7.3448
Non-resonant asymptotics		4.006		7.232	
Near-resonant asymptotics	1.0075		4.1896		7.3416

Table 7.1: The first five SN eigenvalues (that correspond to axially symmetric eigenfunctions) for two identical circular patches of radius $\varepsilon = 0.2$ located on the north and south poles of the unit sphere. The first line presents the numerical results obtained by the accurate method presented in Appendix F; as all digits of these values are exact, they are considered as benchmarks. The second line gives our three-term expansion (7.23a) for the non-resonant case (it is identical to the single-patch asymptotics (7.25)). The third line gives the three-term expansion (7.63), that will be derived in §7.3 for the near-resonant case (see below).

$\tilde{\Psi}_{k'c}$, is taken to be the unique solution to

$$\Delta_{\mathbf{y}} \tilde{\Psi}_{k'c} = 0\,, \quad \mathbf{y} \in \mathbb{R}^3_+\,, \tag{7.27a}$$

$$\partial_{y_3} \tilde{\Psi}_{k'c} + \sigma_0 \tilde{\Psi}_{k'c} = 0\,, \quad y_3 = 0\,,\ (y_1, y_2) \in \Gamma_c\,, \tag{7.27b}$$

$$\partial_{y_3} \tilde{\Psi}_{k'c} = 0\,, \quad y_3 = 0\,,\ (y_1, y_2) \notin \Gamma_c\,, \tag{7.27c}$$

$$\tilde{\Psi}_{k'c}(\mathbf{y}) \sim \frac{1}{|\mathbf{y}|} + \mathcal{O}\left(|\mathbf{y}|^{-2}\right) \quad \text{as} \quad |\mathbf{y}| \to \infty\,, \tag{7.27d}$$

where $\Gamma_c \asymp \varepsilon^{-1}\partial\Omega_c^\varepsilon$. The tilde highlights that we changed here the normalization of $\tilde{\Psi}_{k'c}$ by imposing (7.27d). Comparing this decay with the asymptotic behavior (D.18) of an equivalent eigenfunction $\Psi_{k'c}$ with the conventional $L^2(\Gamma_c)$ normalization, we deduce that

$$\tilde{\Psi}_{k'c} = \frac{2\pi}{\mu_{k'c}\, d_{k'c}} \Psi_{k'c}\,, \tag{7.28}$$

with $d_{k'c}$ being defined in (D.8). We conclude that

$$\int_{\Gamma_c} [\tilde{\Psi}_{k'c}(\mathbf{y})]^2 d\mathbf{y} = \left(\frac{2\pi}{\mu_{k'c}\, d_{k'c}}\right)^2\,. \tag{7.29}$$

Moreover, in our analysis below, we assume that the remaining $N - M$ patches are not in near-resonance in the sense that $\sigma_0 \neq \mu_{ki}$ for all $k \geq 0$ and all $i = M+1, \dots N$.

As similar to the analysis in §7.1, in the outer region we expand u as in (6.5) to obtain (6.6) at each order. We then expand the Steklov eigenvalue as in (6.7), where $\sigma_0 = \mu_{k'c}$. In the inner regions near each Steklov patch, we expand the inner solution as in (6.8) to obtain the inner problems (7.4) at each order.

In contrast to the analysis for the non-resonant case, we obtain in place of (7.7) that the leading-order inner solutions are now

$$\begin{aligned} V_{0i} &= A_i \tilde{\Psi}_{k'c}(\mathbf{y})\,, \quad i = 1, \dots, M\,, \\ V_{0i} &= U_0 \left(1 - w_i(\mathbf{y}; -\sigma_0)\right)\,, \quad i = M+1, \dots, N\,, \end{aligned} \tag{7.30}$$

where $A_1, \dots, A_M$ are constants to be determined. As $|\mathbf{y}| \to \infty$, we have $V_{0i} \to 0$ for $i = 1, \dots, M$ while $V_{0i} \to U_0$ for $i = M+1, \dots, N$. This implies that we can only

match to the leading-order constant outer solution U_0 when $U_0 = 0$. As a result, the leading-order inner solutions near the non-resonant patches vanish, i.e. $V_{0i} = 0$ for $i = M+1, \ldots, N$.

Next, by matching the far-field behavior of V_{0i} for $i = 1, \ldots, M$ to the outer correction U_1 by using the far-field (7.27d) for $\tilde{\Psi}_{k'c}$, we obtain that U_1 satisfies

$$\Delta_{\mathbf{x}} U_1 = 0\,, \quad \mathbf{x} \in \Omega\,; \qquad \partial_n U_1 = 0\,, \quad \mathbf{x} \in \partial\Omega \backslash \{\mathbf{x}_1, \ldots, \mathbf{x}_M\}\,, \tag{7.31a}$$

$$U_1 \sim \frac{A_i}{|\mathbf{x} - \mathbf{x}_1|}\,, \quad \text{as} \quad \mathbf{x} \to \mathbf{x}_i \in \partial\Omega\,, \quad i = 1, \ldots, M\,. \tag{7.31b}$$

The solvability condition for (7.31) yields that

$$\sum_{i=1}^{M} A_i = 0\,. \tag{7.32}$$

In terms of an unknown constant $\overline{U}_1$, the solution to (7.31) is

$$U_1 = \overline{U}_1 + 2\pi \sum_{j=1}^{M} A_j G_s(\mathbf{x}; \mathbf{x}_j)\,, \tag{7.33}$$

where $G_s(\mathbf{x}; \mathbf{x}_j)$ is the surface Neumann Green's function of (3.29). By using the local behavior of G_s given in (3.31) in terms of geodesic coordinates, we obtain as $\mathbf{x} \to \mathbf{x}_i$ that for the resonant patches

$$U_1 \sim \frac{A_i}{\varepsilon|\mathbf{y}|} - \frac{A_i}{2}\log\left(\frac{\varepsilon}{2}\right) - \frac{A_i}{2}\left(\log(y_3 + |\mathbf{y}|) - \frac{y_3(y_1^2 + y_2^2)}{|\mathbf{y}|^3}\right) + \beta_{ci} + \overline{U}_1\,, \quad \text{for} \quad i = 1, \ldots, M\,. \tag{7.34a}$$

In (7.34a), we have defined β_{ci} as the i-th component of the vector $\boldsymbol{\beta}_c$ defined by

$$\boldsymbol{\beta}_c \equiv 2\pi \mathcal{G}_{sc} \mathbf{A}\,, \qquad \text{where} \qquad \mathbf{A} = (A_1, \ldots, A_M)^T\,. \tag{7.34b}$$

Here $\mathcal{G}_{sc}$ is the $M \times M$ Green's matrix representing long-range interactions over the resonant patches, defined by

$$\mathcal{G}_{sc} \equiv \begin{pmatrix} R_s & G_{12} & \cdots & G_{1M} \\ G_{21} & R_s & \cdots & G_{2M} \\ \vdots & \vdots & \ddots & \vdots \\ G_{M1} & \cdots & G_{M,M-1} & R_s \end{pmatrix}\,, \quad R_s \equiv -\frac{9}{20\pi}\,, \quad G_{ij} \equiv G_s(\mathbf{x}_i; \mathbf{x}_j)\,. \tag{7.34c}$$

In contrast, for the non-resonant patches, we have as $\mathbf{x} \to \mathbf{x}_i$ that

$$U_1 \sim \overline{U}_1 + 2\pi \sum_{j=1}^{M} A_j G_s(\mathbf{x}_i; \mathbf{x}_j)\,, \quad \text{for} \quad i = M+1, \ldots, N\,. \tag{7.35}$$

We observe upon comparing (7.34a) and (7.35) that the $\mathcal{O}(\log\varepsilon)$ term only occurs for the resonant patches. As a result, in the inner expansion (6.8) we conclude that $V_{1i} = 0$ for the non-resonant patches $i = M+1, \ldots, N$. Alternatively, for the resonant

patches $i = 1, \ldots, M$, we obtain from the matching condition between the inner and outer solutions that V_{1i} satisfies

$$\Delta_{\mathbf{y}} V_{1i} = 0\,, \quad \mathbf{y} \in \mathbb{R}^3_+\,, \tag{7.36a}$$

$$\partial_{y_3} V_{1i} + \sigma_0 V_{1i} = -\sigma_1 V_{0i}\,, \quad y_3 = 0\,,\ (y_1, y_2) \in \Gamma_c\,, \tag{7.36b}$$

$$\partial_{y_3} V_{1i} = 0\,, \quad y_3 = 0\,,\ (y_1, y_2) \notin \Gamma_c\,, \tag{7.36c}$$

$$V_{1i} \sim -\frac{A_i}{2} + \mathcal{O}(|\mathbf{y}|^{-1})\,, \quad \text{as} \quad |\mathbf{y}| \to \infty\,. \tag{7.36d}$$

To derive the solvability condition for (7.36), which will determine σ_1, we need the following lemma:

LEMMA 7.1. *Consider the inhomogeneous problem for $V(\mathbf{y})$ given by*

$$\Delta_{\mathbf{y}} V = 0\,, \quad \mathbf{y} \in \mathbb{R}^3_+\,, \tag{7.37a}$$

$$\partial_{y_3} V + \sigma_0 V = \mathcal{R}(y_1, y_2)\,, \quad y_3 = 0\,,\ (y_1, y_2) \in \Gamma_c\,, \tag{7.37b}$$

$$\partial_{y_3} V = 0\,, \quad y_3 = 0\,,\ (y_1, y_2) \notin \Gamma_c\,, \tag{7.37c}$$

$$V \sim V_\infty + \mathcal{O}(|\mathbf{y}|^{-1})\,, \quad \textit{as} \quad |\mathbf{y}| \to \infty\,, \tag{7.37d}$$

where V_∞ is a constant. A necessary and sufficient condition for (7.37) to have a solution is that

$$\int_{\Gamma_c} \tilde{\Psi}_{k'c} \mathcal{R}\, dy_1 dy_2 = 2\pi V_\infty\,, \tag{7.38}$$

where $\tilde{\Psi}_{k'c}$ is the unique solution to (7.27) with $\sigma_0 = \mu_{k'c}$. When (7.38) holds, the solution V is unique up to adding an arbitrary multiple of $\tilde{\Psi}_{k'c}$.

Proof. To prove the necessity of (7.38) we apply Green's second identity to V and $\tilde{\Psi}_{k'c}$ over a large hemisphere of radius R in the upper half-space to obtain

$$\int_{\mathbb{R}^3_+} \left(V \Delta_{\mathbf{y}} \tilde{\Psi}_{k'c} - \tilde{\Psi}_{k'c} \Delta_{\mathbf{y}} V \right) d\mathbf{y} = \int_{\Gamma_c} \left[\tilde{\Psi}_{k'c} \left(\partial_{y_3} V + \sigma_0 V \right) - V \left(\partial_{y_3} \tilde{\Psi}_{k'c} + \sigma_0 \tilde{\Psi_{k'c}} \right) \right] d\mathbf{y} \tag{7.39}$$

$$+ 2\pi \lim_{R \to \infty} R^2 \left(V \frac{\partial \tilde{\Psi}_{k'c}}{\partial |\mathbf{y}|} - \tilde{\Psi}_{k'c} \frac{\partial V}{\partial |\mathbf{y}|} \right) \Big|_{|\mathbf{y}| = R}\,.$$

Then, upon imposing the conditions (7.37b) and (7.27b) on the patches, together with using the far-field behaviors (7.37d) and (7.27d), we readily obtain that (7.39) reduces to (7.38). This proves the necessity of (7.38).

We now prove the sufficiency of (7.38). Since $\{\Psi_{kc}|_{\Gamma_c}\}$ form a complete orthonormal basis of $L^2(\Gamma_c)$, any harmonic function V in $\mathbb{R}^3_+$ that decays at infinity and satisfies the mixed Robin-Neumann conditions (7.37b) and (7.37c) can be represented in terms of the eigenfunctions Ψ_{kc}. In other words, a general solution V to (7.37) can be written as

$$V(\mathbf{y}) = V_\infty + \sum_{k=0}^{\infty} \nu_k\, \Psi_{kc}(\mathbf{y})\,, \tag{7.40}$$

with suitable coefficients ν_k. By construction, it satisfies (7.37a), (7.37c), and (7.37d). Substituting this representation into (7.37b), multiplying it by Ψ_{jc}, integrating over $\mathbf{y} \in \Gamma_c$ and using the orthonormality of $\{\Psi_{kc}\}$, we obtain that

$$\nu_j(\sigma_0 - \mu_{jc}) = \int_{\Gamma_c} (\mathcal{R}(\mathbf{y}) - \sigma_0 V_\infty)\Psi_{jc}(\mathbf{y})\, d\mathbf{y}\,. \tag{7.41}$$

Since $\sigma_0 = \mu_{k'c}$, we observe that we must have $\int_{\Gamma_c}(\mathcal{R}(\mathbf{y}) - \sigma_0 V_\infty)\Psi_{k'c}(\mathbf{y})\, d\mathbf{y} = 0$, which is equivalent to (7.38), as is readily seen by using the divergence theorem. When this condition holds, $\nu_{k'}$ remains undetermined (a free parameter). The other coefficients ν_j for any $j \neq k'$ are uniquely given by (7.41).

Finally, when (7.38) holds, the general solution V to (7.37) can be written as $V = V_p + B\tilde{\Psi}_{k'c}$, where B is an arbitrary constant and where V_p is the particular solution of (7.37) satisfying $V_p \sim V_\infty + \mathcal{O}(|\mathbf{y}|^{-2})$ as $|\mathbf{y}| \to \infty$. Since $\tilde{\Psi}_{k'c} \sim 1/|\mathbf{y}|$ as $|\mathbf{y}| \to \infty$, it follows that $V \sim V_\infty + B/|\mathbf{y}|$ as $|y| \to \infty$, where B is arbitrary. ∎

To determine σ_1 from (7.36) we simply apply the solvability condition (7.38) of Lemma 7.1 where we set $V_\infty = -A_i/2$, and $\mathcal{R} = -\sigma_1 V_{0i}$ with $V_{0i} = A_i\tilde{\Psi}_{k'c}$. In this way, by using (7.29), we readily determine in terms of $\mu_{k'c}$ and the weight $d_{k'c} = \int_{\Gamma_c}\Psi_{k'c}\, d\mathbf{y}$ that

$$\sigma_1 = \frac{\pi}{\int_{\Gamma_c}(\tilde{\Psi}_{k'c})^2\, d\mathbf{y}} = \frac{\mu_{k'c}^2 d_{k'c}^2}{4\pi}\,. \tag{7.42}$$

Without loss of generality, as shown in Lemma 7.1 we are free to impose that $V_{1i} \sim -A_i/2 + \mathcal{O}(|\mathbf{y}|^{-2})$ as $|\mathbf{y}| \to \infty$, which ensures that V_{1i} is unique. As a result, from the matching condition we obtain that the outer correction U_2 in (6.5) satisfies (6.6), with no singularities at any $\mathbf{x}_i$ for $i = 1, \ldots, N$. We conclude that $U_2 = \overline{U}_2$, where the constant $\overline{U}_2$ can only be obtained at higher order.

Next, we proceed to determine the SN eigenvalue correction σ_2. For the non-resonant patches $i = M+1, \ldots, N$, we set $V_{0i} = 0$ in (7.4) and use the local behavior (7.35) to derive that the inner correction V_{2i} satisfies

$$\Delta_{\mathbf{y}} V_{2i} = 0\,, \quad \mathbf{y} \in \mathbb{R}^3_+\,, \tag{7.43a}$$

$$\partial_{y_3} V_{2i} + \sigma_0 V_{2i} = 0\,, \quad y_3 = 0\,,\ (y_1, y_2) \in \Gamma_c\,, \tag{7.43b}$$

$$\partial_{y_3} V_{2i} = 0\,, \quad y_3 = 0\,,\ (y_1, y_2) \notin \Gamma_c\,, \tag{7.43c}$$

$$V_{2i} \sim \overline{U}_1 + 2\pi \sum_{j=1}^{M} A_j G_s(\mathbf{x}_i; \mathbf{x}_j)\,, \quad \text{as} \quad |\mathbf{y}| \to \infty\,. \tag{7.43d}$$

The solution to (7.43) for $i = M+1, \ldots, N$ is

$$V_{2i} = \left(\gamma_i + \overline{U}_1\right)\left(1 - w_i(\mathbf{y}; -\sigma_0)\right)\,, \quad \text{where} \quad \gamma_i \equiv 2\pi \sum_{j=1}^{M} A_j G_s(\mathbf{x}_i; \mathbf{x}_j)\,, \tag{7.44}$$

which has the far-field behavior

$$V_{2i} \sim \left(\gamma_i + \overline{U}_1\right)\left(1 - \frac{C_i(-\sigma_0)}{|\mathbf{y}|}\right)\,, \quad \text{as} \quad |\mathbf{y}| \to \infty\,, \quad i = M+1, \ldots, N\,. \tag{7.45}$$

In contrast, for the resonant patches $i = 1, \dots, M$, we obtain from (7.4), together with the $\mathcal{O}(1)$ terms in the local behavior (7.34a), that the inner correction V_{2i} satisfies

$$\Delta_{\mathbf{y}} V_{2i} = 2y_3 V_{0i,y_3y_3} + 2V_{0i,y_3}\,, \quad \mathbf{y} \in \mathbb{R}^3_+\,, \tag{7.46a}$$

$$\partial_{y_3} V_{2i} + \sigma_0 V_{2i} = -\sigma_2 V_{0i}\,, \quad y_3 = 0\,,\ (y_1, y_2) \in \Gamma_c\,, \tag{7.46b}$$

$$\partial_{y_3} V_{2i} = 0\,, \quad y_3 = 0\,,\ (y_1, y_2) \notin \Gamma_c\,, \tag{7.46c}$$

$$V_{2i} \sim \beta_{ci} + \overline{U}_1 - \frac{A_i}{2}\left[\log\left(y_3 + |\mathbf{y}|\right) - \frac{y_3(y_1^2 + y_2^2)}{|\mathbf{y}|^3}\right]\,, \ \text{as} \quad |\mathbf{y}| \to \infty\,. \tag{7.46d}$$

To derive the solvability condition for (7.46), we first need to decompose V_{2i} so as to account for the inhomogeneous term in the PDE (7.46a) as well as the term in the square bracket in (7.46d) in the far-field behavior. More specifically, and as very similar to the analysis in Lemma C.1 of Appendix C, we decompose V_{2i} as

$$V_{2i} = V_{2ip} + V_{2iH}\,, \tag{7.47}$$

where V_{2ip} is given explicitly in terms of $V_{0i} = A_i \tilde{\Psi}_{k'c}$ by

$$V_{2ip} = \frac{y_3^2}{2} V_{0i,y_3} + \frac{y_3}{2} V_{0i} - \frac{1}{2}\int_0^{y_3} V_{0i}(y_1, y_2, \eta)\, d\eta + A_i \mathcal{F}_c(y_1, y_2)\,, \tag{7.48}$$

where $\mathcal{F}_c$ is the unique solution to

$$\Delta_S \mathcal{F}_c = \left(\frac{1}{2}\partial_{y_3}\tilde{\Psi}_{k'c}|_{y_3=0}\right) I_{\Gamma_c}\,; \quad I_{\Gamma_c} \equiv \begin{cases} 1\,, & (y_1, y_2) \in \Gamma_c \\ 0\,, & (y_1, y_2) \notin \Gamma_c\,, \end{cases} \tag{7.49a}$$

$$\mathcal{F}_c \sim \left(\frac{1}{4\pi}\int_{\Gamma_c} \partial_{y_3}\tilde{\Psi}_{k'c}|_{y_3=0}\, d\mathbf{y}\right)\log\rho_0 + o(1)\,, \quad \text{as} \quad \rho_0 \equiv (y_1^2 + y_2^2)^{1/2} \to \infty\,, \tag{7.49b}$$

with $\Delta_S \mathcal{F}_c \equiv \mathcal{F}_{c,y_1y_1} + \mathcal{F}_{c,y_2y_2}$. By applying the divergence theorem to (7.27) we calculate $\int_{\Gamma_c} \partial_{y_3}\tilde{\Psi}_{k'c}|_{y_3=0}\, d\mathbf{y} = -2\pi$. In addition, upon using the relation (7.27b) on Γ_c the solution to (7.49) is written in terms of the free-space Green's function in the plane as

$$\mathcal{F}_c(\mathbf{y}) = -\frac{\mu_{k'c}}{4\pi}\int_{\Gamma_c} \tilde{\Psi}_{k'c}(\mathbf{y}')\log|\mathbf{y} - \mathbf{y}'|\, d\mathbf{y}'\,, \tag{7.50}$$

which satisfies $\mathcal{F}_c \sim -\frac{1}{2}\log\rho_0 + o(1)$ as $\rho_0 \to \infty$.

Then, by repeating a similar calculation as in the proof of Lemma C.1, we conclude that V_{2iH} in (7.47) for $i = 1, \dots, M$ satisfies

$$\Delta_{\mathbf{y}} V_{2iH} = 0\,, \quad \mathbf{y} \in \mathbb{R}^3_+\,, \tag{7.51a}$$

$$\partial_{y_3} V_{2iH} + \sigma_0 V_{2iH} = -\sigma_2 V_{0i} - \sigma_0 A_i \mathcal{F}_c\,, \quad y_3 = 0\,,\ (y_1, y_2) \in \Gamma_c\,, \tag{7.51b}$$

$$\partial_{y_3} V_{2iH} = 0\,, \quad y_3 = 0\,,\ (y_1, y_2) \notin \Gamma_c\,, \tag{7.51c}$$

$$V_{2iH} \sim \beta_{ci} + \overline{U}_1\,, \quad \text{as} \quad |\mathbf{y}| \to \infty\,. \tag{7.51d}$$

To determine σ_2 from (7.51) we simply apply the solvability condition (7.38) of Lemma 7.1 in which we set $V_\infty = \beta_{ci} + \overline{U}_1$ and $\mathcal{R} = -\sigma_2 V_{0i} - \sigma_0 A_i \mathcal{F}_c$ with $V_{0i} = A_i \tilde{\Psi}_{k'c}$. This yields for $i = 1, \ldots, M$ that

$$-2\pi\left(\beta_{ci} + \overline{U}_1\right) = A_i \left[\sigma_2 \int_{\Gamma_c} \left(\tilde{\Psi}_{k'c}\right)^2 d\mathbf{y} + \int_{\Gamma_c} \sigma_0 \tilde{\Psi}_{k'c}\, \mathcal{F}_c\, d\mathbf{y}\right], \tag{7.52}$$

where we identify $\sigma_0 \tilde{\Psi}_{k'c} = -\partial_{y_3} \tilde{\Psi}_{k'c}$ on Γ_c and $\int_{\Gamma_c} (\tilde{\Psi}_{k'c})^2\, d\mathbf{y} = \pi/\sigma_1$ from (7.42).

Finally, upon recalling (7.34b) for β_{ci} and the constraint (7.32), we obtain a matrix eigenvalue problem for $\mathbf{A} \equiv (A_1, \ldots, A_M)^T$ and the eigenvalue parameter α given by

$$\mathcal{G}_{sc}\mathbf{A} + \frac{\overline{U}_1}{2\pi}\mathbf{e}_M = \alpha \mathbf{A}\,, \qquad \mathbf{e}_M^T \mathbf{A} = 0\,, \tag{7.53a}$$

where $\mathbf{e}_M \equiv (1, \ldots, 1)^T \in \mathbb{R}^M$. Here σ_2 is related to α by

$$\sigma_2 = -\frac{\sigma_1}{\pi}\left[4\pi^2\alpha + \mathcal{J}\right], \tag{7.53b}$$

with $\mathcal{J}$ given by

$$\mathcal{J} \equiv \int_{\Gamma_c} \sigma_0\, \tilde{\Psi}_{k'c} \mathcal{F}_c\, d\mathbf{y} = -\frac{\mu_{k'c}^2}{4\pi} \int_{\Gamma_c}\int_{\Gamma_c} \tilde{\Psi}_{k'c}(\mathbf{y})\, \tilde{\Psi}_{k'c}(\mathbf{y}')\, \log|\mathbf{y} - \mathbf{y}'|\, d\mathbf{y}\, d\mathbf{y}'\,, \tag{7.53c}$$

where in the last equality, we used $\sigma_0 = \mu_{k'c}$ and (7.50). By using (7.28), this relation can also be written in terms of the conventionally normalized eigenfunction $\Psi_{k'c}$ as

$$\mathcal{J} = -\frac{\pi}{d_{k'c}^2} \int_{\Gamma_c}\int_{\Gamma_c} \Psi_{k'c}(\mathbf{y})\, \Psi_{k'c}(\mathbf{y}')\, \log|\mathbf{y} - \mathbf{y}'|\, d\mathbf{y}\, d\mathbf{y}'\,, \tag{7.53d}$$

where $d_{k'c} = \int_{\Gamma_c} \Psi_{k'c}\, d\mathbf{y}$. This relation shows that $\mathcal{J}$, and thus the associated correction σ_2 to the SN eigenvalue, are independent of the normalization of $\Psi_{k'c}$.

Since $V_{0i} = A_i \tilde{\Psi}_{k'c}$ for $i = 1, \ldots, M$ and $V_{0i} = 0$ for $i = M+1, \ldots, N$, the PDE normalization condition (7.1) provides the following normalization condition for the matrix eigenvalue problem (7.53):

$$\mathbf{A}^T\mathbf{A} = \sum_{j=1}^{M} A_j^2 \sim \frac{1}{\varepsilon \int_{\Gamma_c} [\tilde{\Psi}_{k'c}]^2\, d\mathbf{y}}\,. \tag{7.53e}$$

By taking the inner product of (7.53a) with $\mathbf{e}_M$, we can isolate $\overline{U}_1$ as

$$\overline{U}_1 = -\frac{2\pi}{M}\mathbf{e}_M^T \mathcal{G}_{sc}\mathbf{A}\,, \tag{7.54}$$

where $\mathbf{A}$ and α is an eigenpair of the $M \times M$ matrix problem

$$\left(\mathbf{I} - \frac{\mathbf{e}_M \mathbf{e}_M^T}{M}\right)\mathcal{G}_{sc}\mathbf{A} = \alpha\mathbf{A}\,, \quad \text{with} \quad \mathbf{e}_M^T\mathbf{A} = 0\,, \tag{7.55}$$

with normalization (7.53e). Here $\mathbf{I}$ is the $M \times M$ identity matrix.

We complete our analysis by deriving the problem for the outer correction U_3 in (6.5), which satisfies (6.6) with singularity conditions at the patch locations. For the resonant patches, as discussed in the proof of Lemma (7.1), we can impose that $V_{2iH} \sim \beta_{ci} + \overline{U}_1 + B_i/|\mathbf{y}|$ as $|\mathbf{y}| \to \infty$, where B_i for $i = 1, \ldots, M$ are unknown constants. For the non-resonant patches, we have that (7.45) provides the singularity behavior for U_3. In this way, we obtain that U_3 satisfies

$$
\begin{aligned}
&\Delta_{\mathbf{x}} U_3 = 0\,, \quad \mathbf{x} \in \Omega\,; \quad \partial_n U_3 = 0\,, \quad \mathbf{x} \in \partial\Omega \backslash \{\mathbf{x}_1, \ldots, \mathbf{x}_N\}\,, \\
&U_3 \sim -\frac{\left(\gamma_i + \overline{U}_1\right) C_i(-\sigma_0)}{|\mathbf{x} - \mathbf{x}_i|}\,, \quad \text{as} \quad \mathbf{x} \to \mathbf{x}_i\,, \quad i = M+1, \ldots, N, \\
&U_3 \sim \frac{B_i}{|\mathbf{x} - \mathbf{x}_i|}\,, \quad \text{as} \quad \mathbf{x} \to \mathbf{x}_i\,, \quad i = 1, \ldots, M\,.
\end{aligned}
\tag{7.56}
$$

The solvability condition for (7.56) provides one equation for $(B_1, \ldots, B_M)^T$:

$$
\sum_{i=1}^{M} B_i = \sum_{i=M+1}^{N} \left(\gamma_i + \overline{U}_1\right) C_i(-\sigma_0)\,,
\tag{7.57}
$$

where γ_i is defined in (7.44). A higher-order analysis can in principle be undertaken to determine a matrix system for $(B_1, \ldots, B_M)^T$.

We summarize our result in the following proposition.

PROPOSITION 5. *Suppose that there are exactly M identical patches, with $2 \le M \le N$, with a common patch shape $\partial\Omega_c^\varepsilon = \partial\Omega_i^\varepsilon$ for $i = 1, \ldots, M$. Let $\{\mu_{kc}\}_{k\ge 0}$ be the spectrum of the local Steklov problem (D.1) of Appendix D on the local common patch $\Gamma_c \asymp \varepsilon^{-1}\partial\Omega_c^\varepsilon$. Then, for any $k \ge 0$ such that $d_{kc} \neq 0$, the Steklov-Neumann (SN) problem (2.12) has $M-1$ eigenvalues $\sigma(\varepsilon)$ (counting multiplicity) for which $\sigma_0 = \lim_{\varepsilon\to 0} \sigma(\varepsilon) = \mu_{kc}$, where μ_{kc} is assumed to be simple. A three-term expansion for these eigenvalues is*

$$
\sigma = \sigma_0 + \varepsilon \log\left(\frac{\varepsilon}{2}\right)\sigma_1 + \varepsilon\sigma_2 + \mathcal{O}(\varepsilon^2 \log\varepsilon)\,,
\tag{7.58}
$$

where σ_1 is given in (7.42) and σ_2 is related via (7.53b) to $M-1$ eigenpairs α and $\mathbf{A} = (A_1, \ldots, A_M)^T$ of the matrix eigenvalue problem (7.55), with normalization condition (7.53e). Moreover, the local behavior of the eigenfunctions on the resonant and non-resonant patches are

$$
\begin{aligned}
&u|_{\Gamma_i} = A_i \tilde{\Psi}_{k'c} + \mathcal{O}(\varepsilon)\,, \quad i = 1, \ldots, M\,, \\
&u|_{\Gamma_i} \sim \varepsilon\left(\gamma_i + \overline{U}_1\right)\left(1 - w_i(\mathbf{y}; -\sigma_0)\right)\,, \quad i = M+1, \ldots, N\,,
\end{aligned}
\tag{7.59}
$$

where $\tilde{\Psi}_{k'c}$ satisfies (7.27). In (7.59), $\overline{U}_1$ and γ_i are defined in (7.54) and (7.44), respectively. In the outer region, the SN eigenfunction is given by

$$
u = \varepsilon\left(\overline{U}_1 + 2\pi \sum_{j=1}^{M} A_j G_s(\mathbf{x}; \mathbf{x}_j)\right) + \mathcal{O}(\varepsilon^2)\,.
\tag{7.60}
$$

We emphasize that in our analysis of this near-resonant case, the eigenvalue corrections σ_1 and σ_2 are obtained upon applying solvability conditions to the inner problems defined near the resonant patches. For the non-resonant case studied in

§7.1, these correction terms were found from solvability conditions on the outer solution. Moreover, in contrast to our main result in Proposition 4 for the non-resonant case, we observe that the SN eigenfunctions for this near-resonant case are concentrated primarily on the resonant patches and that the outer solution in (7.60) is now $\mathcal{O}(\varepsilon)$ smaller than that for the non-resonant case.

The results in Proposition 5 for σ_1 and σ_2 can be simplified for the special case where the common patch shape Γ_c is a disk of radius one ($a_c = 1$), for which $\tilde{\Psi}_{k'c}$ and $\partial_{y_3}\tilde{\Psi}_{k'c}$, depend only on $\rho_0 = (y_1^2 + y_2^2)^{1/2}$ when $y_3 = 0$ and $(y_1, y_2) \in \Gamma_c$. In this special case, where $\mathcal{F}_c = \mathcal{F}_c(\rho_0)$, we write $\mathcal{J}$ in (7.53c) as

$$\mathcal{J} = 2\pi\sigma_0 \int_0^1 \rho_0 \tilde{\Psi}_{k'c}\, \mathcal{F}_c(\rho_0)\, d\rho_0\,. \tag{7.61}$$

Since the problem (7.49) for $\mathcal{F}_c$ is radially symmetric, we find that its first integral is $\rho_0 \mathcal{F}_{c\rho_0} = -\frac{\sigma_0}{2}\int_0^{\rho_0} \eta\tilde{\Psi}_{k'c}(\eta)\, d\eta$ for $0 < \rho_0 < 1$. Upon integrating (7.61) by parts, we use this first integral together with $\mathcal{F}_c(1) = 0$ and $\sigma_0 = \mu_{k'c}$, to conclude that

$$\mathcal{J} = \pi\mu_{k'c}^2 \int_0^1 \frac{1}{\rho_0}\left(\int_0^{\rho_0} \eta\tilde{\Psi}_{k'c}(\eta)\, d\eta\right)^2 d\rho_0\,, \tag{7.62a}$$

$$= \frac{4\pi^3}{d_{k'c}^2} \int_0^1 \frac{1}{\rho_0}\left(\int_0^{\rho_0} \eta\Psi_{k'c}(\eta)\, d\eta\right)^2 d\rho_0\,, \tag{7.62b}$$

where we used (7.28) in the second equality.

7.4. Numerical Comparison. We now consider two examples of our theory for the near-resonant case.

Example I: We first apply our theory to Example II of §7.2 for two identical anti-podal circular patches of radius ε centered at the north and south poles, for which $M = N = 2$ and $a_1 = a_2 = 1$. For such anti-podal patches centered at $\mathbf{x}_1 = (0, 0, 1)$ and $\mathbf{x}_2 = (0, 0, -1)$, the 2×2 Green's matrix $\mathcal{G}_{sc}$ in (7.34c) is circulant symmetric and so the only eigenpair of (7.55) is $\mathbf{A} = A_c(1, -1)^T$ and $\alpha = R_s - G_s(\mathbf{x}_1; \mathbf{x}_2)$, where A_c is a normalization constant. Upon using $R_s = -9/(20\pi)$ and (3.29) for $G_s(\mathbf{x}_1; \mathbf{x}_2)$, we calculate that $\alpha = (\log 2 - 1)/(4\pi)$. By inserting the superscript $^{(k)}$ to distinguish asymptotics for different eigenvalues, we conclude from (7.58) and (7.53b) that there are SN eigenvalues of (2.12) for each $k \geq 0$ given by

$$\sigma(\varepsilon) \sim \mu_{kc} + \varepsilon \log\left(\frac{\varepsilon}{2}\right)\sigma_1^{(k)} - \frac{\varepsilon\sigma_1^{(k)}}{\pi}\left[\pi(\log 2 - 1) + \mathcal{J}^{(k)}\right] + \ldots\,, \tag{7.63}$$

where $\sigma_1^{(k)}$ and $\mathcal{J}^{(k)}$ are given by (7.42) and (7.62), respectively. The numerical values for some local Steklov eigenvalues μ_{kc} and their weights d_{kc} are given in Table D.1 of Appendix D.2. These values can be used to calculate $\sigma_1^{(k)}$ from (7.42).

To illustrate the accuracy of the three-term expansion (7.63), we employ the accurate numerical method from Appendix F to compute the numerical values $\sigma_{\text{num}}^{(j)}$, enumerated by the index $j = 1, 2, 3, \ldots$, that are considered as benchmarks (we recall that these SN eigenvalues correspond to axially symmetric eigenfunctions). Figure 7.3 presents the difference between $\sigma_{\text{num}}^{(j)}$ with $j = 1, 3, 5$, and the three-term expansion (7.63) for near-resonant SN eigenvalues with indices $k = 1, 2, 3$. We also present the difference between $\sigma_{\text{num}}^{(j)}$ with $j = 2, 4$, and the asymptotic values given by (7.25) for non-resonant eigenvalues for a single patch with indices $k = 1, 2$. In both cases, the

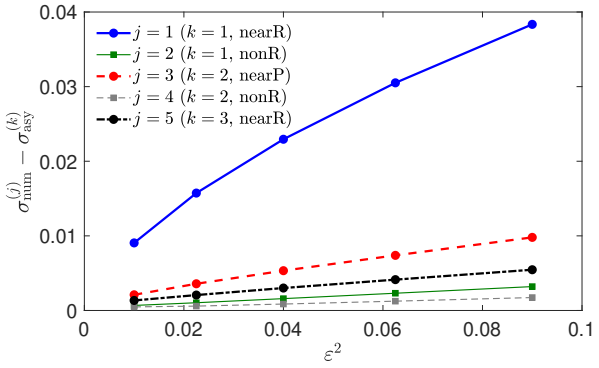

Fig. 7.3: Validation of the three-term expansions for the SN eigenvalues (that correspond to axially symmetric eigenfunctions) in the case of two identical circular patches of radius ε located at the north and south poles of the unit sphere. The difference between the numerical values $\sigma^{(j)}_{\rm num}$ obtained by the method in Appendix F with truncation order $n_{\max} = 2000$, and the asymptotic values $\sigma^{(k)}_{\rm asy}$ given by (7.63) for near-resonant eigenvalues with $k = 1, 2, 3$ and by (7.25) for non-resonant eigenvalues with $k = 1, 2$.

difference is shown as a function of ε^2 to outline the correct form of the asymptotic relations. We can therefore conclude that these relations are very accurate. We also observe that the asymptotic relation for the first (nontrivial) eigenvalue $\sigma^{(1)}$ is the least accurate. Note also that the asymptotic relations for non-resonant eigenvalues are more accurate than those for near-resonant ones.

Example II: Next, we suppose that we have N identical circular patches of a common radius ε (i.e., all $a_i = 1$), with centers located at the vertices of one of the five largest platonic solids that can be inscribed within the unit sphere. For this spatial configuration of patches, where $M = N$ and $N \in \{4, 6, 8, 12, 20\}$, the Green's matrix $\mathcal{G}_{sc}$ is symmetric with a constant row sum, so that $\mathcal{G}_{sc}\mathbf{e}_M = \alpha_M \mathbf{e}_M$. Note that this matrix is in general not circulant. It follows that, up to a normalization condition, the $N - 1$ mutually orthogonal solutions to (7.55) are

$$\mathbf{A}_j = \mathbf{q}_j\,, \quad \text{where} \quad \mathcal{G}_{sc}\mathbf{q}_j = \alpha_j \mathbf{q}_j\,, \quad \mathbf{q}_j^T \mathbf{e}_M = 0 \quad \text{for} \quad j = 2, \ldots, N\,. \tag{7.64}$$

In addition, we obtain from (7.54), that we must have $\overline{U}_1 = 0$ in (7.60). We conclude from (7.58) and (7.53b) that, for each $k \geq 0$, there are $(N - 1)$ SN eigenvalues of (2.12), enumerated by $j = 1, \ldots, N - 1$, given by

$$\sigma(\varepsilon) \sim \mu_{kc} + \varepsilon \log\left(\frac{\varepsilon}{2}\right)\sigma_1^{(k)} - \frac{\varepsilon\sigma_1^{(k)}}{\pi}\left(4\pi^2\alpha_j + \mathcal{J}^{(k)}\right) + \ldots\,, \quad j = 2, \ldots, N\,. \tag{7.65}$$

We remark that $\sigma_1^{(k)}$ and $\mathcal{J}^{(k)}$, as given by (7.42) and (7.62a) respectively, are independent of N and of the locations of the vertices. In this way, determining a three-term expansion for the $(N - 1)$ SN eigenvalues that are in near-resonance with an eigenvalue μ_{kc} of the local Steklov problem reduces to simply finding all of the eigenpairs of the Green's matrix $\mathcal{G}_{sc}$ that are orthogonal to $\mathbf{e}_M$.

In addition, from our analysis in §7.1, we observe from our main result in Proposition 4 that all non-resonant eigenvalues are close to roots of $C(-\sigma_0) = 0$. These roots

are the eigenvalues μ_k^N of the local Steklov eigenvalue problem (D.30) of Appendix D.4 satisfying the far-field Neumann condition (D.30d). In this case, the expansion (7.23a) is independent of the vertex locations of the platonic solids and reduces to

$$\sigma(\varepsilon) \sim \mu_k^N + \varepsilon \frac{E(-\mu_k^N)}{C'(-\mu_k^N)} + \cdots , \tag{7.66}$$

which is the same result derived in Example I of §7.2 for a single Steklov patch.

8. Discussion. In a three-dimensional spherical domain, we have developed and implemented a unified theoretical approach, based on the method of matched asymptotic expansions combined with spectral theory, to analyze the mean first-reaction time (MFRT), the splitting probability, the Steklov-Dirichlet-Neumann (SDN) problem, and the Steklov-Neumann (SN) problem for a collection of small partially reactive patches of arbitrary shape located on the boundary of a sphere. For the MFRT, our analysis extends that of [30] where only perfectly reactive and locally circular patches were considered. In each case, our three-term asymptotic results in the small-patch limit have been favorably compared with full numerical results.

We now discuss a few open problems that are directly related to our study. Firstly, it would be worthwhile to develop an accurate numerical scheme, such as in [89] and [76] for the exterior problem, to validate the homogenization result (4.53) for the effective reactivity k_{eff} for a large collection of small, but equi-distributed, patches on the boundary of a sphere. Secondly, our analysis has been focused only on problems that are *interior* to the sphere. In the companion article [63], we derive the effective reactivity rate for the *exterior* problem where there is a large number of equi-distributed partially reactive surface patches of arbitrary shape, but with small area, on the boundary of a sphere. This analysis extends that of [87] where an effective Robin boundary condition was derived for the case of perfectly reacting but locally circular boundary patches. In turn, it would be worthwhile to analyze the SDN and SN problems *exterior* to a sphere that has a collection of small partially reactive surface patches. Thirdly, our analysis of the SDN and SN problems has left open a few technical issues. In particular, our analysis has provided only the leading-order term for the Steklov eigenparameter for the special case where the corresponding eigenfunction is not axially-symmetric on a circular patch. In addition, for the SN problem, in §7.3 we have only analyzed in detail the *near-resonant* case that will occur when a subset of the patches are identical. We did not provide a similar analysis to investigate *near-resonance* behavior in other, less generic, situations, involving non-identical patches, or when the local Steklov eigenvalue problem near a patch has non-degenerate eigenvalues.

As we stated earlier, the leading-order terms of the derived asymptotic expansions are independent of the actual shape of the bounded domain and thus readily applicable to an arbitrary bounded 3-D domain Ω with a smooth boundary $\partial\Omega$ that contains a collection of N partially reactive surface patches. An important, but completely open, direction is to provide a higher-order asymptotic analysis of our four problems in this more general situation. In this extension, the following surface Neumann Green's function with singularity $\mathbf{x}_i \in \partial\Omega$ plays a key role:

$$\Delta_{\mathbf{x}} G_s = \frac{1}{|\Omega|}, \quad \mathbf{x} \in \Omega; \quad \partial_n G_s = \delta(\mathbf{x} - \mathbf{x}_i), \quad \mathbf{x} \in \partial\Omega; \quad \int_\Omega G_s \, d\mathbf{x} = 0. \tag{8.1a}$$

The local behavior near the singularity $\mathbf{x}_i \in \partial\Omega$ is [110]

(8.1b)
$$G_s(\mathbf{x};\mathbf{x}_i) \sim \frac{1}{2\pi|\mathbf{x}-\mathbf{x}_i|} - \frac{H_i}{4\pi}\log\left[|\mathbf{x}-\mathbf{x}_i| - \hat{n}\cdot(\mathbf{x}-\mathbf{x}_i)\right] + R_i + o(1)\,, \quad \text{as} \quad \mathbf{x}\to\mathbf{x}_i\,,$$

where H_i is the mean curvature to $\partial\Omega$ at $\mathbf{x}=\mathbf{x}_i$ (with $H_i=1$ for the unit sphere), and where the constant R_i is the regular part. Two key challenges are that analytical solutions for G_s are not known for non-spherical domains and that an efficient numerical scheme to compute G_s and R_i is difficult owing to the intricate singularity behavior (8.1b) and the need to ensure the global condition $\int_\Omega G_s\,d\mathbf{x}=0$.

However, by adopting an orthogonal curvilinear coordinate system near each patch, inner problems very similar to that derived for the MFRT in a sphere using geodesic normal coordinates will be obtained. From a preliminary asymptotic analysis of the MFRT satisfying (2.8) in an arbitrary 3-D domain with smooth boundary, we can readily derive a two-term asymptotic expansion for $\overline{u}$ in the form

$$\overline{u} \sim \frac{|\Omega|}{2\pi\overline{C}\varepsilon}\left(1 - \left(\frac{1}{2\overline{C}}\sum_{i=1}^{N} H_i C_i^2\right)\varepsilon\log\varepsilon + \mathcal{O}(\varepsilon)\right)\,, \tag{8.2}$$

where $\overline{C}=\sum_{i=1}^{N} C_i$ and $C_i = C_i(\kappa_i)$ is the local reactive capacitance of the i-th patch. It is an open problem to extend this calculation for the volume-average MFRT to higher order, and to undertake a similar approach to calculate the splitting probability and to analyze the SDN and SN problems in an arbitrary 3-D domain.

Acknowledgements. D.S.G. acknowledges the Simons Foundation for supporting his sabbatical sojourn in 2024 at the CRM (CNRS – University of Montréal, Canada), and the Alexander von Humboldt Foundation for support within a Bessel Prize award. M.J.W. was supported by the NSERC Discovery grant program. We are grateful to Prof. Sean Lawley of the University of Utah for discussions related to the sigmoidal approximation in (3.17).

Appendix A. Geodesic Normal Coordinates to the Unit Sphere Ω.

We define geodesic normal coordinates $\xi=(\xi_1,\xi_2,\xi_3)^T \in (-\pi/2,\pi/2)\times(-\pi,\pi)\times[0,1]$ in $\Omega\cup\partial\Omega$ so that $\xi=0$ corresponds to $\mathbf{x}_i\in\partial\Omega$, with $\xi_3>0$ corresponding to the interior of Ω. Geodesics on $\partial\Omega$ are obtained by setting $\xi_3=0$ and fixing either $\xi_1=0$ or $\xi_2=0$. In terms of the spherical angles $\theta_i\in(0,\pi)$ and $\varphi_i\in[0,2\pi)$ (see Fig. 2.1(b)), and for $|\mathbf{x}_i|=1$, we define the orthonormal vectors

(A.1)
$$\mathbf{x}_i \equiv \begin{bmatrix}\cos\varphi_i\,\sin\theta_i\\ \sin\varphi_i\,\sin\theta_i\\ \cos\theta_i\end{bmatrix}\,,\quad \mathbf{v}_{2i}=\partial_\theta\mathbf{x}_i \equiv \begin{bmatrix}\cos\varphi_i\,\cos\theta_i\\ \sin\varphi_i\,\cos\theta_i\\ -\sin\theta_i\end{bmatrix}\,,\quad \mathbf{v}_{3i}=\mathbf{x}_i\times\partial_\theta\mathbf{x}_i \equiv \begin{bmatrix}-\sin\varphi_i\\ \cos\varphi_i\\ 0\end{bmatrix}\,.$$

The vectors $\mathbf{v}_{2i}$ and $\mathbf{v}_{3i}$ span the tangent plane to the sphere at $\mathbf{x}=\mathbf{x}_i$. We now define the geodesic normal coordinates $\xi=(\xi_1,\xi_2,\xi_3)^T$ by the global transformation

$$\mathbf{x}(\xi) = (1-\xi_3)\left(\cos\xi_1\,\cos\xi_2\,\mathbf{x}_i + \cos\xi_1\,\sin\xi_2\,\mathbf{v}_{2i} + \sin\xi_1\mathbf{v}_{3i}\right)\,. \tag{A.2}$$

We observe that ξ_3 measures the distance of $\mathbf{x}$ to $\partial\Omega$. The curves obtained by setting $\xi_3=0$, and fixing either $\xi_2=0$ or $\xi_1=0$ are, respectively, $\mathbf{x}(\xi_1,0,0)=\cos\xi_1\,\mathbf{x}_i+\sin\xi_1\,\mathbf{v}_{3i}$ or $\mathbf{x}(0,\xi_2,0)=\cos\xi_2\,\mathbf{x}_i+\sin\xi_2\,\mathbf{v}_{2i}$, which correspond to intersections of $\partial\Omega$ with planes spanned by $\{\mathbf{x}_i,\mathbf{v}_{3i}\}$ or $\{\mathbf{x}_i,\mathbf{v}_{2i}\}$, respectively.

To transform the Laplacian from cartesian to geodesic coordinates, we use (A.2) to calculate the scale factors $h_{\xi_j} \equiv |\partial \mathbf{x}/\partial \xi_j|$ for $j = 1, 2, 3$ as

$$h_{\xi_1} = (1-\xi_3)\,, \qquad h_{\xi_2} = (1-\xi_3)\cos\xi_1\,, \qquad h_{\xi_3} = 1\,. \tag{A.3}$$

For the transformation of a generic function $\mathcal{V}(\xi) \equiv u\left(\mathbf{x}(\xi)\right)$, we calculate that

$$\begin{aligned}\Delta_{\mathbf{x}} u &= \frac{1}{h_{\xi_1}h_{\xi_2}h_{\xi_3}}\left[\frac{\partial}{\partial\xi_1}\left(\frac{h_{\xi_2}h_{\xi_3}}{h_{\xi_1}}\mathcal{V}_{\xi_1}\right) + \frac{\partial}{\partial\xi_2}\left(\frac{h_{\xi_1}h_{\xi_3}}{h_{\xi_2}}\mathcal{V}_{\xi_2}\right) + \frac{\partial}{\partial\xi_3}\left(\frac{h_{\xi_1}h_{\xi_2}}{h_{\xi_3}}\mathcal{V}_{\xi_3}\right)\right]\,,\\ &= \frac{(1-\xi_3)^{-2}}{\cos\xi_1}\left[\frac{\partial}{\partial\xi_3}\left((1-\xi_3)^2\cos\xi_1\mathcal{V}_{\xi_3}\right) + \frac{\partial}{\partial\xi_1}\left(\cos\xi_1\mathcal{V}_{\xi_1}\right) + \frac{\partial}{\partial\xi_2}\left(\frac{1}{\cos\xi_1}\mathcal{V}_{\xi_2}\right)\right]\,,\end{aligned}$$

which yields

$$\Delta_{\mathbf{x}} u = \mathcal{V}_{\xi_3\xi_3} - \frac{2}{1-\xi_3}\mathcal{V}_{\xi_3} + \frac{1}{(1-\xi_3)^2\cos^2\xi_1}\mathcal{V}_{\xi_2\xi_2} + \frac{1}{(1-\xi_3)^2\cos\xi_1}\frac{\partial}{\partial_{\xi_1}}\left(\cos\xi_1\mathcal{V}_{\xi_1}\right)\,. \tag{A.4}$$

Next, by introducing the inner, or local variables, $\mathbf{y} = (y_1, y_2, y_3)^T$, defined by

$$\xi_1 = \varepsilon y_1\,, \qquad \xi_2 = \varepsilon y_2\,, \qquad \xi_3 = \varepsilon y_3\,, \tag{A.5}$$

we use the Taylor approximations $(1-\xi_3)^{-1} \sim 1 + \varepsilon y_3$, $(1-\xi_3)^{-2} \sim 1 + 2\varepsilon y_3$, $\cos^2\xi_1 = 1 + \mathcal{O}(\varepsilon^2)$ and $\sin\xi_1 \sim \varepsilon y_1$. We readily obtain that (A.4) reduces to (3.2).

To determine a two-term approximation for the Euclidian distance $|\mathbf{x} - \mathbf{x}_i|$ near the patch, we use (A.5) in (A.2). From a Taylor series approximation we obtain that

$$\mathbf{x} - \mathbf{x}_i = \varepsilon\mathbf{b}_0 - \varepsilon^2\mathbf{b}_1 + \mathcal{O}(\varepsilon^3)\,, \qquad |\mathbf{x} - \mathbf{x}_i|^2 = \varepsilon^2\mathbf{b}_0^T\mathbf{b}_0 - 2\varepsilon^3\mathbf{b}_0^T\mathbf{b}_1 + \mathcal{O}(\varepsilon^4)\,, \tag{A.6a}$$

where $\mathbf{b}_0$ and $\mathbf{b}_1$ are defined by

$$\mathbf{b}_0 = -y_3\mathbf{x}_i + y_2\mathbf{v}_{2i} + y_1\mathbf{v}_{3i}\,, \qquad \mathbf{b}_1 = \frac{1}{2}\left(y_1^2 + y_2^2\right)\mathbf{x}_i + y_3y_2\mathbf{v}_{2i} + y_3y_1\mathbf{v}_{3i}\,. \tag{A.6b}$$

By calculating $\mathbf{b}_0^T\mathbf{b}_0 = y_1^2 + y_2^2 + y_3^2 \equiv \rho^2$ and $\mathbf{b}_0^T\mathbf{b}_1 = y_3\left(y_1^2 + y_2^2\right)/2$, we get

$$|\mathbf{x}-\mathbf{x}_i| \sim \varepsilon\rho - \frac{\varepsilon^2 y_3}{2\rho}\left(y_1^2 + y_2^2\right) + \mathcal{O}(\varepsilon^3)\,, \quad \frac{1}{|\mathbf{x}-\mathbf{x}_i|} \sim \frac{1}{\varepsilon\rho}\left(1 + \frac{\varepsilon y_3}{2\rho^2}(y_1^2 + y_2^2) + \mathcal{O}(\varepsilon^2)\right)\,. \tag{A.7}$$

In matrix form, and to leading order in ε, we can write (A.6) in terms of $\mathbf{y} = (y_1, y_2, y_3)^T$ and an orthogonal matrix $\mathcal{Q}_i$ as

$$\mathbf{y} \sim \varepsilon^{-1}\mathcal{Q}_i^T(\mathbf{x} - \mathbf{x}_i)\,, \quad \text{where} \quad \mathcal{Q}_i \equiv \begin{bmatrix} | & | & | \\ \mathbf{v}_{3i} & \mathbf{v}_{2i} & -\mathbf{x}_i \\ | & | & | \end{bmatrix} \quad \rightarrow \quad |\mathbf{y}| \sim \varepsilon^{-1}|\mathbf{x} - \mathbf{x}_i|\,. \tag{A.8}$$

Since $|\mathbf{x}-\mathbf{x}_i| = \varepsilon\rho + \mathcal{O}(\varepsilon^3)$ when $y_3 = 0$ from (A.7) it follows that for a locally circular Robin patch $\partial\Omega_i^\varepsilon$, we have in terms of local geodesic coordinates that $\left(y_1^2 + y_2^2\right)^{1/2} \leq a + \mathcal{O}(\varepsilon^2)$. Moreover, since the scale factor is $h_{\xi_3} = 1$, the Robin boundary condition on a circular patch is well-approximated in the local geodesic coordinates by

$$-\partial_{y_3}U + \kappa U = 0\,, \qquad \text{for} \quad y_3 = 0\,,\ (y_1^2 + y_2^2)^{1/2} \leq a\,.$$

Finally, by using the scale factors (A.3), the surface area element on the unit sphere, as needed in (6.1), is $d\mathbf{s} = h_{\xi_1} h_{\xi_2}|_{\xi_3=0} d\xi_1 d\xi_2 = \cos(\xi_1) d\xi_1 d\xi_2$.

Appendix B. Asymptotic Behavior of $C_i(\kappa_i)$ as $\kappa_i \ll 1$ for the Disk.

We derive (3.19) of Lemma 3.1 for a disk-shaped patch of radius a_i. To do so, we first introduce $\mathcal{W}(\mathbf{y})$ by

$$w_i(\mathbf{y}) = 1 - C_i \mathcal{W}(\mathbf{y}) \,, \tag{B.1}$$

so that, upon dropping the subscript i, we obtain from (3.3) that $\mathcal{W}$ satisfies

$$\Delta_{\mathbf{y}} \mathcal{W} = 0 \,, \quad \mathbf{y} \in \mathbb{R}^3_+ \,, \tag{B.2a}$$

$$-\partial_{y_3} \mathcal{W} + \kappa \mathcal{W} = 0 \,, \quad y_3 = 0 \,, \, (y_1, y_2) \in \Gamma \,, \tag{B.2b}$$

$$\partial_{y_3} \mathcal{W} = 0 \,, \quad y_3 = 0 \,, \, (y_1, y_2) \notin \Gamma \,, \tag{B.2c}$$

$$\mathcal{W} \sim B(\kappa) - \frac{1}{|\mathbf{y}|} + \ldots \,, \quad \text{as} \quad |\mathbf{y}| \to \infty \,, \tag{B.2d}$$

where the neglected term in (B.2d) is a dipole and where $B(\kappa)$ is related to $C(\kappa)$ by

$$C(\kappa) = \frac{1}{B(\kappa)} \,. \tag{B.3}$$

Here Γ is a disk of radius a. By applying the divergence theorem over the hemisphere $\Omega_R = \{\mathbf{y} = (y_1, y_2, y_3) \,|\, |\mathbf{y}| \le R \,, \, y_3 \ge 0\}$, with boundary $\partial\Omega_R$, we get from (B.2d) that

$$\lim_{R\to\infty} \int_{\partial\Omega_R} \partial_n \mathcal{W} \, d\mathbf{s} = 2\pi \,, \tag{B.4}$$

where ∂_n denotes the outward normal derivative to $\partial\Omega_R$.

For $\kappa \ll 1$, we expand the solution to (B.2) as

$$\mathcal{W} = \frac{b_0}{\kappa} + (\mathcal{W}_1 + b_1) + \kappa \, (\mathcal{W}_2 + b_2) + \kappa^2 \, (\mathcal{W}_2 + b_3) + \ldots \,. \tag{B.5}$$

We substitute (B.5) into (B.2) and collect powers of κ. At leading-order, we choose b_0 so that $\mathcal{W}_1$ satisfies

$$\Delta_{\mathbf{y}} \mathcal{W}_1 = 0 \,, \quad \mathbf{y} \in \mathbb{R}^3_+ \,, \tag{B.6a}$$

$$\partial_{y_3} \mathcal{W}_1 = b_0 \,, \quad y_3 = 0 \,, \, (y_1, y_2) \in \Gamma \,, \tag{B.6b}$$

$$\partial_{y_3} \mathcal{W}_1 = 0 \,, \quad y_3 = 0 \,, \, (y_1, y_2) \notin \Gamma \,, \tag{B.6c}$$

$$\lim_{R\to\infty} \int_{\partial\Omega_R} \partial_n \mathcal{W}_1 \, d\mathbf{s} = 2\pi \,, \qquad \mathcal{W}_1 \sim -\frac{1}{|\mathbf{y}|} + o(1) \,, \quad \text{as} \quad |\mathbf{y}| \to \infty \,. \tag{B.6d}$$

The $o(1)$ condition in (B.6d) determines $\mathcal{W}_1$ uniquely. By applying the divergence theorem to (B.6) over Ω_R, we let $R \to \infty$ to obtain $2\pi - b_0 \pi a^2 = 0$, so that

$$b_0 = \frac{2}{a^2} \,. \tag{B.7}$$

At higher order in κ, for each $m = 2, 3, \ldots$, we will choose b_{m-1} so that $\mathcal{W}_m$ is

the unique solution to

$$\Delta_{\mathbf{y}} \mathcal{W}_m = 0\,, \quad \mathbf{y} \in \mathbb{R}^3_+\,, \tag{B.8a}$$

$$\partial_{y_3} \mathcal{W}_m = \mathcal{W}_{m-1} + b_{m-1}\,, \quad y_3 = 0\,,\ (y_1, y_2) \in \Gamma\,, \tag{B.8b}$$

$$\partial_{y_3} \mathcal{W}_m = 0\,, \quad y_3 = 0\,,\ (y_1, y_2) \notin \Gamma\,, \tag{B.8c}$$

$$\lim_{R\to\infty} \int_{\partial\Omega_R} \partial_n \mathcal{W}_m \, d\mathbf{s} = 0\,, \qquad \mathcal{W}_m \sim o(1)\,, \quad \text{as} \quad |\mathbf{y}| \to \infty\,. \tag{B.8d}$$

By applying the divergence theorem to (B.8) we obtain that $\int_\Gamma (\mathcal{W}_{m-1} + b_{m-1})\, d\mathbf{s} = 0$, which determines b_{m-1} as

$$b_{m-1} = -\frac{1}{\pi a^2} \int_\Gamma \mathcal{W}_{m-1}(y_1, y_2, 0)\, dy_1\, dy_2\,, \qquad m = 2, 3, \ldots\,. \tag{B.8e}$$

With b_0 determined in (B.7), we use the method of images to calculate $\mathcal{W}_1$ as

$$\mathcal{W}_1(\mathbf{y}) = -\frac{1}{\pi a^2} \int_\Gamma \frac{d\xi_1 d\xi_2}{\left[(\xi_1 - y_1)^2 + (\xi_2 - y_2)^2 + y_3^2\right]^{1/2}}\,. \tag{B.9}$$

In particular, for $y_3 = 0$, and with $\rho_0 = (y_1^2 + y_2^2)^{1/2} \le a$, the double integral in (B.9) can be evaluated as

$$\mathcal{W}_1(y_1, y_2, 0) = -\frac{4}{\pi a} E\left(\rho_0/a\right)\,, \quad 0 \le \rho_0 \le a\,, \tag{B.10}$$

where $E(z) \equiv \int_0^{\pi/2} \sqrt{1 - z^2 \sin^2\theta}\, d\theta$ is the complete elliptic integral of the second kind. By using (B.8e) with $m = 2$, and exploiting radial symmetry, we conclude that

$$b_1 = \frac{8}{\pi a^3} \int_0^a \rho_0 E\left(\rho_0/a\right)\, d\rho_0 = \frac{8}{\pi a} \int_0^1 z E(z)\, dz = \frac{16}{3\pi a}\,, \tag{B.11}$$

where we have used $\int_0^1 z E(z)\, dz = 2/3$ from (5.112) of [45].

By using the method of images we calculate that

$$\mathcal{W}_2(\mathbf{y}) = \frac{1}{2\pi} \int_\Gamma \frac{4(\pi a)^{-1} E\left(|\xi|/a\right) - b_1}{\left[(\xi_1 - y_1)^2 + (\xi_2 - y_2)^2 + y_3^2\right]^{1/2}}\, d\xi_1 d\xi_2\,, \tag{B.12}$$

where $|\xi| = (\xi_1^2 + \xi_2^2)^{1/2}$. By evaluating (B.12) on $y_3 = 0$, we obtain on the patch $0 \le \rho_0 \le a$ that

$$\mathcal{W}_2(y_1, y_2, 0) = -\frac{2a}{\pi} b_1 E\left(\frac{\rho_0}{a}\right) + \frac{2}{\pi^2 a} \int_\Gamma \frac{E\left(|\xi|/a\right)}{\left[(\xi_1 - y_1)^2 + (\xi_2 - y_2)^2\right]^{1/2}}\, d\xi_1 d\xi_2\,. \tag{B.13}$$

Upon substituting (B.13) into (B.8e) with $m = 3$, we obtain that

$$b_2 = \frac{4 b_1}{\pi a} \int_0^a \rho_0 E\left(\frac{\rho_0}{a}\right)\, d\rho_0 - \frac{4}{\pi^2 a^3} \int_0^a \rho_0 \mathcal{J}(\rho_0)\, d\rho_0\,, \tag{B.14}$$

where $\mathcal{J}(\rho_0)$ is defined by

$$\mathcal{J}(\rho_0) \equiv \int_\Gamma \frac{E\left(|\xi|/a\right)}{\left[(\xi_1 - y_1)^2 + (\xi_2 - y_2)^2\right]^{1/2}}\, d\xi_1 d\xi_2\,, \qquad \rho_0 = \sqrt{y_1^2 + y_2^2}\,. \tag{B.15}$$

By using (B.11) for b_1 and $\int_0^1 zE(z)\,dz = 2/3$ we can calculate the first term in (B.14). Then, by writing the second integral in (B.15) in polar coordinates we obtain that

(B.16)
$$b_2 = \frac{128}{9\pi^2} - \frac{8}{\pi^2}\int_0^1 \eta\mathcal{H}(\eta)\,d\eta\,, \quad \text{where} \quad \mathcal{H}(\eta) \equiv \int_0^\pi \int_0^1 \frac{E(r)r\,dr\,d\theta}{\left[r^2+\eta^2-2r\eta\cos\theta\right]^{1/2}}\,.$$

Next, we use $\int_0^\pi \left[1+\beta^2-2\beta\cos\theta\right]^{-1/2}\,d\theta = 2(1+\beta)^{-1}K\left(2\sqrt{\beta}/(1+\beta)\right)$ for $0 \le \beta < 1$, where $K(z)$ is the complete elliptic integral of the first kind of modulus z (see (3.6.17) of [45]). We conclude from (B.16) that

$$\mathcal{H}(\eta) = \int_0^1 \frac{2rE(r)}{r+\eta}K\left(\frac{2\sqrt{\eta r}}{r+\eta}\right)\,dr\,. \tag{B.17}$$

We label $A_0 \equiv \int_0^1 \eta\mathcal{H}(\eta)\,d\eta$, in which we use (B.17) for $\mathcal{H}(\eta)$. Upon switching the order of integration and decomposing the resulting integral into two parts we obtain

$$A_0 = \int_0^1 rE(r)\left[\int_0^r \frac{2\eta}{r+\eta}K\left(\frac{2\sqrt{r\eta}}{r+\eta}\right)\,d\eta + \int_r^1 \frac{2\eta}{r+\eta}K\left(\frac{2\sqrt{r\eta}}{r+\eta}\right)\,d\eta\right]\,dr\,. \tag{B.18}$$

To ensure that the modulus of the elliptic functions are on $[0,1]$, we introduce the new variables $s = \eta/r$ and $s = r/\eta$ in the first and second integrals of (B.18), respectively. This yields that

(B.19)
$$A_0 = \int_0^1 2r^2E(r)\left[\int_0^1 \frac{s}{1+s}K\left(\frac{2\sqrt{s}}{1+s}\right)\,ds + \int_r^1 \frac{1}{s^2(1+s)}K\left(\frac{2\sqrt{s}}{1+s}\right)\,ds\right]\,dr\,.$$

Since $0 \le s \le 1$, we use the Landen transformation $K\left(2\sqrt{s}/(1+s)\right) = (1+s)K(s)$ in (B.19) to obtain that

$$A_0 = \int_0^1 2r^2E(r)\left[\int_0^1 sK(s)\,ds + \int_r^1 s^{-2}K(s)\,ds\right]\,dr\,. \tag{B.20}$$

By using the indefinite integrals $\int s^{-2}K(s)\,ds = -s^{-1}E(s)$ and $\int sK(s)\,ds = E(s) - (1-s^2)K(s)$ from (6.12.05) and (6.10.01) of [45] together with $E(0) = K(0) = \pi/2$, we obtain from (B.20) that

$$A_0 = \int_0^1 2r^2E(r)\left[E(1) + \left(-E(1) + r^{-1}E(r)\right)\right]\,dr = \int_0^1 2r\left[E(r)\right]^2\,dr\,. \tag{B.21}$$

In this way, since $A_0 = \int_0^1 \eta\mathcal{H}(\eta)\,d\eta$ we obtain from (B.16) and (B.21) that

$$b_2 = \frac{128}{9\pi^2} - \frac{8}{\pi^2}\int_0^1 2r\left[E(r)\right]^2\,dr\,. \tag{B.22}$$

Finally, upon substituting $B(\kappa) \sim b_0\kappa^{-1} + b_1 + b_2\kappa$ into (B.3), we revert the expansion to conclude that

$$C(\kappa) \sim \frac{\kappa}{b_0} - \frac{b_1\kappa^2}{b_0^2} + \frac{\kappa^3}{b_0^3}\left(b_1^2 - b_0b_2\right) + \dots\,. \tag{B.23}$$

Upon using (B.7), (B.11) and (B.22) in (B.23), we obtain (3.19) of Lemma 3.1. Moreover, we can also readily identify the first three terms in the Taylor expansion (3.8a) as given in (3.16).

Appendix C. Inner Problem Beyond Tangent Plane Approximation.

Omitting the subscript i for the i-th patch, we now analyze the following inner problem that arises at a higher order beyond the tangent-plane approximation:

$$\Delta_{\mathbf{y}}\Phi_2 = -2\left(y_3 w_{y_3y_3} + w_{y_3}\right), \quad \mathbf{y}\in\mathbb{R}^3_+, \tag{C.1a}$$

$$-\partial_{y_3}\Phi_2 + \kappa\Phi_2 = 0, \quad y_3 = 0, \ (y_1,y_2)\in\Gamma, \tag{C.1b}$$

$$\partial_{y_3}\Phi_2 = 0, \quad y_3 = 0, \ (y_1,y_2)\notin\Gamma, \tag{C.1c}$$

$$\Phi_2 \sim \frac{C}{2}\log(y_3+\rho) - \frac{Cy_3}{2\rho^3}(y_1^2+y_2^2) + \frac{E}{\rho} + \ldots, \quad \text{as} \quad \rho\to\infty, \tag{C.1d}$$

where $\rho = (y_1^2+y_2^2+y_3^2)^{1/2}$ and Γ is the Robin patch, which is not necessarily circular. Here $w(\mathbf{y})$ is the solution to the leading-order problem (3.3), where $C = C(\kappa)$ is the coefficient of the monopole in the far-field behavior (3.3d). Our goal is to determine the coefficient E of the monopole term in the far-field (C.1d). The result is as follows:

LEMMA C.1. *The solution to (C.1) can be decomposed as*

$$\Phi_2 = \Phi_{2p} + \Phi_{2h}, \tag{C.2}$$

where

$$\Phi_{2p} = -\frac{y_3^2}{2}w_{y_3} - \frac{y_3}{2}w + \frac{1}{2}\int_0^{y_3} w(y_1,y_2,\eta)\,d\eta + \mathcal{F}(y_1,y_2;\kappa), \tag{C.3}$$

and where $\mathcal{F}(y_1,y_2;\kappa)$, with $\Delta_S\mathcal{F} \equiv \mathcal{F}_{y_1y_1} + \mathcal{F}_{y_2y_2}$, is the unique solution to

(C.4a)

$$\Delta_S\mathcal{F} = q(y_1,y_2;\kappa)I_\Gamma; \ \ q(y_1,y_2;\kappa) \equiv -\left(\frac{1}{2}w_{y_3}|_{y_3=0}\right), \ \ I_\Gamma \equiv \begin{cases} 1, & (y_1,y_2)\in\Gamma \\ 0, & (y_1,y_2)\notin\Gamma, \end{cases}$$

$$\mathcal{F} \sim \frac{C}{2}\log\rho_0 + o(1), \quad \textit{as} \quad \rho_0 \equiv (y_1^2+y_2^2)^{1/2}\to\infty. \tag{C.4b}$$

The logarithmic growth as $\rho_0\to\infty$ in (C.4b) follows by applying the divergence theorem to (C.4a) and recalling (3.4) for C. The $o(1)$ condition in the far-field (C.4b) specifies $\mathcal{F}$ uniquely. In addition, the far-field behavior is

$$\Phi_{2p} \sim -\frac{Cy_3(y_1^2+y_2^2)}{2\rho^3} + \frac{C}{2}\log(y_3+\rho) + o\left(1/\rho\right), \quad \textit{as} \quad \rho\to\infty. \tag{C.5}$$

The remaining term Φ_{2h} in (C.2) satisfies

$$\Delta_{\mathbf{y}}\Phi_{2h} = 0, \quad \mathbf{y}\in\mathbb{R}^3_+, \tag{C.6a}$$

$$-\partial_{y_3}\Phi_{2h} + \kappa\Phi_{2h} = -\kappa\mathcal{F}, \quad y_3 = 0, \ (y_1,y_2)\in\Gamma, \tag{C.6b}$$

$$\partial_{y_3}\Phi_{2h} = 0, \quad y_3 = 0, \ (y_1,y_2)\notin\Gamma, \tag{C.6c}$$

$$\Phi_{2h} \sim \frac{E}{\rho}, \quad \textit{as} \quad \rho\to\infty, \tag{C.6d}$$

where the monopole coefficient $E = E(\kappa)$ is given explicitly by

$$E = -\frac{1}{\pi}\int_\Gamma q(y_1,y_2;\kappa)\,\mathcal{F}(y_1,y_2;\kappa)\,dy_1dy_2, \tag{C.7a}$$

where

$$\mathcal{F}(y_1,y_2;\kappa) = \frac{1}{4\pi}\int_\Gamma q(y_1',y_2',\kappa)\log\left((y_1-y_1')^2 + (y_2-y_2')^2\right)dy_1'dy_2'. \tag{C.7b}$$

In this way, the far-field behavior (C.1d) holds. Finally, in the limit $\kappa\to 0$, the leading-order asymptotics for E is given by (3.23).

Proof. To establish this result, we first show that Φ_{2p} in (C.3) accounts for the the inhomogeneous terms in (C.1a). We readily calculate that

$$\Phi_{2py_3} = -\frac{y_3^2}{2} w_{y_3y_3} - \frac{3}{2} y_3 w_{y_3}\,, \quad \Phi_{2py_3y_3} = -\frac{y_3^2}{2} w_{y_3y_3y_3} - \frac{5}{2} y_3 w_{y_3y_3} - \frac{3}{2} w_{y_3}\,. \tag{C.8}$$

Moreover, we calculate $\Delta_S \Phi_{2p} \equiv \Phi_{2py_1y_1} + \Phi_{2py_2y_2}$, and by using $w_{y_3y_3} = -\Delta_S w$ from (3.3a), we derive

$$\begin{aligned} \Delta_S \Phi_{2p} &= -\frac{y_3^2}{2} \partial_{y_3} \left[\Delta_S w\right] - \frac{y_3}{2} \Delta_S w + \frac{1}{2} \int_0^{y_3} \Delta_S w \, d\eta + \Delta_S \mathcal{F} \\ &= \frac{y_3^2}{2} w_{y_3y_3y_3} + \frac{y_3}{2} w_{y_3y_3} - \frac{1}{2} w_{y_3} + \frac{1}{2} w_{y_3}|_{y_3=0} + \Delta_S \mathcal{F}\,. \end{aligned} \tag{C.9}$$

Upon adding (C.8) and (C.9) we conclude that

$$\Delta_{\mathbf{y}} \Phi_{2p} = \Phi_{2py_3y_3} + \Delta_S \Phi_{2p} = -2\left(y_3 w_{y_3y_3} + w_{y_3}\right) + \left(\Delta_S \mathcal{F} + \frac{1}{2} w_{y_3}|_{y_3=0}\right)\,, \tag{C.10}$$

where the terms on the right-hand side in (C.10) are the inhomogeneous terms for this PDE for Φ_{2p}. It follows that Φ_{2p} satisfies (C.1a) when $\mathcal{F}$ satisfies (C.4a). Consequently, Φ_{2h} satisfies the homogeneous problem (C.6a).

To establish the boundary conditions in (C.6) we observe from (C.8) and (C.3) that $\Phi_{2py_3} = 0$ and $\Phi_{2p} = \mathcal{F}$ on $y_3 = 0$. As a result, upon substituting (C.2) into (C.1b)–(C.1c) we obtain (C.6b)–(C.6c).

Next, we determine the asymptotic far-field behavior of Φ_{2p} as defined in (C.3). We use $w \sim C\rho^{-1}$ as $\rho \to \infty$ with $\rho = (y_3^2 + \rho_0^2)^{1/2}$ where $\rho_0 \equiv (y_1^2 + y_2^2)^{1/2}$. We readily calculate for $\rho \to \infty$ that

$$-\frac{1}{2} y_3^2 w_{y_3} - \frac{1}{2} y_3 w \sim -\frac{C}{2} \frac{y_3 \rho_0^2}{\rho^3}\,, \tag{C.11a}$$

$$\frac{1}{2} \int_0^{y_3} w(y_1, y_2, \eta)\, d\eta \sim \frac{C}{2} \int_0^{y_3} \frac{1}{\left(\eta^2 + \rho_0^2\right)^{1/2}}\, d\eta \sim \frac{C}{2} \left[\log\left(y_3 + \rho\right) - \log \rho_0\right]\,. \tag{C.11b}$$

In this way, it follows that Φ_{2p} in (C.3) has the divergent far-field behavior

$$\Phi_{2p} \sim \frac{C}{2} \log\left(y_3 + \rho\right) - \frac{C y_3}{2\rho^3} \left(y_1^2 + y_2^2\right) - \frac{C}{2} \log \rho_0 + \mathcal{F}\,. \tag{C.12}$$

Therefore, since $\mathcal{F} \sim (C/2) \log \rho_0 + o(1)$ as $\rho_0 \to \infty$ as specified in (C.4b) it follows from (C.12) that $\Phi_{2p} \sim -C y_3 (y_1^2 + y_2^2)/(2\rho^3) + (C/2) \log(y_3 + \rho) + o\left(1/\rho\right)$ as $\rho \to \infty$. Finally, since (C.6) for Φ_{2h} is a Neumann-Robin BVP with a spatially inhomogeneous Robin condition on the patch, we have $\Phi_{2h} = \mathcal{O}(\rho^{-1})$ as $\rho \to \infty$. The expression (C.7) for the monopole coefficient results from using Green's second identity to the problems (3.3) and (C.6) for w and Φ_{2h}, respectively, over a large hemisphere and by calculating $\mathcal{F}$ using the 2-D free-space Green's function. In this way, the far-field behavior (C.1d) for Φ_2 holds.

Finally, we derive the limiting asymptotics (3.23) for E. For $\kappa \to 0$, we obtain from (3.3) that $w = \mathcal{O}(\kappa)$ so that $q = -\left(1/2\right) \partial_{y_3} w \sim \kappa/2$ on Γ. We substitute (C.7b) into (C.7a) and use $q \sim \kappa/2$. Upon eliminating κ by using $C \sim \kappa |\Gamma|/(2\pi)$ for $\kappa \ll 1$, as obtained from (3.8a) and (3.9), we conclude for $\kappa \to 0$ that

$$E \sim -\frac{\kappa^2}{8\pi^2} \int_{\Gamma_i} \int_{\Gamma_i} \log|\mathbf{y} - \mathbf{y}'|\, d\mathbf{y}\, d\mathbf{y}' = -\frac{C^2}{2|\Gamma|^2} \int_{\Gamma_i} \int_{\Gamma_i} \log|\mathbf{y} - \mathbf{y}'|\, d\mathbf{y}\, d\mathbf{y}'\,, \tag{C.13}$$

which establishes (3.23). This completes the proof of Lemma C.1. ∎

We remark that Lemma C.1 applies to a patch Γ of arbitrary shape. However, when Γ is a disk of radius a, the expression for E in (C.7) can be reduced to quadrature and we can determine its limiting asymptotics, as was summarized in Lemma 3.2.

When Γ is a disk, q and $\mathcal{F}$ in (C.4) depend only on $\rho_0 = (y_1^2 + y_2^2)^{1/2}$, so that from (C.4) we readily obtain that $\mathcal{F} = \mathcal{F}(\rho_0;\kappa)$ satisfies $(\rho_0 \mathcal{F}_{\rho_0})_{\rho_0} = \rho_0 q(\rho_0;\kappa)$. We integrate this ODE, impose that $\mathcal{F}(\rho_0;\kappa)$ has no singularity at $\rho_0 = 0$, and we substitute the resulting expression into (C.7a). Exploiting radial symmetry, we determine E as

(C.14)
$$E = -2\int_0^a \rho_0 q(\rho_0;\kappa)\mathcal{F}(\rho_0;\kappa)\,d\rho_0\,; \qquad \mathcal{F}_{\rho_0} = \frac{1}{\rho_0}\int_0^{\rho_0} \eta q(\eta;\kappa)\,d\eta\,, \quad 0 \le \rho_0 \le a\,,$$

with $\mathcal{F} = (C/2)\log a$ at $\rho_0 = a$. Next, we integrate (C.14) by parts to obtain

$$E = -2\left[\mathcal{F}(\rho_0;\kappa)\left(\int_0^{\rho_0} \eta q(\eta;\kappa)\,d\eta\right)\Big|_0^a - \int_0^a \mathcal{F}_{\rho_0}\left(\int_0^{\rho_0} \eta q(\eta;\kappa)\,d\eta\right)\,d\rho_0\right]. \tag{C.15}$$

Then, upon using $\mathcal{F} = (C/2)\log a$ at $\rho_0 = a$, $C = 2\int_0^a \eta q(\eta;\kappa)\,d\eta$ and $\mathcal{F}_{\rho_0}$ from (C.14) we find that (C.15) reduces to (3.24) in Lemma 3.2.

For $\kappa = \infty$, we calculate (3.24) analytically. By using (3.14) for $q = q(\rho_0;\infty)$, $C = C(\infty) = 2a/\pi$ and $\int_0^{\rho_0} \eta/\sqrt{a^2-\eta^2}\,d\eta = a - \sqrt{a^2-\rho_0^2}$, we obtain from (3.24) that

$$\begin{aligned} E(\infty) &= -\frac{[C(\infty)]^2}{2}\log a + \frac{2}{\pi^2}\int_0^a \frac{1}{\rho_0}\left[a - \sqrt{a^2-\rho_0^2}\right]^2\,d\rho_0\,, \\ &= -\frac{2a^2}{\pi^2}\log a + \frac{2a^2}{\pi^2}\int_0^1 \frac{1}{x}\left(2 - x^2 - 2\sqrt{1-x^2}\right)\,dx\,, \\ &= -\frac{2a^2}{\pi^2}\log a + \frac{2a^2}{\pi^2}\left(\frac{3}{2} - \log 4\right). \end{aligned}$$

In this way, we recover the expression for $E(\infty)$ given in (3.26a) of Lemma 3.2.

Finally, we calculate E when $\kappa \ll 1$ and Γ is a disk. Instead of using (C.13), we can proceed more directly. When $\kappa \ll 1$, we find from (3.3) that $-\partial_{y_3} w \sim \kappa$ on $y_3 = 0$, $(y_1, y_2) \in \Gamma$, so that from (C.4), $q(\rho_0;\kappa) \sim \kappa/2$ on $0 \le \rho_0 \le a$. By evaluating the integrals in (3.24), and using $C \sim \kappa a^2/2$ for $\kappa \ll 1$, we obtain (3.26b) of Lemma 3.2 for E when $\kappa \ll 1$.

Appendix D. Computation and Analysis of Reactivity Capacitance.

In this Appendix, we derive an exact representation for the reactivity capacitance $C_i(\kappa_i)$ in the general case of an arbitrary patch. We then analyze its properties for the case of a circular patch.

D.1. Arbitrary patch. The solution $w_i(\mathbf{y};\kappa_i)$ of the mixed BVP (3.3) is the key element for our asymptotic analysis. As this BVP is formulated for the i-th patch Γ_i, independently of the other patches, its solution can be searched separately for different patches so that the index i will be kept fixed throughout this appendix. As an explicit solution is not available even for circular patches, we search for a suitable spectral representation of $w_i(\mathbf{y};\kappa_i)$. For this purpose, we employ the *local* Steklov

eigenvalue problem defined in an upper half-space by

$$\Delta_{\mathbf{y}} \Psi_{ki} = 0\,, \quad \mathbf{y} \in \mathbb{R}^3_+\,, \tag{D.1a}$$

$$\partial_n \Psi_{ki} = \mu_{ki} \Psi_{ki}\,, \quad y_3 = 0\,,\ (y_1, y_2) \in \Gamma_i\,, \tag{D.1b}$$

$$\partial_n \Psi_{ki} = 0\,, \quad y_3 = 0\,,\ (y_1, y_2) \notin \Gamma_i\,, \tag{D.1c}$$

$$\Psi_{ki}(\mathbf{y}) = \mathcal{O}\left(1/|\mathbf{y}|\right) \quad \text{as} \quad |\mathbf{y}| \to \infty\,. \tag{D.1d}$$

This spectral problem can be reduced to the exterior Steklov problem in the whole space $\mathbb{R}^3$. The latter has a discrete spectrum [19], whereas its eigenfunctions are necessarily either symmetric, or antisymmetric with respect to the horizontal plane. The symmetric ones satisfy the Neumann boundary condition (D.1c). In the following, we focus only on these symmetric eigenmodes and enumerate them by the index $k = 0, 1, 2, \ldots$ such that the associated eigenvalues form an increasing sequence:

$$0 < \mu_{0i} < \mu_{1i} \leq \cdots \nearrow +\infty\,, \tag{D.2}$$

with the principal eigenvalue μ_{0i} being simple and strictly positive. Importantly, the restrictions $\Psi_{ki}(\mathbf{y})|_{\Gamma_i}$ onto Γ_i form a complete orthonormal basis in $L^2(\Gamma_i)$:

$$\int_{\Gamma_i} \Psi_{ki} \Psi_{k'i}\, d\mathbf{y} = \delta_{k,k'}\,. \tag{D.3}$$

As discussed in [56], the restriction of the Neumann Green's function onto Γ_i turns out to be the kernel of an integral operator that determines the eigenpairs μ_{ki} and $\Psi_{ki}(\mathbf{y})$. In our setting, the restriction of the Neumann Green's function in the half-space onto a patch on the horizontal plane is $1/(2\pi|\mathbf{y} - \mathbf{y}'|)$ and yields the following identity:

$$\frac{1}{2\pi|\mathbf{y} - \mathbf{y}'|} = \sum_{k=0}^{\infty} \frac{\Psi_{ki}(\mathbf{y}) \Psi_{ki}(\mathbf{y}')}{\mu_{ki}}\,, \quad \text{for} \quad \mathbf{y}, \mathbf{y}' \in \Gamma_i\,. \tag{D.4}$$

This identity can also be recast as an eigenvalue problem

$$\int\limits_{\Gamma_i} \frac{1}{2\pi|\mathbf{y} - \mathbf{y}'|} \Psi_{ki}(\mathbf{y}')\, d\mathbf{y}' = \frac{1}{\mu_{ki}} \Psi_{ki}(\mathbf{y})\,, \quad \text{for} \quad \mathbf{y} \in \Gamma\,, \tag{D.5}$$

whose eigenpairs are enumerated by $k = 0, 1, \ldots$.

The completeness of the basis of $\{\Psi_{ki}\}$ in $L^2(\Gamma_i)$ allows us to decompose the restriction of $w_i(\mathbf{y}; \kappa_i)$ to Γ_i and thus to search the solution of (3.3) in the form:

$$w_i(\mathbf{y}; \kappa_i) = \sum_{k=0}^{\infty} \eta_{ki} \Psi_{ki}(\mathbf{y})\,. \tag{D.6}$$

The unknown coefficients η_{ki} can be found from imposing the boundary condition (3.3b):

$$\sum_{k'=0}^{\infty} \eta_{k'i} (\mu_{k'i} + \kappa_i) \Psi_{k'i}(\mathbf{y}) = \kappa_i\,, \quad \text{for} \quad \mathbf{y} \in \Gamma_i\,. \tag{D.7}$$

Multiplying (D.7) by $\Psi_{ki}(\mathbf{y})$ and integrating the resulting expression over Γ_i, we get

$$\eta_{ki} = \frac{\kappa_i\, d_{ki}}{\mu_{ki} + \kappa_i}\,, \quad \text{with} \quad d_{ki} = \int_{\Gamma_i} \Psi_{ki}\, d\mathbf{y}\,, \tag{D.8}$$

where we used the orthonormality condition (D.3). We therefore deduced the following spectral representation:

$$w_i(\mathbf{y};\kappa_i) = \kappa_i \sum_{k=0}^{\infty} \frac{d_{ki}}{\mu_{ki}+\kappa_i}\Psi_{ki}(\mathbf{y}), \quad \mathbf{y}\in\mathbb{R}^3_+. \tag{D.9}$$

As a consequence, the charge density becomes

$$q_i(\mathbf{y};\kappa_i) = \frac{1}{2}\partial_n w_i(\mathbf{y};\kappa_i) = \frac{\kappa_i}{2}\sum_{k=0}^{\infty}\frac{d_{ki}\mu_{ki}}{\mu_{ki}+\mu}\Psi_{ki}(\mathbf{y})\,, \quad \text{for} \quad \mathbf{y}\in\Gamma_i\,. \tag{D.10}$$

Moreover, setting $\kappa_i = -\sigma$ and evaluating the derivative with respect to σ gives

$$w_{ci}(\mathbf{y};-\sigma) = \partial_\sigma w_i(\mathbf{y};-\sigma) = -\sum_{k=0}^{\infty}\frac{\mu_{ki}d_{ki}}{(\mu_{ki}-\sigma)^2}\Psi_{ki}(\mathbf{y})\,. \tag{D.11}$$

These spectral expansions imply that if $\sigma = \mu_{ki}$ for some integer $k \geq 0$, then there is no solution $w_i(\mathbf{y};-\sigma)$.

According to the definition (3.4), the reactive capacitance can be found as

$$C_i(\kappa_i) = \frac{1}{2\pi}\int_{\Gamma_i}\partial_n w_i\, d\mathbf{y} = \frac{\kappa_i}{2\pi}\sum_{k=0}^{\infty}\frac{\mu_{ki}d_{ki}^2}{\mu_{ki}+\kappa_i}\,. \tag{D.12}$$

Equation (D.12) is one of the main results of this appendix. In particular, its derivative, given by (3.7), is strictly positive. As a result, the capacitance $C_i(\infty)$ is an upper bound for $C_i(\kappa_i)$ for $\kappa_i > 0$. Another upper bound, which is useful for small κ_i, reads

$$C_i(\kappa_i) \leq \frac{\kappa_i}{2\pi}\sum_{k=0}^{\infty} d_{ki}^2 = \frac{\kappa_i\,|\Gamma_i|}{2\pi}\,, \tag{D.13}$$

where the second equality follows from (D.17), which is shown below. We conclude that the eigenvalues μ_{ki} and the spectral weights d_{ki}, for which $d_{ki} \neq 0$, fully determine the reactive capacitance and its properties. It is worth noting that a dilation of the patch Γ_i by $a_i > 0$ implies

$$\text{If} \;\; \Gamma_i' = a_i\Gamma_i\,, \quad \text{then} \quad \mu_{ki}' = \mu_{ki}/a_i, \quad d_{ki}' = a_i\, d_{ki}\,, \tag{D.14}$$

where we used the $L^2(\Gamma_i)$ normalization of eigenfunctions.

In the limit $\kappa_i \to 0$, the geometric series expansion of each fraction in (D.12) yields the Taylor expansion

$$C_i(\kappa_i) = -a_i\sum_{n=1}^{\infty} c_{ni}\,(-\kappa_i a_i)^n\,, \quad \text{with} \quad c_{ni} = \frac{1}{2\pi a_i^{n+1}}\sum_{k=0}^{\infty}\frac{d_{ki}^2}{\mu_{ki}^{n-1}}\,. \tag{D.15}$$

The coefficient c_{1i} can be found by expanding the unity on the complete basis of eigenfunctions $\{\Psi_{ki}\}$,

$$\sum_{k=0}^{\infty} d_{ki}\Psi_{ki}(\mathbf{y}) = 1\,, \quad \text{for} \quad \mathbf{y}\in\Gamma_i\,, \tag{D.16}$$

while its integral over $\mathbf{y} \in \Gamma_i$ yields

$$\sum_{k=0}^{\infty} d_{ki}^2 = |\Gamma_i| \,, \tag{D.17}$$

where $|\Gamma_i|$ denotes the area of Γ_i. This shows that $F_{ki} = d_{ki}^2/|\Gamma_i|$ can be interpreted as the relative weight of the k-th eigenpair. Applying the divergence theorem to (D.1), we observe that the coefficient d_{ki} determines the far-field behavior of $\Psi_{ki}(\mathbf{y})$ in the form

$$\Psi_{ki}(\mathbf{y}) \sim \frac{\mu_{ki} d_{ki}}{2\pi|\mathbf{y}|} + \ldots \,, \quad \text{as} \quad |\mathbf{y}| \to \infty \,. \tag{D.18}$$

According to (D.17), we get

$$c_{1i} = \frac{|\Gamma_i|}{2\pi a_i^2} \,. \tag{D.19}$$

It is convenient to derive a closed-form representation for the coefficients c_{2i} and c_{3i} to facilitate their numerical computation without solving the Steklov eigenvalue problem. To this end, we integrate (D.5) over $\mathbf{y} \in \Gamma_i$ to get

$$\int_{\Gamma_i} \Psi_{ki}(\mathbf{y})\, \omega_i(\mathbf{y})\, d\mathbf{y} = \frac{d_{ki}}{\mu_{ki}} \,, \qquad \text{where} \qquad \omega_i(\mathbf{y}) \equiv \int_{\Gamma_i} \frac{d\mathbf{y}'}{2\pi|\mathbf{y}-\mathbf{y}'|} \,. \tag{D.20}$$

Multiplying this relation by $d_{ki}/(2\pi)$ and summing over k, we find

$$c_{2i} = \frac{1}{2\pi a_i^3} \sum_{k=0}^{\infty} \frac{d_{ki}^2}{\mu_{ki}} = \frac{1}{2\pi a_i^3} \sum_{k=0}^{\infty} \int_{\Gamma_i} \Psi_{ki}(\mathbf{y})\, \omega_i(\mathbf{y})\, d\mathbf{y} \int_{\Gamma_i} \Psi_{ki}(\mathbf{y}')\, d\mathbf{y}'$$

$$= \frac{1}{2\pi a_i^3} \int_{\Gamma_i} \omega_i(\mathbf{y}) \left(\int_{\Gamma_i} \underbrace{\sum_{k=0}^{\infty} \Psi_{ki}(\mathbf{y})\, \Psi_{ki}(\mathbf{y}')}_{=\delta(\mathbf{y}-\mathbf{y}')}\, d\mathbf{y}' \right) d\mathbf{y} \;= \frac{1}{2\pi a_i^3} \int_{\Gamma_i} \omega_i(\mathbf{y})\, d\mathbf{y} \,, \tag{D.21}$$

where we used the completeness of the basis of eigenfunctions Ψ_{ki} in $L^2(\Gamma)$. In the same vein, we have

$$c_{3i} = \frac{1}{2\pi a_i^4} \sum_{k=0}^{\infty} \frac{d_{ki}^2}{\mu_{ki}^2} = \frac{1}{2\pi a_i^4} \sum_{k=0}^{\infty} \int_{\Gamma_i} \Psi_{ki}(\mathbf{y})\, \omega_i(\mathbf{y})\, d\mathbf{y} \int_{\Gamma_i} \Psi_{ki}(\mathbf{y}')\, \omega_i(\mathbf{y}')\, d\mathbf{y}'$$

$$= \frac{1}{2\pi a_i^4} \int_{\Gamma_i} \omega_i(\mathbf{y}) \left(\int_{\Gamma_i} \omega_i(\mathbf{y}') \underbrace{\sum_{k=0}^{\infty} \Psi_{ki}(\mathbf{y})\, \Psi_{ki}(\mathbf{y}')}_{=\delta(\mathbf{y}-\mathbf{y}')}\, d\mathbf{y}' \right) d\mathbf{y} = \frac{1}{2\pi a_i^4} \int_{\Gamma_i} \omega_i^2(\mathbf{y})\, d\mathbf{y} \,. \tag{D.22}$$

These two representations allow one to compute the coefficients c_{2i} and c_{3i} numerically for any patch shape without solving the exterior Steklov problem. In other words, we managed to represent these coefficients in purely geometric terms.

k	0	1	2	3	4	5	6	7
μ_{ki}	1.1578	4.3168	7.4602	10.602	13.744	16.886	20.028	23.169
d_{ki}	1.7524	0.2298	0.1000	0.0587	0.0397	0.0291	0.0225	0.0180
d_{ki}^2/π	0.9775	0.0168	0.0032	0.0011	0.0005	0.0003	0.0002	0.0001
μ_{ki}^N	0	4.1213	7.3421	10.517	13.677	16.831	19.981	23.128
F_{ki}^N	1	0.1195	0.0782	0.0587	0.0471	0.0394	0.0339	0.0297

Table D.1: The first eight Steklov eigenvalues μ_{ki} for the unit disk Γ_i ($a_i = 1$) in the upper half-space that correspond to axially symmetric eigenfunctions, for which the weights d_{ki} are nonzero. These values were obtained via a numerical diagonalization of a truncated matrix representing the Dirichlet-to-Neumann operator, with the truncation order 100 (see details in [55]). Note that the reduction of the truncation order to 50 does not affect the shown digits, assuring the high quality of this computation. The last two rows present the first eight eigenvalues μ_{ki}^N, corresponding to axially symmetric eigenfunctions, of the Steklov problem (D.30), and the associated weights $F_{ki}^N = \pi[\Psi_{ki}^N(\infty)]^2$; see [68, 56] for their numerical computation.

A numerical computation of the function $\omega_i(\mathbf{y})$ requires integration of the singular kernel $1/|\mathbf{y}-\mathbf{y}'|$. To avoid technical issues, it is convenient to recall that $\Delta_2|\mathbf{y}-\mathbf{y}'| = 1/|\mathbf{y}-\mathbf{y}'|$, where Δ_2 is the two-dimensional Laplace operator. As a consequence, one has

$$\omega_i(\mathbf{y}) = \frac{1}{2\pi}\int\limits_{\Gamma_i} \Delta_2|\mathbf{y}-\mathbf{y}'|\,d\mathbf{y}' = -\frac{1}{2\pi}\int\limits_{\partial\Gamma_i} \frac{(\mathbf{n}_{\mathbf{y}'}\cdot(\mathbf{y}-\mathbf{y}'))}{|\mathbf{y}-\mathbf{y}'|}\,d\mathbf{y}'\,, \tag{D.23}$$

where $\mathbf{n}_{\mathbf{y}'}$ is the unit normal vector to the boundary of the patch, oriented outward from Γ_i. In this way, the original integral over a planar region Γ_i is reduced to an integral over its one-dimensional boundary that avoids singularities. Using $\nabla_{\mathbf{y}}|\mathbf{y}-\mathbf{y}'| = (\mathbf{y}-\mathbf{y}')/|\mathbf{y}-\mathbf{y}'|$ and the divergence theorem, we can rewrite the integral in (D.21) as

$$c_{2i} = -\frac{1}{4\pi^2 a_i^3}\int\limits_{\partial\Gamma_i} d\mathbf{y}\int\limits_{\partial\Gamma_i} |\mathbf{y}-\mathbf{y}'|(\mathbf{n}_{\mathbf{y}}\cdot\mathbf{n}_{\mathbf{y}'})\,d\mathbf{y}'\,. \tag{D.24}$$

D.2. Circular Patch. For a circular patch Γ_i, the exterior Steklov problem was studied in [55]. In particular, an efficient numerical procedure for constructing the eigenvalues and eigenfunctions was developed by using oblate spheroidal coordinates. Moreover, the axial symmetry of this setting implies that only axially symmetric eigenfunctions do contribute to $w_i(\mathbf{y};\kappa_i)$ in (D.9) and related quantities (in fact, the coefficients d_{ki} in (D.8) vanish for non-axially symmetric eigenfunctions). As a consequence, we can focus exclusively on axially symmetric eigenmodes that we still enumerate by the index $k = 0, 1, 2, \ldots$.

Using the numerical procedure from [55], we compute μ_{ki} and d_{ki} by diagonalizing an appropriate truncated matrix. The first eight eigenvalues μ_{ki} and coefficients d_{ki} for the unit disk are shown in Table D.1. One sees that the principal eigenmode provides the dominant contribution of 98%, the next one gives 1.7%, whereas all the remaining eigenmodes are almost negligible. In other words, the infinite sum in (3.8a) can be truncated to only a few terms to get very accurate results for c_{ni}. For instance, keeping only the first two terms in the spectral expansion (3.8a) determining c_{ni} and

substituting the data from Table D.1, we find

$$c_{ni} \approx \frac{0.4888}{(1.1578)^{n-1}} + \frac{0.0084}{(4.3168)^{n-1}}\,, \quad \text{for} \quad n \geq 2\,. \tag{D.25}$$

This explicit approximation gives $c_{2i} \approx 0.4241$ and $c_{3i} \approx 0.3651$, which perfectly agree with the exact values from (3.16). While the exact computation of c_{ni} rapidly becomes very cumbersome (see Appendix B), the approximation (D.25) is fully explicit.

We also note that an alternative exact computation of c_{2i} and c_{3i} to that done in Appendix B can be achieved using the integral representations (D.21) and (D.22). Setting $\mathbf{y} = (r, \phi)$ and $\mathbf{y}' = (1, \phi')$ in polar coordinates, we first evaluate the integral in (D.23) as

$$\omega_i(\mathbf{y}) = -\frac{1}{2\pi} \int_0^{2\pi} \frac{r\cos(\phi - \phi') - 1}{\sqrt{1 + r^2 - 2r\cos(\phi - \phi')}} = \frac{2}{\pi} E(|\mathbf{y}|)\,, \tag{D.26}$$

where $E(z)$ is the complete elliptic integral of the second kind. As a consequence, we get immediately that

$$c_{2i} = \frac{2}{\pi} \int_0^1 r\, E(r)\, dr = \frac{4}{3\pi}\,, \qquad c_{3i} = \frac{4}{\pi^2} \int_0^1 r\, \left[E(r)\right]^2\, dr \approx 0.3651\,. \tag{D.27}$$

We also observe that c_{2i} could also be found directly from (D.24):

$$c_{2i} = -\frac{1}{4\pi^2} \int_0^{2\pi} \left(\int_0^{2\pi} \sqrt{2 - 2\cos(\phi - \phi')}\cos(\phi - \phi')\, d\phi' \right) d\phi = \frac{4}{3\pi}\,. \tag{D.28}$$

D.3. The Large-Reactivity Limit. While the fast decay of d_{ki}^2 allows one to keep only few terms in the analysis of the small-reactivity limit $\kappa_i \to 0$, all eigenmodes become relevant in the opposite limit $\kappa_i \to \infty$ of high reactivity. In the case of the unit disk (i.e., $a_i = 1$), the solution of (3.3) can be related to the potential Φ introduced and studied in [65]. In fact, the divergence theorem applied to (3.3) yields $\kappa_i \int_{\Gamma_i} (1 - w_i(\mathbf{y}; \kappa_i))\, d\mathbf{y} = 2\pi C_i(\kappa_i)$, so that $(1 - w_i)/C_i = 2\pi\Phi$, where Φ is the unique solution of equations (12-14) from [65]. As a consequence, the asymptotic relations (2,3,11) derived in [65] (with $D = 1$) imply, in our notations, that

$$C_i(\kappa_i) \approx \frac{2}{\pi} - \frac{2\left(\log\kappa_i + \log 2 + \gamma_e + 1\right)}{\pi^2 \kappa_i} \quad \text{as} \quad \kappa_i \to \infty\,, \tag{D.29}$$

where $\gamma_e \approx 0.5772\ldots$ is the Euler constant. Figure D.1 illustrates an excellent agreement between the numerically computed values of $C_i(\kappa_i)$ and the asymptotic relation (D.29).

D.4. Alternative Representation and Zeros of the Function $C_i(\kappa_i)$. As discussed in §7, the leading-order term in the asymptotic expansion of the SN problem is determined by (7.10), which requires finding zeros of the sum of $C_i(-\sigma_0)$. We now discuss the relation between the zeros of $C_i(-\sigma_0)$ and the spectrum of an additional local Steklov eigenvalue problem (see also [56]).

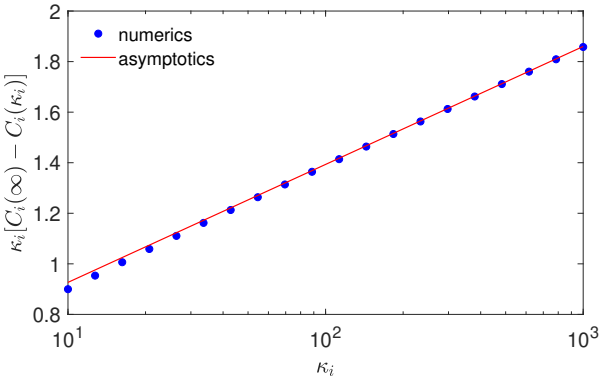

Fig. D.1: Asymptotic behavior of $C_i(\kappa_i)$ at large κ_i for the unit disk Γ_i ($a_i = 1$). The numerical results (symbols) computed from (D.12) are well-predicted by the asymptotic formula (D.29) when κ_i is large.

For this purpose, we consider the following exterior Steklov problem:

$$\Delta_{\mathbf{y}} \Psi_{ki}^N = 0\,, \quad \mathbf{y} \in \mathbb{R}^3_+\,, \tag{D.30a}$$

$$\partial_n \Psi_{ki}^N = \mu_{ki}^N \Psi_{ki}^N\,, \quad y_3 = 0\,,\ (y_1, y_2) \in \Gamma_i\,, \tag{D.30b}$$

$$\partial_n \Psi_{ki}^N = 0\,, \quad y_3 = 0\,,\ (y_1, y_2) \notin \Gamma_i\,, \tag{D.30c}$$

$$|\mathbf{y}|^2\, |\nabla \Psi_{ki}^N(\mathbf{y})| \to 0\,, \quad \text{as} \quad |\mathbf{y}| \to \infty\,. \tag{D.30d}$$

This spectral problem, which was formulated in [68], admits infinitely many nontrivial solutions $\{\mu_{ki}^N, \Psi_{ki}^N\}$, enumerated by $k = 0, 1, \ldots$, such that the eigenvalues form an ordered sequence,

$$0 = \mu_{0i}^N < \mu_{1i}^N \le \mu_{2i}^N \le \ldots \nearrow +\infty, \tag{D.31}$$

whereas the restrictions $\Psi_{ki}^N|_{\Gamma_i}$ onto Γ_i form a complete orthonormal basis of $L^2(\Gamma_i)$. The spectral problem differs from the former problem (D.1) by the imposed behavior of eigenfunctions at infinity. In fact, while (D.1d) can be interpreted as a Dirichlet condition at infinity, (D.30d) implements a vanishing flow condition, which is a sort of Neumann condition at infinity. The distinctions between these two cases were investigated in a much more general setting in [2]. It is trivial to check that a constant function $\Psi_{0i}^N = 1/\sqrt{|\Gamma_i|}$ is a solution of (D.30), with the trivial eigenvalue $\mu_{0i}^N = 0$. As the other eigenfunctions Ψ_{ki}^N must be orthogonal to Ψ_{0i}^N in $L^2(\Gamma_i)$, one has $\int_{\Gamma_i} \Psi_{ki}^N \, d\mathbf{y} = 0$ for any $k > 0$. Note that the condition (D.30d) does not require vanishing of Ψ_{ki}^N at infinity, i.e., Ψ_{ki}^N may have a constant non-zero limit as $|\mathbf{y}| \to \infty$. For a circular patch, the first eight eigenvalues μ_{ki}^N corresponding to axially symmetric eigenfunctions, are given in the last row of Table D.1 (see [56] for the details on their numerical computation).

The exterior Steklov problems (D.1) and (D.30) provide complementary spectral tools for our asymptotic analysis. It is therefore instructive to discuss several relations between the eigenpairs of these problems. For some indices k and k', let us multiply (D.1a) by $\Psi_{k'i}^N$, multiply (D.30a) with k' by Ψ_{ki}, subtract these equations, integrate over a large hemisphere, apply the Green's formula, and use the boundary conditions

and the asymptotic behavior at infinity to get

$$\left(\mu_{ki} - \mu^N_{k'i}\right) \int_{\Gamma_i} \Psi_{ki}(\mathbf{y}) \Psi^N_{k'i}(\mathbf{y})\, d\mathbf{y} = \mu_{ki} d_{ki} \Psi^N_{k'i}(\infty)\,. \tag{D.32}$$

This identity allows us to characterize the spectra of the two problems. In (7.3), we introduced the resonant set $\mathcal{P}_i$ as the union of all eigenvalues μ_{ki} for which $d_{ki} \neq 0$:

$$\mathcal{P}_i \equiv \bigcup_{k=0}^{\infty} \{\mu_{ki} \mid d_{ki} \neq 0\}\ . \tag{D.33}$$

The union of the remaining eigenvalues is then denoted by

$$\mathcal{P}_i^0 \equiv \bigcup_{k=0}^{\infty} \{\mu_{ki} \mid d_{ki} = 0\}\ . \tag{D.34}$$

We emphasize that the intersection of these two sets is not necessarily empty, i.e., there may exist indices $k \neq k'$ such that $\mu_{ki} = \mu_{k'i}$, $d_{ki} \neq 0$ and $d_{k'i} = 0$. In analogy, one can define two sets for the spectral problem (D.30) by

$$\mathcal{P}_i^N \equiv \bigcup_{k=0}^{\infty} \left\{\mu^N_{ki} \mid \Psi^N_{ki}(\infty) \neq 0\right\}\ , \tag{D.35a}$$

$$\mathcal{P}_i^{0,N} \equiv \bigcup_{k=0}^{\infty} \left\{\mu^N_{ki} \mid \Psi^N_{ki}(\infty) = 0\right\}\ . \tag{D.35b}$$

We now prove the following statement.

LEMMA D.1. *One has*

$$\mathcal{P}_i^0 = \mathcal{P}_i^{0,N}\,, \qquad \mathcal{P}_i \cap \mathcal{P}_i^N = \emptyset\,. \tag{D.36}$$

Proof. Let us first prove that $\mathcal{P}_i^0 \subset \mathcal{P}_i^{0,N}$ in the first relation. If $\mu_{ki} \in \mathcal{P}_i^0$, the right-hand side of (D.32) is zero for all $k' = 0, 1, \ldots$. Since the eigenfunctions $\{\Psi^N_{k'i}\}$ form a complete basis of $L^2(\Gamma_i)$, an eigenfunction Ψ_{ki} cannot be orthogonal to all eigenfunctions $\Psi^N_{k'i}$, implying that there exists an index k' such that $\mu_{ki} = \mu^N_{k'i}$. As a consequence, the associated eigenfunction Ψ_{ki} satisfies both (D.1) and (D.30) so that it must decay faster than $\mathcal{O}\left(1/|\mathbf{y}|\right)$, and thus $\Psi_{ki}(\infty) = 0$. We conclude that $\mu_{ki} \in \mathcal{P}_i^{0,N}$. The opposite inclusion $\mathcal{P}_i^{0,N} \subset \mathcal{P}_i^0$ in the first relation of (D.36) is proved in the same way.

In turn, if $\mu_{ki} \in \mathcal{P}_i$ and $\mu_{k'i} \in \mathcal{P}_i^N$, the right-hand side of (D.32) is nonzero, implying that $\mu_{ki} \neq \mu_{k'i}$ and that the eigenfunctions Ψ_{ki} and $\Psi^N_{k'i}$ are not orthogonal to each other. This proves the second relation in (D.36). ∎

Another practical consequence of the identity (D.32) is the possibility to re-expand an eigenfunction from one basis on the eigenfunctions from the other basis. More precisely, if $\mu_{ki} \in \mathcal{P}_i \backslash \mathcal{P}_i^0$, then

$$\Psi_{ki}(\mathbf{y}) = \sum_{k'=0}^{\infty} (\Psi_{ki}, \Psi^N_{k'i})_{L^2(\Gamma_i)} \Psi^N_{k'i}(\mathbf{y}) = \mu_{ki} d_{ki} \sum_{k'=0}^{\infty} \frac{\Psi^N_{k'i}(\infty)}{\mu_{ki} - \mu^N_{k'i}} \Psi^N_{k'i}(\mathbf{y})\,, \quad \mathbf{y} \in \Gamma_i\,; \tag{D.37}$$

similarly, if $\mu^N_{k'i} \in \mathcal{P}^N_i \backslash \mathcal{P}^0_i$, then

(D.38)
$$\Psi^N_{k'i}(\mathbf{y}) = \sum_{k=0}^{\infty} (\Psi^N_{k'i}, \Psi_{ki})_{L^2(\Gamma_i)} \Psi_{ki}(\mathbf{y}) = \Psi^N_{k'i}(\infty) \sum_{k=0}^{\infty} \frac{\mu_{ki} d_{ki}}{\mu_{ki} - \mu^N_{k'i}} \Psi_{ki}(\mathbf{y}) \,, \quad \mathbf{y} \in \Gamma_i \,.$$

The complementary nature of the Steklov problems (D.1) and (D.30) suggest that the reactive capacitance can actually be expressed in terms of the eigenpairs $\{\mu^N_{ki}, \Psi^N_{ki}\}$, as shown in the following lemma.

LEMMA D.2. *For any $\kappa_i \notin \mathcal{P}^N_i$, one has*

$$\frac{1}{C_i(\kappa_i)} = \frac{1}{C_i(\infty)} + 2\pi \sum_{k=0}^{\infty} \frac{[\Psi^N_{ki}(\infty)]^2}{\mu^N_{ki} + \kappa_i} \,. \tag{D.39}$$

Proof. To prove (D.39), we consider an auxiliary function

$$\tilde{w}_i(\mathbf{y}; \kappa) = \frac{w_i(\mathbf{y}; \infty)}{C_i(\infty)} - \frac{w_i(\mathbf{y}; \kappa)}{C_i(\kappa)} \,, \tag{D.40}$$

which, by construction and via (3.3), satisfies

$$\Delta_{\mathbf{y}} \tilde{w}_i = 0 \,, \quad \mathbf{y} \in \mathbb{R}^3_+ \,, \tag{D.41a}$$

$$\partial_n \tilde{w}_i + \kappa \tilde{w}_i = \kappa \left(\frac{1}{C_i(\infty)} - \frac{1}{C_i(\kappa)} \right) + \frac{\partial_n w_i(\mathbf{y}; \infty)}{C_i(\infty)} \,, \quad y_3 = 0 \,, \, (y_1, y_2) \in \Gamma_i \,, \tag{D.41b}$$

$$\partial_n \tilde{w}_i = 0 \,, \quad y_3 = 0 \,, \, (y_1, y_2) \notin \Gamma_i \,, \tag{D.41c}$$

$$\tilde{w}_i(\mathbf{y}) \sim o(1/|\mathbf{y}|) \,, \quad \text{as} \quad |\mathbf{y}| \to \infty \,. \tag{D.41d}$$

Since the decay of this function at infinity does not include the monopole term $1/|\mathbf{y}|$, it can decomposed onto the Steklov eigenfunctions $\{\Psi^N_{ki}\}$, with the coefficients obtained from the boundary condition:

$$\tilde{w}_i(\mathbf{y}; \kappa) = \frac{1}{C_i(\infty)} - \frac{1}{C_i(\kappa)} + \frac{1}{C_i(\infty)} \sum_{k=0}^{\infty} \frac{\left(\partial_n w_i(\mathbf{y}; \infty), \Psi^N_{ki}\right)_{L^2(\Gamma_i)}}{\mu^N_{ki} + \kappa} \Psi^N_{ki}(\mathbf{y}) \,, \tag{D.42}$$

where we used $\Psi^N_{0i}(\mathbf{y}) = 1/\sqrt{|\Gamma_i|}$ for the first two terms. Multiplying (D.30a) by $w_i(\mathbf{y}; \infty)$, multiplying (3.3a) with $\kappa_i = \infty$ by $\Psi^N_{ki}(\mathbf{y})$, subtracting these equations, integrating them over a large hemisphere, applying the Green's formula, the boundary conditions and the decay at infinity, we get

$$\int_{\Gamma_i} \Psi^N_{ki}(\mathbf{y}) \left(\partial_n w_i(\mathbf{y}; \infty)\right) d\mathbf{y} = 2\pi C_i(\infty) \Psi^N_{ki}(\infty) \,, \tag{D.43}$$

that determines the scalar product in (D.42). Finally, in the limit $|\mathbf{y}| \to \infty$, the left-hand side of (D.42) vanishes, yielding the spectral expansion (D.39). ∎

While the original representation (3.5) allowed us to get the upper bound (D.13), the alternative expansion (D.39) gives access to lower bounds. For instance, one has

$$\frac{1}{C_i(\kappa_i)} \leq \frac{1}{C_i(\infty)} + \frac{2\pi}{\kappa_i |\Gamma_i|} + 2\pi \sum_{k=1}^{\infty} \frac{[\Psi^N_{ki}(\infty)]^2}{\mu^N_{ki}} \,. \tag{D.44}$$

The last sum can computed by comparing the Taylor series of $1/C_i(\kappa_i)$ as $\kappa_i \to 0$ with (3.8a), from which

$$\frac{1}{C_i(\infty)} + 2\pi \sum_{k=1}^{\infty} \frac{[\Psi_{ki}^N(\infty)]^2}{\mu_{ki}^N} = \frac{4\pi^2 a_i^3 c_{2i}}{|\Gamma_i|^2}\,, \tag{D.45}$$

where the coefficient c_{2i} is given by (3.9). We conclude that

$$C_i(\kappa_i) \geq \frac{\kappa_i |\Gamma_i|}{2\pi} \left(1 + \frac{2\pi a_i^3 c_{2i}}{|\Gamma_i|} \kappa_i\right)^{-1}. \tag{D.46}$$

We remark that if the last term in (D.44) is neglected, we recover our sigmoidal approximation (3.12). The smallness of this last term as compared to $1/C_i(\infty)$ may explain the high accuracy of this approximation.

From the representation (D.39), it is clear that, when κ_i approaches $-\mu_{ki}^N$ such that $\Psi_{ki}^N(\infty) \neq 0$, the right-hand side of (D.39) diverges, so that $C_i(-\kappa_i)$ vanishes. In other words, any element of $\mathcal{P}_i^N$ is a zero of the function $C_i(-\kappa)$. In the following lemma, we prove that all zeros of $C_i(-\kappa)$ are in $\mathcal{P}_i^N$.

LEMMA D.3. *Let $\mathcal{Z}_0$ be the set of zeros of the function $C_i(-\mu)$, and $\mathcal{P}_i^N$ be the subset of eigenvalues μ_{ki}^N such that $\Psi_{ki}^N(\infty) \neq 0$. Then $\mathcal{Z}_0 = \mathcal{P}_i^N$.*

Proof. We first prove that $\mathcal{P}_i^N \subset \mathcal{Z}_0$. This inclusion follows directly from (D.39) but we provide an alternative argument here.

We recall from (3.3) that $C_i(-\mu)$ is obtained from the solution to

$$\Delta_{\mathbf{y}} w_i = 0\,, \quad \mathbf{y} \in \mathbb{R}^3_+\,, \tag{D.47a}$$

$$\partial_n w_i - \mu w_i = -\mu\,, \quad y_3 = 0\,,\, (y_1, y_2) \in \Gamma_i\,, \tag{D.47b}$$

$$\partial_n w_i = 0\,, \quad y_3 = 0\,,\, (y_1, y_2) \notin \Gamma_i\,, \tag{D.47c}$$

$$w_i \sim \frac{C_i(-\mu)}{|\mathbf{y}|} + \mathcal{O}(|\mathbf{y}|^{-2})\,, \quad \text{as} \quad |\mathbf{y}| \to \infty\,. \tag{D.47d}$$

By applying Green's second identity to w_i and Ψ_{ki}^N, which satisfies (D.30), over a large hemisphere of radius R in the upper half-plane we pass to the limit $R \to \infty$ to obtain

$$0 = \int_{\mathbb{R}^3_+} \left(w_i\, \Delta_{\mathbf{y}} \Psi_{ki}^N - \Psi_{ki}^N\, \Delta_{\mathbf{y}} w_i\right) d\mathbf{y} = \int_{\Gamma_i} \left(w_i\, \partial_n \Psi_{ki}^N - \Psi_{ki}^N\, \partial_n w_i\right) d\mathbf{y} \\ + 2\pi \lim_{R\to\infty} R^2 \left(w_i \frac{\partial \Psi_{ki}^N}{\partial |\mathbf{y}|} - \Psi_{ki}^N \frac{\partial w_i}{\partial |\mathbf{y}|}\right)\Big|_{|\mathbf{y}|=R}. \tag{D.48}$$

Then, upon using the Steklov conditions (D.30b) and (D.47b) on Γ_i, together with the far-field behaviors (D.30d) and (D.47d) for Ψ_{ki}^N and w_i, we find that (D.48) reduces to

$$\left(\mu_{ki}^N - \mu\right) \int_{\Gamma_i} w_i \Psi_{ki}^N\, d\mathbf{y} + \mu \int_{\Gamma_i} \Psi_{ki}^N\, dy + 2\pi \Psi_{ki}^N(\infty) C_i(-\mu) = 0\,. \tag{D.49}$$

Owing to the decay behavior (D.30d), we obtain from the divergence theorem that for $k > 0$, for which $\mu_{ki}^N > 0$, we have $\int_{\Gamma_i} \Psi_{ki}^N\, d\mathbf{y} = \left(\mu_{ki}^N\right)^{-1} \int_{\Gamma_i} \partial_n \Psi_{ki}^N\, d\mathbf{y} = 0$. As a result, (D.49) simplifies to

$$\left(\mu_{ki}^N - \mu\right) \int_{\Gamma} w_i \Psi_{ki}^N\, d\mathbf{y} = -2\pi \Psi_{ki}^N(\infty) C_i(-\mu)\,. \tag{D.50}$$

We conclude that if an eigenfunction Ψ_{ki}^N does not vanish at infinity, then the function $C_i(-\mu)$ must vanish at $\mu = \mu_{ki}^N$. By its definition (3.5), $C_i(-\mu)$ also vanishes at $\mu = \mu_{0i}^N = 0$. This proves that $\mathcal{P}_i^N \subset \mathcal{Z}_0$.

Let us now prove the opposite inclusion $\mathcal{Z}_0 \subset \mathcal{P}_i^N$, i.e., there is no other zero of $C_i(-\mu)$ than those determined by the eigenvalues μ_{ki}^N. Assume that there exists $\mu' > 0$ such that $-\mu' \in \mathcal{Z}_0$ but $-\mu' \notin \mathcal{P}_i^N$. Since the basis of eigenfunctions Ψ_{ki}^N is complete in $L^2(\Gamma_i)$, there is a unique solution to the inhomogeneous problem

$$\Delta_{\mathbf{y}} U = 0\,, \quad \mathbf{y} \in \mathbb{R}^3_+\,, \tag{D.51a}$$

$$\partial_n U - \mu' U = f\,, \quad y_3 = 0\,,\ (y_1, y_2) \in \Gamma_i\,, \tag{D.51b}$$

$$\partial_n U = 0\,, \quad y_3 = 0\,,\ (y_1, y_2) \notin \Gamma_i\,, \tag{D.51c}$$

$$|\mathbf{y}|^2\, |\nabla U(\mathbf{y})| \to 0\,, \quad \text{as} \quad |\mathbf{y}| \to \infty\,, \tag{D.51d}$$

where we set $f = (\Psi_{0i})|_\Gamma$. The divergence theorem implies

$$0 = \int_{\Gamma_i} \partial_n U \, d\mathbf{y} = \mu' \int_{\Gamma_i} U \, d\mathbf{y} + d_{0i}\,, \tag{D.52}$$

where d_{0i} is given by (D.8). On one hand, upon multiplication of (D.16) by U and integration over Γ_i, while using (D.52), we obtain

$$-\frac{d_{0i}}{\mu'} = \int_\Gamma U \, d\mathbf{y} = \sum_{k=0}^{\infty} d_{ki} \int_{\Gamma_i} U \Psi_{ki} \, d\mathbf{y}\,. \tag{D.53}$$

On the other hand, upon applying Green's second identity to U and Ψ_{ki} over a large hemisphere in the upper half-plane and passing to the limit we obtain

$$0 = \int_{\mathbb{R}^3_+} (\Psi_{ki} \Delta_{\mathbf{y}} U - U \Delta_{\mathbf{y}} \Psi_{ki}) \, d\mathbf{y} = \mu_{ki} d_{ki} U(\infty) + (\mu' - \mu_{ki}) \int_{\Gamma_i} U \Psi_{ki} \, d\mathbf{y} + \delta_{0,k}\,, \tag{D.54}$$

due to the orthonormality of Ψ_{ki} to Ψ_{0i}. Upon solving (D.54) for $\int_{\Gamma_i} U \Psi_{ki} \, d\mathbf{y}$, we obtain from (D.52) and the Steklov eigenfunction expansion of $C_i(\mu)$ in (D.12), that

$$-d_{0i} = \mu' \left[\frac{d_{0i}}{\mu_{0i} - \mu'} + U(\infty) \sum_{k=0}^{\infty} \frac{\mu_{ki} d_{ki}^2}{\mu_{ki} - \mu'} \right] = \frac{d_{0i} \mu'}{\mu_{0i} - \mu'} - 2\pi U(\infty) C_i(-\mu')\,. \tag{D.55}$$

Since μ' was assumed to be a zero of $C_i(-\mu)$, we conclude that $-d_{0i} = d_{0i}\mu'/(\mu_{0i} - \mu')$. Given that $d_{0i} \neq 0$, this yields that $\mu_{0i} = 0$, which contradicts the strict positivity of the principal eigenvalue μ_{0i}. We conclude that the second inclusion $\mathcal{Z}_0 \subset \mathcal{P}_i^N$ must also hold. Therefore, $\mathcal{Z}_0 = \mathcal{P}_i^N$. ∎

D.5. Relation to Dirichlet-to-Neumann operators. The dual character of the Steklov problems (D.1) and (D.30) can be further understood from the tight relation between the associated Dirichlet-to-Neumann operators $\mathcal{D}_i$ and $\mathcal{D}_i^N$. The operator $\mathcal{D}_i$ associates to a function $f \in H^{1/2}(\Gamma_i)$ on the patch Γ_i another function $g = \mathcal{D}_i f = (\partial_n u)|_{\Gamma_i} \in H^{-1/2}(\Gamma_i)$ on the same patch, where u is the unique solution of the BVP

$$\Delta u = 0 \quad \text{in } \mathbb{R}^3_+\,, \qquad u = f \quad \text{on } y_3 = 0,\ (y_1, y_2) \in \Gamma_i\,, \tag{D.56a}$$

$$\partial_n u = 0 \quad \text{on } y_3 = 0,\ (y_1, y_2) \notin \Gamma_i\,, \qquad u \to 0 \quad \text{as } |\mathbf{y}| \to \infty\,. \tag{D.56b}$$

The operator $\mathcal{D}_i^N$ acts similarly, i.e., $g = \mathcal{D}_i^N f = (\partial_n u^N)|_{\Gamma_i}$, where u^N satisfies the similar BVP, except for the asymptotic decay $|\mathbf{y}|^2|\nabla u^N| \to 0$ at infinity. The spectral properties of the operators $\mathcal{D}_i$ and $\mathcal{D}_i^N$ were investigated in a more general setting in [2, 19]. It is easy to check that μ_{ki} and $\Psi_{ki}|_{\Gamma_i}$ are the eigenpairs of $\mathcal{D}_i$, whereas μ_{ki}^N and $\Psi_{ki}^N|_{\Gamma_i}$ are the eigenpairs of $\mathcal{D}_i^N$. Moreover, Theorem 5.9 from [2] states that these two operators differ by a rank-one perturbation:

(D.57)
$$\mathcal{D}_i f = \mathcal{D}_i^N f + \frac{1}{\beta_i}(f, \varphi_i)_{L^2(\Gamma_i)}\varphi_i\,, \qquad \text{where } \varphi_i = \mathcal{D}_i 1 \quad \text{and} \quad \beta_i = (1, \varphi_i)_{L^2(\Gamma_i)}$$

(even though this statement was proved for a slightly different setting of exterior problems in the whole space, the arguments seem to straightforwardly apply to our case, see further discussion in [19]). Since (D.56) with $f = 1$ is identical to (3.3) with $\kappa_i = \infty$, one gets

(D.58)
$$\varphi_i = \mathcal{D}_i 1 = (\partial_n w_i(\mathbf{y}; \infty))|_{\Gamma_i}\,, \qquad \beta_i = 2\pi C_i(\infty)\,,$$

where the second relation follows from the divergence theorem.

Many former relations can be rapidly recovered by using the operators $\mathcal{D}_i$ and $\mathcal{D}_i^N$. To illustrate this point, we first note that, according to (D.4), $1/(2\pi|\mathbf{x}-\mathbf{y}|)$ is the kernel of the inverse of $\mathcal{D}_i$ so that the function ω_i, defined in (3.10), can be formally written as $\omega_i = \mathcal{D}_i^{-1}1$ (the operator $\mathcal{D}_i$ is invertible because all its eigenvalues are strictly positive). The projections of this relation onto a constant function or onto itself yield immediately that

(D.59a)
$$\int_{\Gamma_i} \omega_i(\mathbf{y}) d\mathbf{y} = (1, \mathcal{D}_i^{-1}1)_{L^2(\Gamma_i)} = \sum_{k=0}^{\infty} \frac{d_{ki}^2}{\mu_{ki}}\,,$$

(D.59b)
$$\int_{\Gamma_i} [\omega_i(\mathbf{y})]^2 d\mathbf{y} = (\mathcal{D}_i^{-1}1, \mathcal{D}_i^{-1}1)_{L^2(\Gamma_i)} = \sum_{k=0}^{\infty} \frac{d_{ki}^2}{\mu_{ki}^2}\,,$$

from which follows the representations (3.9) for the coefficients c_{2i} and c_{3i}.

Appendix E. Computation and Analysis of the Monopole Term E_i.

We aim at computing numerically the coefficient E_i given by (3.24) for the circular patch Γ_i of radius a_i. Upon changing the integration variables, we represent it as

(E.1)
$$E_i(\kappa_i) = -\frac{C_i^2(\kappa_i)}{2}\log a_i + a_i^2 \mathcal{E}_i(\kappa_i a_i)\,,$$

where

(E.2)
$$\mathcal{E}_i(\mu) = 2\int_0^1 \frac{1}{r}\left(\int_0^r r' a_i q_i(a_i r'; \mu/a_i)\, dr'\right)^2 dr$$

now corresponds to the unit disk. By recalling the limiting asymptotics in (3.26), we observe that $\mathcal{E}_i(\infty) = (3 - 4\log 2)/\pi^2$ and that $\mathcal{E}_i(\mu) \approx \mu^2/32$ as $\mu \to 0$.

In order to compute the integral in (E.2), one can employ the spectral representation (D.10) of the density $q_i(\mathbf{y}; \kappa_i)$. The presence of the factor μ_{ki} in the numerator of (D.10) deteriorates the numerical convergence of the spectral expansion, thus requiring higher truncation orders. Therefore, it is convenient to use the identity (D.16) to represent this function as

(E.3)
$$q_i(\mathbf{y}; \kappa_i) = \frac{\kappa_i}{2}\left(1 - \kappa_i \sum_{k=0}^{\infty} \frac{d_{ki}\,\Psi_{ki}(\mathbf{y})}{\mu_{ki} + \kappa_i}\right), \quad \text{for} \quad \mathbf{y} \in \Gamma_i\,,$$

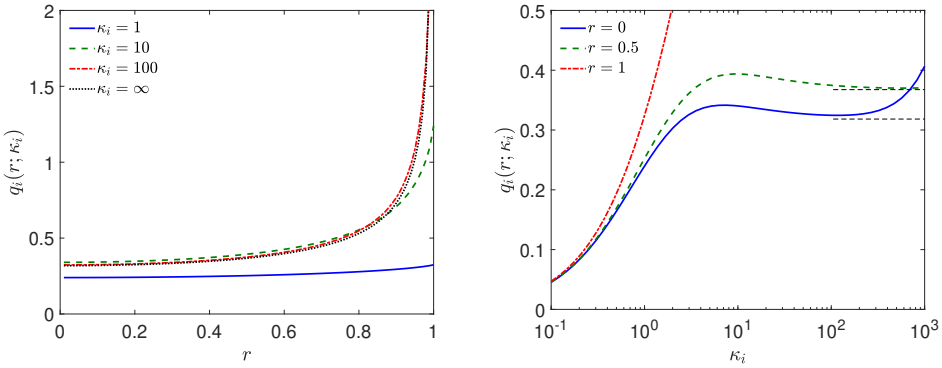

(a) $q_i(r;\kappa_i)$ versus r for three κ_i **(b)** $q_i(r;\kappa_i)$ versus κ_i for three r

Fig. E.1: (a): The density $q_i(r;\kappa_i)$ for the unit disk ($a_i = 1$) as a function of r, for different values of κ_i, as indicated in the legend. The three curves were obtained by truncating the series in (E.3) at $k \le 500$. The black dashed curve presents the exact expression (3.14). **(b):** The density $q_i(r;\kappa_i)$ as a function of κ_i, for three fixed r. Here we used the truncation up to 1000 terms; nevertheless, the obtained q_i at $r = 0$ exhibits erroneous behavior at large κ_i, since it does not approach its limit $1/(\pi\sqrt{1-r^2})$, as indicated by dashed horizontal line.

which exhibits a faster convergence. Repeating this trick, we get an even faster converging representation for $\mathbf{y} \in \Gamma_i$ given by

$$q_i(\mathbf{y};\kappa_i) = \frac{\kappa_i}{2}\left(1 - \kappa_i\left[\frac{2a_i}{\pi}E(|\mathbf{y}|/a_i) - \kappa_i\sum_{k=0}^{\infty}\frac{d_{ki}\,\Psi_{ki}(\mathbf{y})}{\mu_{ki}(\mu_{ki}+\kappa_i)}\right]\right), \quad \text{for} \quad \mathbf{y} \in \Gamma_i\,, \tag{E.4}$$

where $E(z)$ is the complete elliptic integral of the second kind.

Figure E.1(a) illustrates the behavior of the density q_i versus r for the unit disk ($a_i = 1$). As expected, this density approaches its limiting form $q_i(\mathbf{y};\infty)$ as $\kappa_i \to \infty$. Curiously, for a fixed r, q_i is not a monotone increasing function of κ_i, as illustrated in Fig. E.1(b). Finally, we highlight that even the use of large truncation orders does not fully resolve the issue of the numerical accuracy at large κ_i, especially for small r.

In Fig. E.2, we plot the numerically computed $E_i(\kappa_i) = \mathcal{E}_i(\kappa_i)$ versus κ_i for $\kappa_i < 0$ for the unit disk ($a_i = 1$). In computing $\mathcal{E}_i$ from (E.2), we numerically evaluated the integral in (E.2) with the discretization step $\delta r = 10^{-4}$, where q_i was estimated from the series (E.3) truncated to either 200 terms (crosses) or to 1000 terms (line). An excellent agreement between these two results confirms the accuracy of our numerical computation. Despite the vertical asymptotes (the poles of $C_i(\kappa_i)$), the function $E_i(\kappa_i)$ remains always positive.

In turn, Fig. 3.3 shows the dependence of the coefficient $E_i(\kappa_i)$ on κ_i for $\kappa_i > 0$. In contrast to that for $C_i(\kappa_i)$, this dependence is not monotonous. We expect that this is a result of the non-monotone approach of $q_i(\mathbf{y};\kappa_i)$ to $q_i(\mathbf{y};\infty)$, as discussed earlier. It is also worth noting that the numerical computation for large κ_i requires large truncation orders; in fact, the truncation order 100 was not sufficient for $\kappa_i \ge 100$ (two curves start to deviate from each other). Even the large truncation order 500 becomes insufficient for $\kappa_i \ge 1000$ (not shown). To overcome this difficulty, we propose

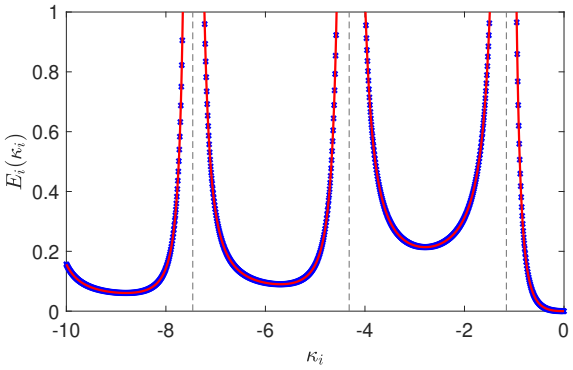

Fig. E.2: The numerically computed $E_i(\kappa_i)$ for $\kappa_i < 0$ for a circular patch Γ_i with $a_i = 1$. Vertical dashed lines indicate three poles $\{-\mu_{ki}\}$ of $C_i(\kappa_i)$, which are also the poles of q_i and thus of E_i. Crosses correspond to the truncation order $k_{\max} = 200$, whereas line presents the result for $k_{\max} = 1000$.

below a simple empirical formula (E.6) for $E_i(\kappa_i)$ that closely predicts the numerically computed value on the entire range $\kappa_i > 0$. The remarkable accuracy of this simple approximation was illustrated in Fig. 3.3.

Empirical Approximation of E for the Unit Disk. The non-monotonic behavior of $E_i(\kappa_i)$ makes its approximation trickier. For this reason, we consider the ratio $E_i(\kappa_i)/C_i^2(\kappa_i)$, which turns out to be a monotone decreasing function of κ_i that ranges from $1/8$ at $\kappa_i = 0$ to $3/4 - \log 2$ as $\kappa_i \to \infty$. This behavior suggests to approximate it for the unit disk as

$$\frac{E_i(\kappa)}{C_i^2(\kappa)} \approx \frac{3}{4} - \log 2 + \frac{1}{\frac{1}{\log 2 - 5/8} + f(\kappa)}\,, \tag{E.5}$$

where $f(\kappa)$ is a suitable increasing function of κ (such that $f(0) = 0$ and $f(\infty) = \infty$). Choosing $f(\kappa) = 3.04\,\kappa^{0.88}$, one can make this approximation accurate, but it still requires the computation of $C_i(\kappa)$ via its spectral representation (D.12). Applying the empirical approximation $C^{\rm app}(\kappa) = 2\kappa/(\pi\kappa + 4)$ from (3.17) for $C_i(\kappa)$, we get a fully explicit empirical approximation on $\kappa > 0$ for the unit disk:

$$E^{\rm app}(\kappa) = \frac{4\kappa^2}{(\pi\kappa + 4)^2}\left(\frac{3}{4} - \log 2 + \frac{1}{\frac{1}{\log 2 - 5/8} + 5.17\,\kappa^{0.81}}\right), \tag{E.6}$$

where we adjusted the function $f(\kappa)$ to ensure higher accuracy. The closeness of this approximation was shown in Fig. 3.3.

Appendix F. Improved Numerics for the SN Problem.

In this appendix, we devise an accurate numerical method to treat the SN problem (2.12) for the unit sphere with either one circular patch, or two circular patches centered at the north and south poles. To do so, we employ a general expansion of an axially symmetric harmonic function U in spherical coordinates in terms of Legendre polynomials $P_n(z)$, given by

$$V(r,\theta) = \sum_{n=0}^{\infty} c_n r^n P_n(\cos\theta)\,. \tag{F.1}$$

The unknown coefficients c_n are determined from the mixed boundary condition:

$$\partial_n V = \mu I_{\Omega_a} V, \tag{F.2}$$

where I_{Ω_a} is the indicator function of the patches Ω_a. The substitution of the expansion (F.1) yields

$$\sum_{n=0}^{\infty} c_n n P_n(\cos\theta) = \mu \sum_{n=0}^{\infty} c_n P_n(\cos\theta) I_{\Omega_a}(\theta)\,. \tag{F.3}$$

Multiplying this equation by $P_m(\cos\theta)\sin\theta$ and integrating over $\theta \in (0,\pi)$, we get a system of linear equations

(F.4)

$$m c_m = \mu \sum_{n=0}^{\infty} K_{m,n} c_n\,, \qquad K_{m,n} = (m+1/2) \int_0^{\pi} \sin\theta\, P_m(\cos\theta) P_n(\cos\theta) I_{\Omega_a}(\theta) d\theta\,.$$

As the left-hand side vanishes at $m = 0$, it is convenient to isolate the coefficient c_0 from this relation at $m = 0$ as

$$c_0 = -\frac{1}{K_{00}} \sum_{n=1}^{\infty} K_{0,n} c_n\,. \tag{F.5}$$

We substitute it into the above system to get

$$m c_m = \mu \left(-\frac{K_{m,0}}{K_{0,0}} \sum_{n=1}^{\infty} K_{0,n} c_n + \sum_{n=1}^{\infty} K_{m,n} c_n \right) \quad \text{for} \quad m = 1, 2, \ldots\,. \tag{F.6}$$

This system of linear equations can be written in a matrix form as

$$\mathbf{M}\mathbf{C} = \frac{1}{\mu}\mathbf{C}\,, \tag{F.7}$$

where $\mathbf{C}$ is the vector of coefficients $c_1, c_2, \ldots$, and

$$\mathbf{M}_{m,n} = \frac{1}{m}\left(K_{m,n} - \frac{K_{m,0} K_{0,n}}{K_{0,0}} \right) \quad \text{for} \quad m, n = 1, 2, \ldots\,. \tag{F.8}$$

A numerical diagonalization of the truncated matrix $\mathbf{M}$ allows one to determine the eigenvalues μ of the SN problem.

For a single patch of angle ε_1 at the north pole, an explicit representation of the elements $K_{m,n}$ was given in Appendix D.3 of [48] as

$$K^{(1)}_{m,n}(\varepsilon_1) = \sum_{k=0}^{\min\{m,n\}} B^k_{mn} \frac{P_{m+n-2k-1}(\cos\varepsilon_1) - P_{m+n-2k+1}(\cos\varepsilon_1)}{2(m+n-2k)+1}\,, \tag{F.9}$$

where

$$B^k_{mn} = \frac{A_k A_{m-k} A_{n-k}}{A_{m+n-k}} \frac{2m+2n-4k+1}{2m+2n-2k+1}\,, \quad A_k = \frac{\Gamma(k+1/2)}{\sqrt{\pi}\,\Gamma(k+1)}\,, \quad A_0 = 1\,. \tag{F.10}$$

For a single patch of angle ε_2 at the south pole, one can use the symmetry of Legendre polynomials, $P_n(1-x) = (-1)^n P_n(x)$, to get

$$K^{(2)}_{m,n}(\varepsilon_2) = (-1)^{m+n} K^{(1)}_{m,n}(\varepsilon_2)\,. \tag{F.11}$$

$n_{\max}$	ε	0.1	0.15	0.2	0.25	0.30
1000	$\sigma^{(1)}$	4.0646	4.0362	4.0080	3.9801	3.9523
2000	$\sigma^{(1)}$	4.0644	4.0361	4.0080	3.9801	3.9523

Table F.1: Numerical approximation for the first SN eigenvalue $\sigma^{(1)}_{\text{num}}$ for a single circular patch of radius ε on the unit sphere for various values of ε and two different truncations of the matrix $\mathbf{M}$.

When there are two patches, the matrix element $K_{m,n}$ is the sum of these two contributions.

We emphasize that $V(r,\theta)$ in (F.1) is constructed to be axially symmetric (i.e., independent of the angle ϕ). In other words, this numerical procedure gives access exclusively to axially symmetric eigenfunctions of the SN problem. In a similar way, one can construct non-axially-symmetric eigenfunctions by using a representation in the form $e^{im\phi}r^n P_n^m(\cos\theta)$ with associated Legendre polynomials $P_n^m(z)$, see similar constructions in [55, 56].

Numerical Results for One Patch. For validation purpose, we consider the case of a single patch of radius ε at the north pole. We compute the first SN eigenvalue by truncating the matrix $\mathbf{M}$ to the size $n_{\max} \times n_{\max}$. Our numerical results for the first eigenvalue, labeled by $\sigma^{(1)}_{\text{num}}$, for different ε and two different truncations $n_{\max}$ are shown in Table F.1. From this table we observe that increasing $n_{\max}$ by a factor of two does not significantly change our numerical estimate for the first SN eigenvalue, which confirms the high accuracy of our numerical method. The favorable comparison between the first two numerically computed SN eigenvalues and their asymptotic predictions in (7.25a) is shown in Fig. 7.1.

REFERENCES

[1] B. Alberts, D. Bray, J. Lewis, M. Raff, K. Roberts, and J. D. Watson. *Molecular Biology of the Cell*. Garland, New York, 3rd edition, 1994.

[2] W. Arendt and ter Elst A. F. M. The Dirichlet-to-Neumann operator on exterior domains. *Poten. Anal.*, 43:313–340, 2015.

[3] J. W. S. Baron Rayleigh. *The Theory of Sound*, volume 2. Dover, New York, 2nd edition, 1945.

[4] O. Bénichou, M. Moreau, and G. Oshanin. Kinetics of stochastically gated diffusion-limited reactions and geometry of random walk trajectories. *Phys. Rev. E*, 61:3388–3406, 2000.

[5] O. Bénichou and R. Voituriez. Narrow escape time problem: Time needed for a particle to exit a confining domain through a small window. *Phys. Rev. Lett*, 100:168105, 2008.

[6] A. M. Berezhkovskii, L. Dagdug, V. A. Lizunov, J. Zimmerberg, and S. M. Bezrukov. Communication. Clusters of absorbing disks on a reflecting wall: Competition for diffusing particles. *J. Chem. Phys.*, 136:211102, 2012.

[7] A. M. Berezhkovskii, Y. A. Makhnovskii, M. I. Monine, V. Y. Zitserman, and S. Y. Shvartsman. Boundary homogenization for trapping by patchy surfaces. *J. Chem. Phys.*, 121:11390–11394, 2004.

[8] A. M. Berezhkovskii, M. I. Monine, C. B. Muratov, and S. Y. Shvartsman. Homogenization of boundary conditions for surfaces with regular arrays of traps. *J. Chem. Phys.*, 124:036103, 2006.

[9] H. C. Berg and E. M. Purcell. Physics of chemoreception. *Biophys. J.*, 20(2):193–219, 1977.

[10] O. G. Berg and P. H. von Hippel. Diffusion-controlled macromolecular interactions. *Ann. Rev. Biophys. Biophys. Chem.*, 14:131–160, 1985.

[11] A. Bernoff, A. Lindsay, and D. Schmidt. Boundary homogenization and capture time distributions of semipermeable membranes with periodic patterns of reactive sites. *SIAM Multi. Model. Simul.*, 16:1411–1447, 2018.

[12] P. C. Bressloff. Target competition for resources under multiple search-and-capture events with stochastic resetting. *Proc. R. Soc. A*, 476:20200475, 2020.
[13] P. C. Bressloff. Asymptotic analysis of extended two-dimensional narrow capture problems. *Proc. Roy. Soc. A.*, 477:20200771, 2021.
[14] P. C. Bressloff. Asymptotic analysis of target fluxes in the three-dimensional narrow capture problem. *SIAM Multi. Model Simul.*, 19(2):612–632, 2021.
[15] P. C. Bressloff. Encounter-based reaction-subdiffusion model I: Surface adsorption and the local time propagator. *J. Phys. A: Math. Theor.*, 56:435004, 2023.
[16] P. C. Bressloff. Encounter-based reaction-subdiffusion model II: Partially absorbing traps and the occupation time propagator. *J. Phys. A: Math. Theor.*, 56:435005, 2023.
[17] P. C. Bressloff and S. D. Lawley. Stochastically gated diffusion-limited reactions for a small target in a bounded domain. *Phys. Rev. E.*, 92(6):062117, 2015.
[18] P. C. Bressloff and J. Newby. Stochastic models of intracellular transport. *Rev. Mod. Phys.*, 85:135–196, 2013.
[19] L. Bundrock, A. Girouard, D. S. Grebenkov, M. Levitin, and I. Polterovich. The exterior Steklov problem for Euclidean domains. *in preparation*, 2025.
[20] D. F. Calef and J. M. Deutch. Diffusion-controlled reactions. *Ann. Rev. Phys. Chem.*, 34:493–524, 1983.
[21] P. T. Callaghan. *Principles of Nuclear Magnetic Resonance Microscopy*. Clarendon, Oxford, 1991.
[22] A. Cengiz and S. D. Lawley. Narrow escape with imperfect reactions. *Phys. Rev. E*, 110:054127, 2024.
[23] A. Chaigneau and D. S. Grebenkov. First-passage times to anisotropic partially reactive targets. *Phys. Rev. E*, 105:054146, 2022.
[24] A. Chaigneau and D. S. Grebenkov. A numerical study of the generalized Steklov problem in planar domains. *J. Phys. A: Math. Theor*, 57:445201, 2024.
[25] S. J. Chapman, R. Erban, and S. Isaacson. Reactive boundary conditions as limits of interaction potentials for Brownian and Langevin dynamics. *SIAM J. Appl. Math.*, 76:368–390, 2016.
[26] X. Chen and A. Friedman. Asymptotic analysis for the narrow escape problem. *SIAM J. Math. Anal.*, 43:2542–2563, 2011.
[27] J. Cherry, A. E. Lindsay, A. Navarro Hernandez, and B. Quaife. Trapping of planar Brownian motion: Full first passage time distributions by kinetic Monte Carlo, asymptotic, and boundary integral methods. *SIAM Multi. Model Simul.*, 20:1284–1314, 2022.
[28] C. Chevalier, O. Bénichou, B. Meyer, and R. Voituriez. First-passage quantities of Brownian motion in a bounded domain with multiple targets: A unified approach. *J. Phys. A: Math. Theor.*, 44:025002, 2011.
[29] A. F. Cheviakov and M. J. Ward. Optimizing the principal eigenvalue of the Laplacian in a sphere with interior traps. *Math. Computer Model.*, 53:1394–1409, 2011.
[30] A. F. Cheviakov, M. J. Ward, and R. Straube. Anasymptotic analysis of the mean first passage time for narrow escape problems. Part II. The sphere. *SIAM Multi. Model Simul.*, 8:836–870, 2010.
[31] A. F. Cheviakov and D. Zawada. Narrow-escape problem for the unit sphere: Homogenization limit, optimal arrangements of large number of traps, and the N^2 conjecture. *Phys. Rev. E.*, 87:042118, 2013.
[32] B. Colbois, A. Girouard, C. Gordon, and D. Sher. Some recent developments on the Steklov eigenvalue problem. *Rev. Mat. Complut.*, 37:1–161, 2024.
[33] F. C. Collins and G. E. Kimball. Diffusion-controlled reaction rates. *J. Coll. Sci.*, 4:425–437, 1949.
[34] S. Condamin, O. Bénichou, V. Tejedor, R. Voituriez, and J. Klafter. First-passage time in complex scale-invariant media. *Nature*, 450:77–80, 2007.
[35] D. Coombs, R. Straube, and M. J. Ward. Diffusion on a sphere with localized traps: Mean first passage time, eigenvalue asymptotics, and Fekete points. *SIAM J. Appl. Math*, 70:302–332, 2009.
[36] J. Cortés, D. T. Le, R. Iehl, and T. Siméon. Simulating ligand-induced conformational changes in proteins using a mechanical disassembly method. *Phys. Chem. Chem. Phys.*, 12:8268–8276, 2010.
[37] L. Dagdug, J. Peña, and I. Pompa-García. *Diffusion Under Confinement. A Journey Through Counterintuition*. Springer Cham, 2024.
[38] M. Delgado, M. J. Ward, and D. Coombs. Conditional mean first passage times to small traps in a 3-D domain with a sticky boundary: Applications to T cell searching behavior in lymph nodes. *SIAM Multi. Model. Simul.*, 13:1224–1258, 2015.

[39] V. I. Fabrikant. *Applications of Potential Theory to Mechanics: A Selection of New Results*. Monograph in the Series: Mathematics and its Applications, Kluwer Academic Publishers, Dordrecht, 1989.
[40] M. Felici, M. Filoche, and B. Sapoval. Diffusional screening in the human pulmonary acinus. *J. Appl. Physiol.*, 94(5):2010–2016, 2003.
[41] D. W. Fox and J. R. Kuttler. Sloshing frequencies. *Z. Angew. Math. Phys.*, 34:668–696, 1983.
[42] M. Galanti, D. Fanelli, and F. Piazza. Conformation-controlled binding kinetics of antibodies. *Scient. Rep.*, 6:18976, 2016.
[43] A. Girouard and I. Polterovich. Spectral geometry of the Steklov problem. *J. Spectr. Th.*, 7:321–359, 2017.
[44] A. Godec and R. Metzler. First passage time distribution in heterogeneity controlled kinetics: Going beyond the mean first passage time. *Sci. Rep.*, 6:20349, 2016.
[45] I. S. Gradshteyn and I. M. Ryzhik. *Tables of Integrals, Series, and Products; Eds. A. Jeffrey, D. Zwillinger*. Seventh Edition, Academic Press, 2007.
[46] D. S. Grebenkov. NMR survey of reflected Brownian motion. *Rev. Mod. Phys.*, 79:1077–1137, 2007.
[47] D. S. Grebenkov. Universal formula for the mean first passage time in planar domains. *Phys. Rev. Lett.*, 117:260201, 2016.
[48] D. S. Grebenkov. Spectral theory of imperfect diffusion-controlled reactions on heterogeneous catalytic surfaces. *J. Chem. Phys.*, 151:104108, 2019.
[49] D. S. Grebenkov. Diffusion toward non-overlapping partially reactive spherical traps: Fresh insights onto classic problems. *J. Chem. Phys.*, 152:244108, 2020.
[50] D. S. Grebenkov. Joint distribution of multiple boundary local times and related first-passage time problems with multiple targets. *J. Stat. Mech.*, 2020:103205, 2020.
[51] D. S. Grebenkov. Paradigm shift in diffusion-mediated surface phenomena. *Phys. Rev. Lett.*, 125:078102, 2020.
[52] D. S. Grebenkov. Statistics of diffusive encounters with a small target: Three complementary approaches. *J. Stat. Mech.*, 2022, 2022.
[53] D. S. Grebenkov. Diffusion-controlled reactions with non-Markovian binding/unbinding kinetics. *J. Chem. Phys.*, 158:214111, 2023.
[54] D. S. Grebenkov. Encounter-based approach to the escape problem. *Phys. Rev. E*, 107:044105, 2023.
[55] D. S. Grebenkov. Spectral properties of the Dirichlet-to-Neumann operator for spheroids. *Phys. Rev. E*, 109:055306, 2024.
[56] D. S. Grebenkov. Mixed Steklov-Neumann problem: Asymptotic analysis and applications to diffusion-controlled reactions. *accepted to SIAM Multi. Model. Simul.; preprint on ArXiv: 2409.00213v1*, 2025.
[57] D. S. Grebenkov and A. Chaigneau. The Steklov problem for exterior domains: Asymptotic behavior and applications. *J. Math. Phys.*, 66:061502, 2025.
[58] D. S. Grebenkov, R. Metzler, and G. Oshanin. Strong defocusing of molecular reaction times results from an interplay of geometry and reaction control. *Commun. Chem.*, 1:96, 2018.
[59] D. S. Grebenkov, R. Metzler, and G. Oshanin. Full distribution of first exit times in the narrow escape problem. *New J. Phys.*, 21:122001, 2019.
[60] D. S Grebenkov, R. Metzler, and G. Oshanin. *Target Search Problems*. Springer Cham, 2024.
[61] D. S. Grebenkov and G. Oshanin. Diffusive escape through a narrow opening: New insights into a classic problem. *Phys. Chem. Chem. Phys.*, 119:2723–2739, 2017.
[62] D. S. Grebenkov and S. Traytak. Semi-analytical computation of Laplacian Green functions in three-dimensional domains with disconnected spherical boundaries. *J. Comput. Phys.*, 379:91–117, 2019.
[63] D. S. Grebenkov and M. J. Ward. The effective reactivity for capturing Brownian motion by partially reactive patches on a spherical surface. *submitted, SIAM Multi. Model. Simul. (32 pages)*, 2025.
[64] D.S. Grebenkov. Diffusion-controlled reactions: An overview. *Molecules*, 28:7570, 2023.
[65] T. Guérin, M. Dolgushev, O. Bénichou, and R. Voituriez. Imperfect narrow escape problem. *Phys. Rev. E*, 107:034134, 2023.
[66] T. Guérin, N. Levernier, O. Bénichou, and R. Voituriez. Mean first-passage times of non-markovian random walkers in confinement. *Nature*, 534:356–359, 2016.
[67] P. Hänggi, P. Talkner, and M. Borkovec. Reaction-rate theory: fifty years after Kramers. *Rev. Mod. Phys.*, 62:251–341, 1990.
[68] P. Henrici, B. A. Troesch, and L. Wuytack. Sloshing frequencies for a half-space with circular or strip-like aperture. *Z. Angew. Math. Phys.*, 21:285–318, 1970.
[69] D. Holcman and Z. Schuss. Escape through a small opening: Receptor trafficking in a synaptic

membrane. *J. Stat. Phys.*, 117:975–1014, 2004.
[70] D. Holcman and Z. Schuss. Diffusion escape through a cluster of small absorbing windows. *J. Phys. A: Math. Theor.*, 41:155001, 2008.
[71] D. Holcman and Z. Schuss. Control of flux by narrow passages and hidden targets in cellular biology. *Phys. Progr. Report*, 76:074601, 2013.
[72] D. Holcman and Z. Schuss. The narrow escape problem. *SIAM Rev.*, 56:213–257, 2014.
[73] J. E. House. *Principles of Chemical Kinetics*. Academic press, 2007.
[74] S. A. Iyaniwura, T. Wong, C. B. Macdonald, and M. J. Ward. Optimization of the mean first passage time in near-disk and elliptical domains in 2-D with small absorbing traps. *SIAM Rev.*, 63:525–555, 2021.
[75] J. D. Jackson. *Classical Electrodynamics*. Wiley, New York, 2nd Edition, 1945.
[76] J. Kaye and L. Greengard. A fast solver for the narrow capture and narrow escape problems in the sphere. *J. Comput. Phys. X*, 5:100047, 2020.
[77] V. G. Kiselev. Fundamentals of diffusion MRI physics. *NMR Biomed.*, 30:e3602, 2017.
[78] V. Kozlov and N. Kuznetsov. The ice-fishing problem: The fundamental sloshing frequency versus geometry of holes. *Math. Methods Appl. Sci.*, 27:289–312, 2004.
[79] V. Kurella, J. Tzou, D. Coombs, and M. J. Ward. Asymptotic analysis of first passage time problems inspired by ecology. *Bull. Math Bio.*, 77:83–125, 2015.
[80] P. Lagerstrom. *Matched Asymptotic Expansions: Ideas and Techniques, Applied Mathematical Sciences, 76*. Springer-Verlag, New York, 1988.
[81] D. A. Lauffenburger and J. Linderman. *Receptors: Models for Binding, Trafficking, and Signaling*. Oxford University Press, Oxford, 1993.
[82] S. D. Lawley and J. P. Keener. A new derivation of Robin boundary conditions through homogenization of a stochastically switching boundary. *SIAM J. Appl. Dyn. Syst.*, 14:1845–1867, 2015.
[83] S. D. Lawley, A. E. Lindsay, and C. E. Miles. Receptor organization determines the limits of single-cell source location detection. *Phys. Rev. Lett,*, 125:018102, 2020.
[84] M. Levitin, D. Mangoubi, and I. Polterovich. *Topics in Spectral Geometry: (Graduate Studies in Mathematics, vol. 237)*. American Mathematical Society, 2023.
[85] M. Levitin, L. Parnovski, I. Polterovich, and D. Sher. Sloshing, Steklov and corners: Asymptotics of sloshing eigenvalues. *J. Anal. Math.*, 146:65–125, 2022.
[86] K. Lindenberg, G. Oshanin, and Metzler R. (Eds.). *Chemical Kinetics: Beyond the Textbook*. New Jersey: World Scientific, 2019.
[87] A. E. Lindsay, A. Bernoff, and M. J. Ward. First passage statistics for the capture of a Brownian particle by a structured spherical target with multiple surface traps. *SIAM Multi. Model. Simul.*, 15:74–109, 2017.
[88] A. E. Lindsay and A. J. Bernoff. Boundary homogenization and capture time distributions of semi-permeable membranes with periodic patterns of reactive sites. *SIAM Multi. Model Simul.*, 16(3):1411–1447, 2018.
[89] A. E. Lindsay and A. J. Bernoff. Numerical approximation of diffusive capture rates by planar and spherical surfaces with absorbing pores. *SIAM J. Appl. Math.*, 78(1):266–290, 2018.
[90] M. Lüking, J. Elf, and Y. Levy. Conformational change of transcription factors from search to specific binding: A lac repressor case study. *J. Phys. Chem. B*, 126:9971–9984, 2022.
[91] J. S. Marshall. Analytical solutions for an escape problem in a disc with an arbitrary distribution of exit holes along its boundary. *J. Stat. Phys.*, 165:920–952, 2016.
[92] J. Masoliver. *Random Processes: First-Passage and Escape*. World Scientific Publishing, 2018.
[93] V. G. Maz'ya, S. A. Nazarov, and B. A. Plamenevskii. Asymptotic expansions of the eigenvalues of boundary value problems for the Laplace operator in domains with small holes. *Math. USSR Izv.*, 24:321–345, 1985.
[94] R. Metzler, G. Oshanin, and S. (Eds.) Redner. *First-passage Phenomena and Their Applications*. Singapore: World Scientific, 2014.
[95] C. B. Muratov and S. Y. Shvartsman. Boundary homogenization for periodic arrays of absorbers. *SIAM Multi. Model. Simul.*, 7:44–61, 2008.
[96] A. M. North. Diffusion-controlled reactions. *Q. Rev. Chem. Soc.*, 20:421–440, 1966.
[97] S. Ozawa. Singular variation of domains and eigenvalues of the Laplacian. *Duke Math. J.*, 48:767–778, 1981.
[98] F. Piazza. The physics of boundary conditions in reaction-diffusion problems. *J. Chem. Phys.*, 157:234110, 2022.
[99] S. Pillay, M. J. Ward, A. Peirce, and T. Kolokolnikov. An asymptotic analysis of the mean first passage time for narrow escape problems: Part I: Two-dimensional domains. *SIAM Multi. Model. Simul.*, 8:803–835, 2010.

[100] C. E. Plunkett and S. D. Lawley. Boundary homogenization for partially reactive patches. *SIAM Multi. Model. Simul.*, 22:784–810, 2024.
[101] B. Punia, S. Chaudhury, and A. B. Kolomeisky. Understanding the reaction dynamics on heterogeneous catalysts using a simple stochastic approach. *J. Phys. Chem. Lett.*, 12:11802–11810, 2021.
[102] S. Redner. *A Guide to First-Passage Time Processes*. Cambridge University Press, Cambridge, U.K., 2001.
[103] D. Reguera, G. Schmid, P. S. Burada, J.-M. Rubí, P Reimann, and P. Hänggi. Entropic transport: Kinetics, scaling, and control mechanisms. *Phys. Rev. Lett.*, 96:130603, 2006.
[104] J. Reingruber and D. Holcman. Gated narrow escape time for molecular signaling. *Phys. Rev. Lett.*, 103:148102, 2009.
[105] M. Reva, D. DiGregorio, and D. S. Grebenkov. A first-passage approach to diffusion-influenced reversible binding and its insights into nanoscale signaling at the presynapse. *Sci. Rep.*, 11:5377, 2021.
[106] S. Rice. *Diffusion-Limited Reactions*. Elsevier, Amsterdam, The Netherlands, 1985.
[107] J.-F. Rupprecht, O. Bénichou, D. S. Grebenkov, and R. Voituriez. Exit time distribution in spherically symmetric two-dimensional domains. *J. Stat. Phys.*, 158:192–230, 2015.
[108] Z. Schuss. *Brownian Dynamics at Boundaries and Interfaces in Physics, Chemistry and Biology*. Springer, New York, 2013.
[109] Z. Schuss, A. Singer, and D. Holcman. The narrow escape problem for diffusion in cellular microdomains. *Proc. Nat. Acad. Sci. USA*, 104:16098–16103, 2007.
[110] A. S. Silbergleit, I. Mandel, and I. M. Nemenman. Potential and field singularity at a surface point charge. *J. Math. Phys.*, 44:4460–4466, 2003.
[111] A. Singer, Z. Schuss, and D. Holcman. Narrow escape, Part II: The circular disk. *J. Stat. Phys.*, 122:465–489, 2006.
[112] A. Singer, Z. Schuss, and D. Holcman. Narrow escape, Part III: Non-smooth domains and Riemann surfaces. *J. Stat. Phys.*, 122:491–509, 2006.
[113] A. Singer, Z. Schuss, and D. Holcman. Narrow escape and leakage of Brownian particles. *Phys. Rev. E.*, 78:051111, 2009.
[114] A. Singer, Z. Schuss, D. Holcman, and R. S. Eisenberg. Narrow escape, Part I. *J. Stat. Phys.*, 122:437–463, 2006.
[115] I. N. Sneddon. *Mixed Boundary Value Problems in Potential Theory*. North-Holland Pub. Co., 1966.
[116] S. D. Traytak. Competition effects in steady-state diffusion-limited reactions: Renormalization group approach. *J. Chem. Phys.*, 105:10860, 1996.
[117] S. D. Traytak and M. Tachiya. Diffusion-controlled reactions in an electric field: Effects of an external boundary and competition between sinks. *J. Chem. Phys.*, 107:9907–9920, 1997.
[118] M. J. Ward, W. D. Henshaw, and J. B. Keller. Summing logarithmic expansions for singularly perturbed eigenvalue problems. *SIAM J. Appl. Math.*, 53(3):799–828, 1993.
[119] M. J. Ward and J. B. Keller. Strong localized perturbations of eigenvalue problems. *SIAM J. Appl. Math.*, 53(3):770–798, 1993.
[120] G. H. Weiss. Overview of theoretical models for reaction rates. *J. Stat. Phys.*, 42:3–36, 1986.
[121] G. Wilemski and M. Fixman. General theory of diffusion-controlled reactions. *J. Chem. Phys.*, 58:4009–4019, 1973.
[122] Y. Ye, A. Chaigneau, and D. S. Grebenkov. Escape-from-a-layer approach for simulating the boundary local time in Euclidean domains. *J. Comput. Phys.*, 537:114099, 2025.
[123] H.-X. Zhou and R. Zwanzig. A rate process with an entropy barrier. *J. Chem. Phys.*, 94:6147–6152, 1991.